COMPARING AND EVALUATING TWO PHYSICALLY-BASED MODELS: OPENLISEM AND SCOOPS3D, FOR LANDSLIDE VOLUME PREDICTION

CHIYANG MA
FEBRUARY 2018

SUPERVISORS:
Dr. Cees. van Westen
Prof. Dr. Vector. Jetten
Dr. Olga. Mavrouli

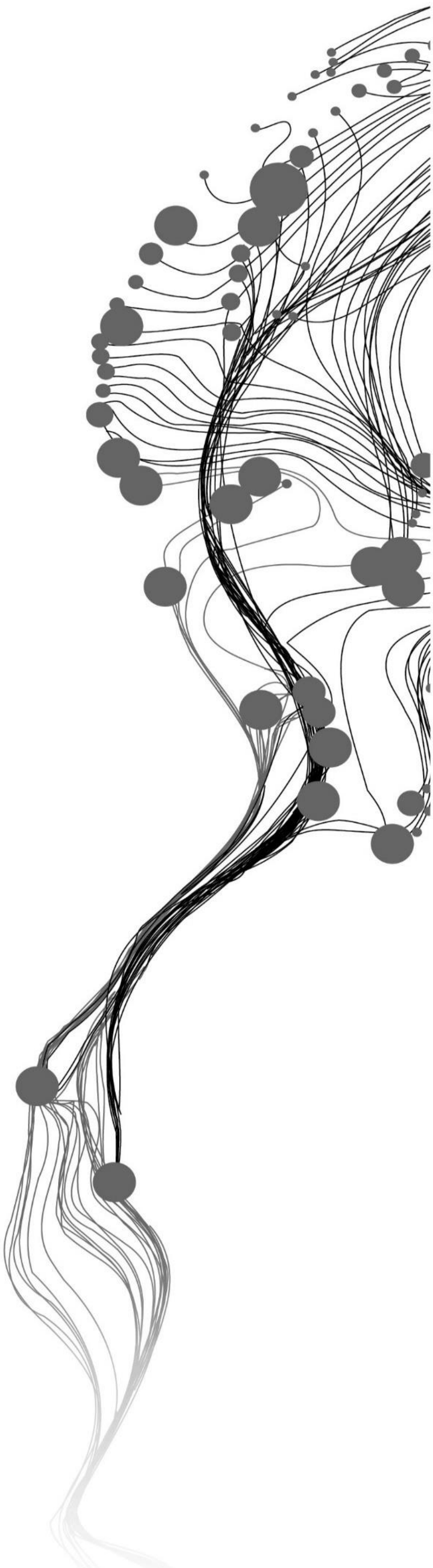

COMPARING AND EVALUATING TWO PHYSICALLY-BASED MODELS: OPENLISEM AND SCOOPS3D, FOR LANDSLIDE VOLUME PREDICTION

Chiyang Ma
Enschede, The Netherlands, February, 2018

Thesis submitted to the Faculty of Geo-Information Science and Earth Observation of the University of Twente in partial fulfilment of the requirements for the degree of Master of Science in Geo-information Science and Earth Observation.
Specialization: Applied Earth Sciences – Natural Hazards and Disaster Risk Management (AES-NHSRM)

SUPERVISORS:
Dr. Cees. van Westen (First supervisor)
Prof. Dr. Victor Jetten (Second supervisor)
Dr. Olga. Mavrouli (Third supervisor)

THESIS ASSESSMENT BOARD:
Prof. Dr. Norman Kerle (Chair)
Prof. Dr. Harry Seijmonsbergen (External examiner)

ABSTRACT

Potential landslide volume is an important parameter expressing potential landslide magnitude. With potential landslide volume, the landslide hazard and risk assessment can be carried out, and decisions on mitigation plans and budget measures can be made. However, due to the lack of underground information related to potential failure surface, it is hard to make a prediction for landslide volume.

Some physically-based modelling methods can be applied to predict landslide volumes by analyzing slope stabilities of slopes and determining potential failure surface. However, different models have different assumptions to define potential failure surface and analyze slope stability, the predicted landslides and their volumes may be also different. On the other hand, different models have different input data requirements, thus the difficulties for a successful application could also be different.

The main objective of this study is to compare two Geographic Information System (GIS) based distributed models: OpenLISEM and Scoops3D, in terms of landslide volume prediction. Due to the difficulties related to the acquisition of input data, a hypothetical dataset has been developed to perform the model comparison. The hypothetical dataset represented a volcanic environment by assigning the properties of volcanic ash soils to the virtual soils. Three scenarios were developed based on the hypothetical volcanic environment. In scenario 1, the initial soil thickness was initially determined to be homogeneous 10 meters by mimicking an explosive eruption where volcanic ash homogeneously rains down and covers the whole terrain. Based on scenario 1, the optimal internal model parameters of OpenLISEM and Scoops3D were determined, and a critical soil thickness was calculated using OpenLISEM by removing landslides from the terrain. Scenario 2 and 3 were based on this critical soil thickness. Wetting front and pore water pressure caused by groundwater level were considered as triggering factors for scenario 2 and 3, respectively. The landslides simulated by OpenLISEM and Scoops3D in three scenarios were compared using four comparing strategies: landslide number, location, volume, and area-volume statistical relationship.

The comparison results from sensitivity analysis on internal model parameters reveal that the internal model parameters can significantly influence the landslide volume prediction. These parameters should be very carefully selected when applying these two models. When determining critical soil thickness, it was found that there is no successive failures in OpenLISEM once the potential slope failures are cleared out of the terrain. Whereas there still are slope failures in Scoops3D when potential slope failures are cleared out of the terrain. This behavior indicates that OpenLISEM is more logical than Scoops3D. From comparisons under three scenarios, it was found that OpenLISEM and Scoops3D produce very different landslides in terms of number, location, and volume. Then volumes produced by Scoops3D are much larger than OpenLISEM, and Scoops3D tends to produce relatively round landslides. Sometimes, Scoops3D may cut into the bedrock and produce extremely large volume. This behavior also indicates that Scoops3D may lead to unexpected results.

Keywords: potential failure surface, potential landslide volume, physically-based modelling, soil thickness.

ACKNOWLEDGEMENTS

Firstly, I would like to thank my parents. Their endless love and support make my life. Without them, I cannot imagine what the life will be like.

I would like to express my deepest gratitude to my three supervisors, Dr. Cees Van Westen, professor Dr. Victor Jetten, and Dr. Olga Mavrouli. During the whole process, they never lose patience and never feel disappointed with me. Their great help is not only about the thesis, but also about the life. I appreciate that I can know you and be your MSc student. I cannot forget this learning experience.

I would also like to thank my Chinese supervisor, Dr. Xi'an Li. Thanks for supporting me to come to ITC, and also thanks for the great supporting when I was in China.

The same gratitude gives to Drs. Nanette Kingma, Ir. Bart Krol, Dr. Janneke Ettema. Thanks for the great help when I first came to ITC, and thanks for the great consolations you give me when I feel frustrated. You prevent me from breakdown.

Many special thanks to Ph.D. candidate Bastian van den Bout, Ph.D. student Chenxiao Tang, and Dr. Jianqiang Zhang. Thanks for spending so much time with me to teach me how to do the research. Also thanks for providing me the OpenLISEM model and research data. Your patience and intelligence lead my road. Without you, I cannot finish my thesis.

My appreciation also goes to all the teachers in ESA department. From you, I learned a lot, I will not forget the pleasant learning experience from you.

I also would like to thank all my friends in ITC. Your smile and company make my life in the Netherlands full of joy. Wish all the best to you.

TABLE OF CONTENTS

1. INTRODUCTION

1.1. Background

Landslides, defined as the movement of a mass of rock, debris, or soil down a slope, are one of the deadliest natural hazards in the world (Fell et al., 2008). Landslides can be triggered by earthquakes, extreme precipitation, and human activities such as road cutting, deforestation, and excavation. Landslides can cause significant damage and casualties to people and property. Engineering designs and practice, such as retaining walls and anchor cables to mitigate or even eliminate the threat from landslides require suitable information on landslide volume (Chen et al., 2014). Landslide hazard and risk assessment have also been playing an important role in minimizing the loss of lives and damage to properties (Dai et al., 2002; Wang et al., 2005).

The potential landslide volume is an important parameter in landslide studies because:

- Landslide volume is the best way to express the individual landslide magnitude. In the quantitative analysis of landslide risk, landslide magnitude-frequency relationship is one of the critical components, which quantifies the number of landslides that occur at different sizes (Malamud et al., 2004; Corominas et al., 2014). The prior studies have proposed several ways to express landslide magnitude, including volume (Malamud et al., 2004), total landslide area (Guzzetti et al., 2002), landslide area density, and landslide number density (Dai et al., 2011). Among those, the volume is preferable because it can reflect the realistic landslide size.
- It is very important in engineering practice. With the knowledge of the potential landslide volume, engineers can make decision on mitigation plans and budget measures to deal with landslide hazards (Hungr et al., 2005; Wang et al., 2005; de Falco et al., 2012; Chen et al., 2014; Loew et al., 2017).
- It is a fundamental parameter in analyzing secondary hazards. For example, potential landslide volume may determine the co-event damming of rivers, or determine the post-event debris flows (Fan et al., 2012; Calvo et al., 2015).

The potential landslide volume is considered as the volume of the material between the ground surface and the potential failure surface. The potential failure surfaces are often geologic discontinuities or changes in soil, which could experience a decrease in strength and evolve into failure surfaces when the water table rises or rainwater infiltrates and accumulates in discontinuities. Knowing the position and geometry of such discontinuities is required for landslide volume prediction. However, it is difficult to acquire such information beforehand (or even after) the event due to the scarcity and complexity of the underground information (Marchesini et al., 2009).

Direct methods, including trenching, drilling boreholes, and geophysical methods, can be used to directly measure the position and geometry of the geologic discontinuities. For example, the geophysical methods like seismic methods, acoustic methods, or electromagnetic methods utilize seismic waves, acoustic waves, or electromagnetic waves to penetrate into the soil or rock and detect the internal anomalies underneath the ground. Although the direct methods can give intuitive interpretations of potential slip surfaces, enough sampling points and appropriate distribution of sampling points are required, which is sometimes impossible in an inaccessible area. Additionally, both money- and labor-consuming drawbacks also limit their applications in landslide volume prediction (McCann and Forster, 1990; Jongmans and Garambois, 2007; Lollino et al., 2015).

Some physical models may also be applied to predict landslide volume. By inputting terrain data, soil parameters (soil cohesion, soil internal friction angle), hydrological parameters, soil thickness, etc., the physical models can mimic the underground situations. Based on the mimicked underground situations, physical models can simulate the unstable slopes and the corresponding potential failure surfaces by analyzing slope stabilities.

Physical models adopt two different principles to analyze slope stability, one is limit equilibrium models (LEMs), another is finite element models (FEMs). Most of the physical models adopt LEMs to carry out slope stability analysis (Abramson et al., 2002). The idea of LEMs is to predefine failure surfaces for slopes and analyze the stabilities of those predefined failure surfaces. The slope stability analysis is built on physical laws of equilibrium of forces or moments of the predefined failure surface, which can be mathematically expressed through an equation calculating the factor of safety for that surface (FoS, the ratio between stabilizing force and the destabilizing force; Duncan et al., 2014). The FoS greater than 1 indicates stable conditions, FoS equal to 1 indicates metastable conditions, and FoS less than 1 indicates unstable conditions. The predefined failure surface corresponding to unstable slopes (FoS less than 1) can be determined as the ultimate potential failure surface. And the materials between that failure surface and the ground surface can then be taken as potential landslide volumes.

However, the LEMs are only suitable for rigid masses that simultaneously fail down without progress deformation, and the calculated FoS is uniformly distributed along each predefined failure surface (Krahn, 2003). For failures that are caused by complex mechanisms such as progressively creep or brittle fracture, dynamic loading, and liquefaction of weak layer, etc., LEMs are not suitable anymore (Reid et al., 2015), and more complex numerical models such as FEMs should be used.

In contrast to LEM, FEMs do not predefine failure surface. This type of models first split a slope into a finite number of elements (meshes), then the forces and strains for each element are calculated using the corresponding constitutive laws. The potential failure surface can be found by solving those constitutive equations. The advantages of FEM include the ability to simulate site-specific features such as tension cracks and external loads. However, the quality of simulations using FEM depend on the user-defined mesh, if the defined mesh is too coarse, the results will not be good. Moreover, this kind of models needs accurate geologic boundary conditions and sophisticated input parameters, which in some cases limit their applications.

Nevertheless, most of the physical models that can be used to simulate landslide volume adopt LEM. These models include CLARA (Hungr et al., 1989), TSLOPE3 (Pyke, 1991), 3D-SLOPE (Lam and Fredlund, 1993), 3-DSLOPEGIS (Xie et al., 2003), r.slope.stability (Mergili et al., 2014), Scoops3D (Reid et al., 2015), and OpenLISEM (Van den Bout et al., 2017), etc. Among these models, the CLARA, TSLOPE3, and 3D-SLOPE can only deal with the individual slopes, whereas the r.slope.stability, Scoops3D, and OpenLISEM are spatially distributed models, which are based on Geographic Information System (GIS) and can be applied over a large area. OpenLISEM and Scoops3D can be run in Windows system, whereas the r.slope.stability model has been run on Linux system. Thus this study applies OpenLISEM and Scoops3D to carry out a comparison for predicting landslide volume.

1.2. Problem statement

OpenLISEM and Scoops3D may behave very differently for landslide volume prediction due to the different assumptions related to potential failure surface and slope stability analysis, or due to the internal model parameters. For example, Scoops3D utilizes a number of spheres to cut the terrain and generate a number of intersections between spheres and the terrain, the slope stabilities are analyzed based on the intersections. And a series of model parameters are used to define such searching process. Different search strategies may lead to different landslides. Whereas OpenLISEM predefines a planar shape of failure surface for each raster cell of DEM, the slope stabilities are analyzed based on every individual raster cells. Because different raster cell may have different failure depth, the combination of a group of individual failure surfaces of raster cells will lead to an overall irregular slip surface. For model applications, it is very useful and necessary to evaluate the effect of model assumptions on landslide volume simulation. However, no such comparison has been made.

Apart from the available models, the data requirements for the successful applications of these models are even more problematic. For example, the underground conditions, such as soil depth, soil types, geotechnical and hydrological properties, geologic structures, and discontinuity patterns are often essential components in landslide prediction, but such data is often unavailable. Researchers tend to use empirical models to estimate input data, but there is a lot of uncertainties in them, and validation is needed to make them acceptable.

1.3. Research objectives and research questions

The general objective of this research is to compare and evaluate two physical models, OpenLISEM and Scoops3D for landslide volume prediction.

Three specific objectives are proposed and eight corresponding research questions are formulated to accomplish the general objective.

1. To create controlled environments and to develop the respective datasets for comparison of landslide volume using OpenLISEM and Scoops3D.

   (1) How to create a suitable dataset in terms of topography, soil thickness and geotechnical properties, that can be imported into OpenLISEM and Scoops3D?

   (2) How to analyze the effect of rainfall on the landslide occurrence and volume using these models?

2. To compare the characteristics of the landslides predicted by OpenLISEM and Scoops3D.

   (3) Do the model parameters and model setup influence the landslide volume? And how?

   (4) What parameters to use for the comparison between the modelling results?

   (5) What are the major differences between the results from the two models in terms of number, volume distribution of the predicted landslides? What causes these differences?

3. To provide recommendations on the adequacy of OpenLISEM and Scoops3D for landslide volume calculation

   (6) Which are the fundamental assumptions of each model for the landslide volume calculation?

   (7) Based on what criteria should one choose one model or the other for landslide volume calculation?

   (8) Which are the limitations in each case?

1.4. The organization of the thesis and workflow

This thesis consists of six chapters:

Chapter one-Introduction. This chapter describes the research background, research objectives, and research questions.

Chapter two-Methods for landslide volume estimation. This chapter reviews the major methods for landslide volume measurement (post-event) as well as for landslide volume prediction (pre-event). The physically-based modelling methods are emphasized in this chapter.

Chapter three-Descriptions of the two models: OpenLISEM and Scoops3D. This chapter describes OpenLISEM and Scoops3D in terms of model assumptions, volume simulation, triggering mechanisms, input data requirements, as well as the model calibration options.

Chapter four-Methodology. This chapter explains the methodology adopted in this study. Fig. 1-1 briefly illustrates the major points for methodology. Through literature review, soil parameters were derived. Together with DEM and initial soil thickness (homogeneous 10 meters), the scenario 1 was analyzed. Based on scenario 1, sensitivity analysis on internal model parameters and the calculation of critical soil thickness has been done. With optimal model parameters and critical soil thickness, another two scenarios were analyzed. Then the landslides of the three scenarios were compared in terms of number, location, volume, and the area-volume statistical relationship.

Chapter five-results and analysis. This chapter analyzes all the model results, including sensitivity analysis on model parameters, critical soil thickness, and simulated landslides in three scenarios.

Chapter six-discussion, conclusions, and recommendations. This chapter presents the main limitations of this study, as well as the main findings and recommendations in this study.

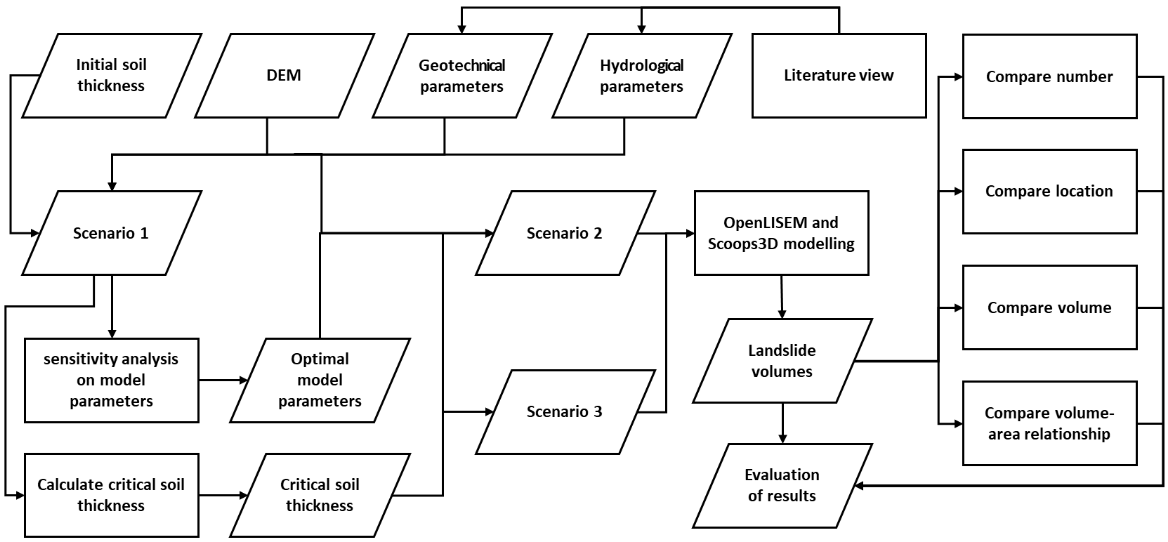

Fig. 1-1: *The workflow in this study.*

2. METHODS FOR LANDSLIDE VOLUME ESTIMATION

Landslide volume-related studies have been mainly focusing on existing landslides, and very few studies have attempted to predict potential landslide volume. This chapter presents several methods for landslide volume measurement (post-event) as well as for landslide volume prediction (pre-event). The first section briefly summarizes three main methods for landslide volume estimation, namely field measurement methods, elevation subtraction methods, and statistical methods. The second section introduces two types of methods for landslide volume prediction: namely field measurements, and physically-based modelling methods. It has to be clarified in the beginning that landslide volume is determined by the failure surface, thus the methods to estimate or predict landslide volume can be transformed into methods to detect or predict failure surface.

2.1. Post-event landslide volume estimation

Generally, there are three major methods to estimate the existing landslide volume: field measurement methods, elevation subtraction methods, and statistical methods. In this section, these three methods, as well as their advantages and disadvantages are briefly reviewed.

2.1.1. Field measurement methods

Field measurements are done in-situ with non-destructive methods (geomorphological and geological survey, geophysical prospecting) and destructive methods (drilling, pits and trenching etc.). The aims of these methods in landslide investigation are to investigate or detect landslide boundaries and to position the underground slip surface based on the fact that the landslide mass has different physical properties from the surrounding materials (Göktürkler et al., 2008; Pazzi et al., 2016). After acquiring the underground slip surface, the landslide volume can be derived by subtracting the elevation of the slip surface from post-event Digital Elevation Model (DEM), or by simply multiplying the landslide area with the depth, or using other geometric methods. From the perspective of slip surface geometry, a hemi-ellipsoid will be used to assume the geometry of landslide mass, and the landslide volume can be calculated by the hemi-ellipsoid volume formula:

$$V = (\pi/6) \cdot D_r W_r L_r \quad [2\text{-}1]$$

where D_r, W_r, L_r are respectively the depth (m), width (m), and length (m) of the rapture surface (Adegbe et al., 2014; Cruden and Varnes, 1996; Dewitte et al., 2008; Dewitte and Demoulin, 2005). However, it does

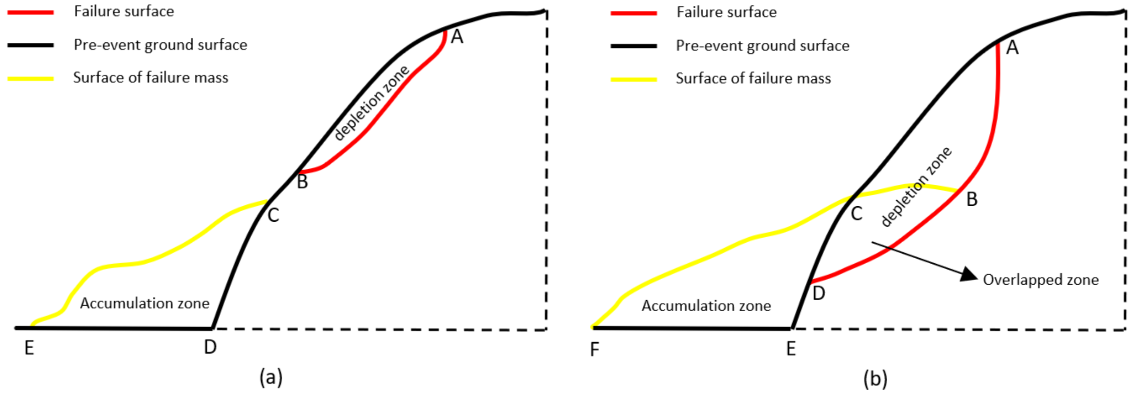

Fig. 2-1: *Figure shows accumulation and depletion zones of a landslide.*

not take into account the specific form of failure surface and specific geomorphology of single landslide types into account, and it is an oversimplified formula.

Notably, the slip surface is different from the failure surface (the slip surface contains the failure surface). Fig. 2-1 can be used to illustrate the difference between slip surface and failure surface. In Fig. 2-1 (a), the failure surface is the red curve A-B, whereas the slip surface is the curve A-B-C-D-E. In Fig. 2-1 (b), the failure surface is the red curve A-B-D, whereas the slip surface is the curve A-B-D-E-F. The field measurements can be used to directly measure slip surface, the calculated landslide volume is regarded as the post-event volume (volume between surface C-E and surface C-D-E in Fig. 2-1 (a); and volume between B-C-F and surface B-D-E-F in Fig. 2-1 (b)).

Among these field measurement methods, geophysical methods have gained an increasing attention and a considerable development in recent years due to the availability of cheap computer power, increasing reliability and accuracy, and its flexibility compared to other methods (Hack, 2000; Jongmans and Garambois, 2007). Often there is a geophysical contrast between the landslide body and the underlying bedrock. Geophysical techniques can detect such contrast using different forms of impulses such as seismic waves, acoustic waves, and electromagnetic waves, etc. According to the different form of impulses and imagining techniques, geophysical methods can be categorized into seismic methods, electromagnetic methods, geo-electrical or resistivity methods, self-potential (SP), acoustic emission, borehole geophysical methods and micro-gravity methods, etc. (McCann & Forster, 1990; Hack, 2000). The detailed principles of these methods are described by (Keller et al., 2002).

McCann and Forster (1990) reviewed the applications some geophysical methods under different geological settings for detecting slip surface and delineating the lateral extent of the landslide area. They also pointed out that despite the fact that conventional methods (drilling, pits and trenching) are more direct and accurate compared with geophysical methods, they are more expensive and hard to deploy on the steep or irregular ground. Besides, conventional methods can only provide a limited number of isolated single-point data.

Another comprehensive review is given by Jongmans and Garambois (2007), who presented the applications of main geophysical techniques at the time between 1990 and 2007 for different landslide types under different geological contexts. Meanwhile, they also explicitly compared the advantages and disadvantages of these techniques in terms of deployability, reliability, and requirement, and introduced the most recent 3D and 4D (spatial and temporal dimension) techniques such as electrical tomography technique and permanent geophysical monitoring systems, which are very useful for assessing the landslide volume.

The recent applications of geophysical methods for slip surface determination and landslide volume estimation are often coupled with other techniques (Deparis et al., 2008; Naudet et al., 2008; Pazzi et al., 2017). Naudet et al. (2008) integrated geophysical and geomorphological surveys to reconstruct the slip geometry of a landslide triggered by snowmelt-triggered in southern Italy. De Bari et al. (2011) combined geophysical measurements, aerial photogrammetry, and geological and geomorphological surveys to estimate the volume of a translational landslide situated in Basilicata region, southern Italy.

Although geophysical methods are capable of detecting internal structure (slip surface) of the landslide mass, they are still underdeveloped and relatively little used for slip surface detection because 1) these techniques only provide images depicting physical parameters which are not directly linked to geological and mechanical properties; 3) these techniques are highly dependent on geological contexts; 2) there is always a trade-off between image resolution and penetration depth, which depends on the size of landslide mass; 3) the solutions to the image results are not unique and need geomorphic surveys and borehole data to calibrate them; 4) the expert knowledge of geophysics is needed to get a reliable interpretation; 5) the combination of different geophysical techniques is necessary to acquire a reliable result, making it time- and money-consuming (Jongmans et al., 2009).

2.1.2. Elevation subtraction methods

Landslide volume can be estimated by subtracting pre- and post-event topography (Kerle, 2002). The elevation subtraction methods can be directly used to calculate landslide volume if the multi-temporal DEMs are available, or can be follow-ups of the field measurement methods which also mean to reconstruct slip surface and subtract slip surface from the post-event DEM. The pre- and post-failure DEMs can be derived from three general sources: 1) ground surveys (including total station, electronic theodolites, Global Positioning System (GPS) units, etc.); 2) digitized cartographic documents (existing hardcopy topographic maps); 3) remote sensing techniques (including airborne and satellite photogrammetric/stereo methods, airborne laser scanning (LiDAR), and airborne and satellite radar systems; Wilson, 2012).

According to the different degree of separation between depletion zone and failure mass (Fig. 2-1), the subtraction of pre- and post-event DEMs can derive different landslide volumes. In Fig. 2-1 (a), the failure mass is completely separated from the depletion zone. For such type of landslides, the subtraction between pre- and post-event DEMs can derive both pre-event volume (volume between pre-event ground surface and failure surface A-B) and post-event volume (volume between post-event DEM and surface C-D-E). In Fig. 2-1 (b), the part of the failure surface (surface B-D) is covered by failure mass. For such type of landslides, the subtraction between pre- and post-event DEMs can only derive post-event volume (volume between post-event DEM and surface C-D-E-F). The pre-event volume cannot be calculated because the underground surface B-D is unknown.

There are many studies on volume estimation using pre- and post-DEM subtraction methods. For example, Barbarella et al. (2000) investigated the evolution of a landslide situated in the Bracigliano village, Italy and estimated its volume using multi-temporal DEMs. In their study, DEMs were derived from different sources: a hardcopy cartography, ground surveying (total station), and aero-photogrammetric data, so they also compared and evaluated the resultant volumes derived from different DEM sources. Similarly, Kerle (2002) investigated a flank collapse that occurred at Casita volcano (Nicaragua) and calculated its volume using DEMs from three different sources: ground survey (total station), photogrammetric techniques and digitized cartographic material. In his study, different methods and their respective accuracies, as well as the problems in terms of volume calculation were completely evaluated. Based on multi-temporal DEMs, Van Westen and Getahun (2003) investigated the activity of the Tessina landslide located in North Eastern Italy and calculated its volume for different time periods. Bichler et al. (2004) compared three different methods for calculating landslide volume: subtraction of DEMs, geophysical methods, and field observation and measurements, and they concluded that geophysical methods gave the best approximation in their case. Other examples include Dewitte and Demoulin (2005), Baldi et al. (2005), Hapke (2005), Chen et al. (2006), Du and Teng (2007), Dewitte et al. (2008), Kasai et al. (2009), Baldo et al. (2009), Ventura et al. (2011), Tseng et al. (2013), Nikolaeva et al. (2014), Chen et al. (2014).

The major drawbacks and limitations of pre- and post-event elevation subtraction methods include: (1) the poor quality of many pre-event DEMs, especially when dealing with unexpected events (Kerle, 2002). In most of the cases, historical hardcopy documents would be used to generate the contour line and pre-event DEM. However errors would be brought in when digitized and interpolation of contour line (Kerle, 2002); (2) difference source of DEMs may result in co-registration errors, and consequently lead to undesirable volume results, especially in mountainous areas; (3) when the failure surface is partly covered by the failure mass (Fig. 2-1 (b)), the subtraction of pre- and post-event DEMs can only provide post-event volume. Pre-event volume can be very different from post-event volume because the decrease of density of the failed mass would lead to an increase of the failure volume (Chen et al., 2006), as well as the fragmentation and entrainment of bed material during the mass movement would lead to an increase of the failure volume (Zhan et al., 2017).

2.1.3. Statistical Methods

Landslide volume can also be estimated using statistical equations which express relationships between landslide volume and landslide-related factors. Such landslide-related factors can be geometrical characteristics such as surface area, length, width, and ratio of height to length, etc. (Brunetti et al,. 2009; Larsen et al., 2010; Klar et al., 2011; Tseng et al., 2013; Xu et al., 2013; Xu et al., 2014; Amirahmadi et al., 2016; Xu et al., 2016), or landslide triggering factors, for example, Keefer (1994) linked volumes of landslides in a seismically active region to the earthquake magnitude and seismic moment, Dai and Lee (2001) investigated relationships between landslide volume and precipitation.

Among these relationships, the volume-area relationship is regarded as the most frequently used one. The mathematical form of this type of relationships can be expressed by a general equation:

$$V_L = \alpha A_L^{\beta} \quad [2\text{-}2]$$

where V_L (m^3) refers to landslide volume, α to a constant, A_L (m^2) to the landslide area, β to the scaling exponent. This relationship was firstly proposed by Simonett (1967) who examined about 201 landslides in mountains on the north-central coast of New Guinea. Later on, other researchers developed their own volume-area relationships based on local landslide datasets (Rice et al., 1969; Innes,1983; Hovius et al.,1997; Guthrie and Evans, 2004; Korup, 2005; ten Brink et al., 2006; Imaizumi and Sidle, 2007; Guzzetti et al., 2008; Imaizumi et al., 2008; Larsen et al., 2010; Tseng et al., 2013; Xu et al., 2013; Xu et al., 2014; Amirahmadi et al., 2016; Xu et al., 2016).

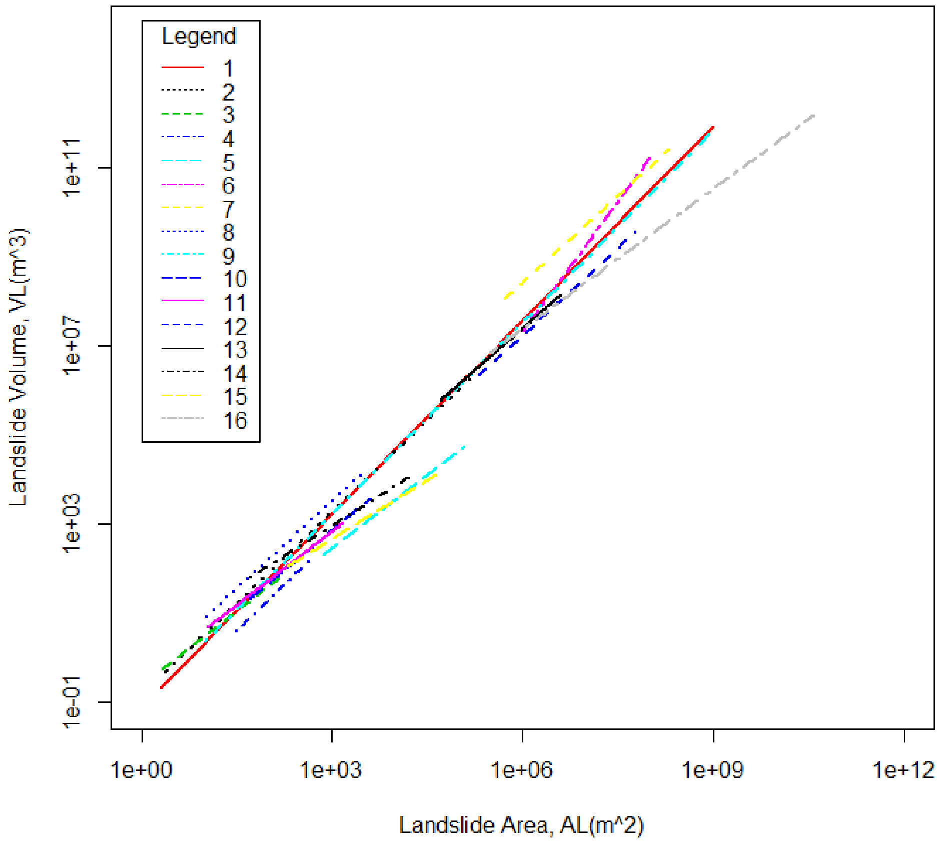

Fig. 2-2: *16 landslide volume-area relationships (in log-log scale) proposed in 16 literature and summarized in Guzzetti et al. (2009). Thick red line (#1) is the relationship that proposed by Guzzetti et al. (2009). The corresponding 16 literature can be found in Table 2-1.*

Guzzetti et al. (2009) investigated volume-area relationships for 677 landslides of slide type selected from a global database, and derived their volume-area relationship:

$$V_L = 0.074 \times A_L^{1.45} \qquad [2\text{-}1]$$

They also compared the results with the existing volume-area relationships in literature. Fig. 2-2 and Table 2-1 summaries these empirical relationships. The number 1-16 indicate the literature number, which can also be found in Table 2-1. They found that most of the relationships show a similar trend, and the volume-area relationships are largely independent from the physiographic settings. The geomorphological or mechanical properties (cohesion and internal friction angle) of the failure mass, landslide types, and the criteria adopted to estimate landslide volume do not significantly affect the relationships. Klar et al. (2011) demonstrated this independence from the perspective of the failure mechanism, where they varied cohesion from 0.001kpa to 200kpa in their study and derived the scaling exponent β is ranging from 1.32 to 1.38.

Table 2-1: *Empirical relationships between landslide area A_L and landslide volume V_L proposed by 16 literature (source: Guzzetti et al., 2009).*

ID	Equation	Min. A_L (m^2)	Max. A_L (m^2)	Source
1	$V_L = 0.074 \times A_L^{1.45}$	2×10^0	1×10^9	Guzzetti et al. (2009)
2	$V_L = 0.074 \times A_L^{1.45}$	2.3×10^3	1.9×10^5	Simonett (1967)
3	$V_L = 0.074 \times A_L^{1.45}$	2.1×10^0	2×10^2	Rice et al. (1969)
4	$V_L = 0.074 \times A_L^{1.45}$	3×10^1	5×10^2	Innes (1983)
5	$V_L = 0.074 \times A_L^{1.45}$	7×10^2	1.2×10^5	Guthrie and Evans (2004)
6	$V_L = 0.074 \times A_L^{1.45}$	$>1\times10^6$		Korup (2005)
7	$V_L = 0.074 \times A_L^{1.45}$	5×10^5	2×10^8	ten Brink et al. (2006)
8	$V_L = 0.074 \times A_L^{1.45}$	1×10^1	3×10^3	Imaizumi and Sidle (2007)
9	$V_L = 0.074 \times A_L^{1.45}$	1×10^1	1×10^9	Guzzetti et al. (2008)
10	$V_L = 0.074 \times A_L^{1.45}$	5×10^1	4×10^3	Imaizumi et al. (2008)
11	$V_L = 0.074 \times A_L^{1.45}$	1.1×10^1	1.5×10^3	Rice and Foggin (1971)
12	$V_L = 0.074 \times A_L^{1.45}$	2×10^5	6×10^7	Abele (1974)
13	$V_L = 0.074 \times A_L^{1.45}$	5×10^4	3.9×10^6	Whitehouse (1983)
14	$V_L = 0.074 \times A_L^{1.45}$	5×10^1	1.6×10^4	Larsen and Torres Sanchez (1998)
15	$V_L = 0.074 \times A_L^{1.45}$	2×10^2	5.2×10^4	Martin et al. (2002)
16	$V_L = 0.074 \times A_L^{1.45}$	3×10^5	3.9×10^{10}	Haflidason et al. (2005)

However, it is worthwhile to notice the reliability of the information of landslide areas and volumes used to determine the volume-area relationships. Most of the landslide areas that were used to build volume-area relationships were derived from landslide inventory maps. The problem consists in how to distinguish the individual landslides in landslide inventory maps. Many smaller landslides of different type and age can be nested inside of larger landslides, which are often ignored in landslide inventory maps, especially for geomorphological inventory maps. To overcome this problem, a multi-temporal landslide inventory map is needed, and a sufficient level of detail in mapping individual landslides. Moreover, for landslide inventories in which the depletion area is separately mapped from the deposition area, the merged area (depletion plus deposition) should be used for statistical analysis (Guzzetti et al., 2008; Tseng et al., 2013). Some studies only utilized depletion area (Imaizumi and Sidle, 2007; Imaizumi et al., 2008), whereas some studies only utilized deposition area (Innes, 1983), leading to an inaccurate estimation of total landslide area. Furthermore, many landslide volumes are simply calculated by multiplying landslide surface areas and average landslide depths, which can lead to overestimated landslide volumes (Larsen and Sanchez, 1998; Martin et al., 2002). These uncertainties related to the landslide types and geological environments, which sometimes make the accurate volume-area relationships very different to acquire.

2.2. Landslide volume prediction

As mentioned above, very few studies have been done for landslide volume prediction, mainly because the slope instability itself is hard to forecast, let alone the difficulties of obtaining reliable and representative information on the slip geometry of the unstable slope (Meric et al., 2005). There are two main methods that can potentially predict the volume of potential landslides: field measurements and physically-based modelling methods. In this section, these two methods are briefly described.

2.2.1. Direct Measurement methods

Geophysical and drilling methods can be applied to detect the potential failure surface of impending failures because they can reveal details about weathered zone, hydrological system, and geological structures (discontinuities) underneath the ground surface (Robain et al., 1996; Ritz et al., 1999; Jongmans and Garambois, 2007), which are generally regarded as weak layers in slopes and could evolve into failure surfaces. Some studies also utilized geological survey methods to detect potential failure surface, for example, Zhang et al. (2013) investigated fracture orientation of fractured rock slope, and based on this they analyzed critical failure surface. The most frequently used methods are geophysical methods coupled with drilling methods. And for possible reactivations of old landslides, the problem of finding and representing the rupture surface is the same as for the post-event methods that were described in the previous section of this chapter.

Lebourg et al. (2005) carried out a three-dimensional electrical resistivity tomography method to investigate a potential deep-seated landslide in France, and predicted that the potential volume of the constructed sliding body is 5 million cubic meter. Deparis et al. (2008) combined geophysical methods with remote sensing techniques to characterize the geometry and fracture pattern of a potentially unstable cliff in France. Other examples applied geophysical methods to predict potential failure surface are Chambers et al. (2011), Kotyrba et al. (2015), Pazzi et al. (2017).

Generally speaking, geophysical methods can give relatively accurate and detailed information on the sub-surface. They have been a common approach for engineering projects, and often coupled with slope stability analysis. However, due to the reasons mentioned in section 2.1.1, these methods cannot be frequently used in landslide volume prediction, especially for studies at a large scale.

2.2.2. Physically-based modelling Method

Physically-based modelling methods are based on the physical laws to analyze potential landslide occurrence and volume. By inputting terrain data, soil parameters (soil cohesion, soil internal friction angle, bulk density), hydrological parameters (infiltration capacity, saturated hydraulic conductivity), soil thickness, etc., physical models can mimic the underground situations. Based on the mimicked underground situations, physical models can estimate potentially unstable slopes and the corresponding potential failure surfaces by analyzing slope stabilities. Physical models adopt two different types of principles to analyze slope stability: limit equilibrium models (LEM), and numerical models (the most frequently used numerical models are finite element models (FEM)).

The limit equilibrium models predefine potential failure surface and investigate the equilibrium state (the equilibrium of forces or moments) of the predefined failure surface. The equilibrium state is expressed by a ratio, FoS, between the upslope stabilizing force R and the downslope destabilizing force T:

$$\mathrm{FoS} = \frac{R}{T} \qquad [2\text{-}2]$$

Where FoS is the factor of safety for predefined failure surface. FoS > 1 indicates stable condition, FoS = 1 indicates metastable condition, while FoS < 1 indicates unstable condition. Notably, the unstable condition can only exist in modelling results, in reality, such unstable situation cannot exist unless the slopes are affected by the external factors, such as rainfall or earthquake, etc. Equation 2-4 is only a general form of expression of limit equilibrium models, it can be expanded by adding seismic terms if there are a seismic effects, or water table terms if the water table variation affects the slope stability.

Assumptions of limit equilibrium model are: (1) the failure mass consists of rigid materials and slides along a single failure plane (Mergili et al., 2014); (2) failure occurs simultaneously along the potential slip surface without progressive movement, FoS is uniform everywhere along the predefined slip surfaces (one predefined slip surface has one single FoS); (3) the deformation and strain of the potential failure mass, as well as dynamic loading are ignored (Duncan and Wright, 2005). Limit equilibrium models can be applied to one-, two-, or three-dimensional stability analysis.

The finite element models do not predefine failure surface. This type of models first split a slope into a finite number of elements, then the force and strain for each element are calculated using the corresponding constitutive laws (Kanjanakul and Chub-uppakarn, 2013). The potential failure surface can be found by solving those constitutive equations. The advantages of finite element models include the ability to simulate site-specific features such as tension cracks and external loads. However, this kind of models needs accurate geologic boundary conditions and sophisticated input parameters, which in many cases limit their applications.

Most physical models adopt limit equilibrium models to analyze slope stability (as mentioned in section 1.1). In these models, the potential landslide volume can be calculated by:

(1) Predefining slip surface;

(2) Analyzing the stabilities for predefined slip surfaces;

(3) Computing the corresponding volumes.

According to different limit equilibrium models the and different ways to predefine failure surfaces, the limit-equilibrium-models-based physical models can be classified as one-, two-, and three-dimensional models.

2.2.2.1. One-dimensional model

The one-dimensional (1-D) slope stability model, also termed as infinite slope model, is the simplest but most used model. The important assumptions of the infinite slope model are: (1) the topographic surface is infinitely long compared with the soil depth; (2) the potential slip surface is predefined as the bottom of the soil layer; (3) the potential slip surface and topographic surface are of planar shape and parallel with each other (Fig. 2-3(left)). According to these assumptions, the infinite slope can be regarded as an individual unit (without slicing) when applying the limit equilibrium method to analyze its stability, which significantly simplifies the slope stability analysis. The equation of limit equilibrium method in infinite slope model is (Graham, 1984):

$$FoS = \frac{c' + z(\gamma Cos^2\alpha - \rho a_h N cos\alpha sin\alpha - \gamma_w m \cdot Cos^2\alpha)tan\varphi'}{z(\gamma sin\alpha cos\alpha + \rho a_h N cos^2\alpha)} \qquad [2\text{-}3]$$

Where c' (kPa) is the effective soil cohesion, z (m) is soil depth, γ (kN/m^3) is the unit weight of soil, α (°) is the terrain surface inclination, ρ (kg/m^3) is the bulk density of soil, a_h (m/s^{-2}) is the horizontal peak ground acceleration (PGA) for rock, N (-) is the amplification coefficient of seismic acceleration for soil material, γ_w (kN/m^3) is the unit weight of water, m (-) is the ratio between groundwater depth Z_w (m) and soil depth Z (m), ϕ' (°) is the soil effective internal friction angel. The effective soil cohesion and internal friction angle are different from soil cohesion and internal friction angle, the former takes into account the buoyancy of the soils below the groundwater level, whereas the latter does not, indicating a dry condition.

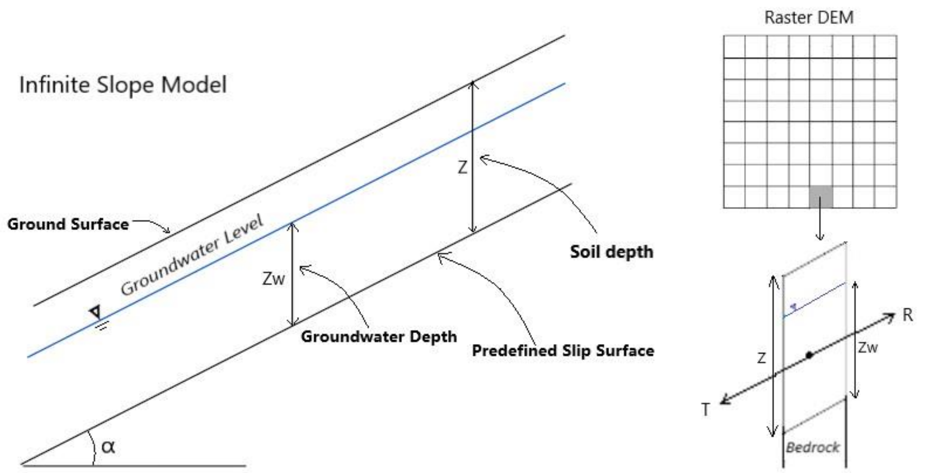

Fig. 2-3: *The infinite slope model (Left) and its application in raster GIS (Right).*

The assumptions of the infinite slope model facilitate its application in GIS-based environments (Murphy and Vita-Finzi, 1991; Van Westen and Terlien, 1996; Mergili et al., 2014), where all the calculations are based on individual DEM pixels and inter-pixel forces are ignored because the failure is assumed to be infinitely long and wide. By incorporating the infinite slope model into GIS environments, the landslide volume can be simulated because each raster cell can be considered as an infinite slope and the failure width can be represented by pixel size (Fig. 2-3 (right)).

So far, a large number of models have been developed using infinite slope model in GIS (Montgomery and Dietrich, 1994; Van Westen and Terlien, 1995; Wu and Sidle, 1995; Pack et al., 1998; Baum et al., 2010; Lee and Park, 2015), including SHALSTAB (Montgomery and Dietrich, 1994), SINMAP (Pack et al., 2003), and STARWARS+PROBSTAB (Van Beek, 2002), etc. Many of them are coupled with two-dimensional hydrological models to estimate the effect of the change of groundwater level or the transient rainfall infiltration on slope stability. Some studies also incorporated seismic-related models, such as Newmark's displacement model and ground motion attenuation model, into infinite slope model to simulate earthquake-induced landslides (Miles and Ho 1999; Luzi et al. 2000; Randall et al. 2000; Jibson et al. 2000; Khazai and Sitar, 2000; Refice and Capolongo, 2002).

However, due to the assumptions, infinite slope model only works well for shallow and translational landslides with the cohesionless material, for deep-seated landslides whose slip surfaces are no longer plane and the materials are cohesive, this model is not suitable anymore (Mergili et al., 2014).

2.2.2.2. Two-dimensional model

In two-dimensional (2-D) slope stability models, the slope stability analysis which is based on the slope profiles derived from the DEM along the steepest slope gradient is performed outside the GIS environment. SlopeW (GEO-SLOPE International, 2010) is one 2D model. Unlike 1-D model, 2-D models do not constrain the geometry of predefined slip surfaces, and the geometry can be circular, elliptical or spiral, etc. Above the predefined slip surface, the potential failure mass should be equally or unequally partitioned into many vertical slices. The FoS of each slice is calculated using the equation 2-5, and then summed up to calculate the overall FoS for the entire slope. The inter-slice forces can also be considered in the calculation procedure (Duncan and Wright, 2005).

The advantages of two-dimensional slope stability models are (1) the flexible geometry of slip surface (circular, elliptical or spiral, etc.); (2) the applicability for both shallow and deep-seated landslides; (3) the presence of many existing models with many reasonable limit equilibrium models ; (4) the combination of many hydrological models (Anderson and Howes, 1985; Van Asch et al., 1993).

The disadvantages of 2-D slope stability models are (1) the inapplicability in GIS environment (Van Westen and Terlien, 1995); (2) the inevitable subjectivity resulting from the selection of dangerous slope when the investigation is performed over a large area; (3) the ignorance of the width and the topography of the slope (Mergili et al., 2014); (4) the inconvenience related to the data conversion from GIS to external two-dimensional slope stability models (Van Westen and Terlien, 1995); (5) the difficulties related to the representation of the spatially distributed results (Xie et al., 2003).

Notably, for potential landslide volume prediction, 2-D slope stability models are obviously not suitable because the models can only provide two-dimensional slip surface without width information, as well as their inapplicability in GIS environment where the width can be represented by pixel size.

2.2.2.3. Three-dimensional model

In reality, potential slip surface is often of three-dimensional (3-D) geometry, thus a 3-D model for potential landslide volume simulation is more rational than 1- D model. The advent of 3-D landslide analysis can date back to 70s last century. The 3-D models were firstly applied for individual slope stability analysis. The implementation was performed outside the GIS using software such as CLARA (Hungr, 1988), TSLOPE3 (Pyke, 1991), and 3D-SLOPE (Lam and Fredlund, 1993). Later on, GIS-based 3-D models were developed, allowing for the simulation over a large area. The examples include OpenLISEM (Van den Bout et al., 2017), Scoops3D (Reid et al., 2015), and r.slope.stability (Mergili et al., 2014). Among the existing 3-D models, the geometry of predefined slip surface can be sphere, ellipsoid, truncated ellipsoid, etc.

2.2.2.4. The uncertainties related to physical models

The input data and internal model parameters can bring in uncertainties when simulating landslides. In the GIS-based analysis, from the data preparation to the final result generation, uncertainty may be introduced or magnified at each stage (Davis and Keller, 1997). The source of uncertainty is the spatial and temporal variation of the geotechnical and geometric parameters. Geotechnical parameters consist of soil cohesion, soil internal friction angle, unit weight of soil, soil thickness, and depth to groundwater etc., which are determined in the field or in the laboratory. Uncertainties regarding geotechnical and hydrological parameters are introduced by (1) the horizontal and vertical variability of soil material (heterogeneity) that cannot be represented by only a limited number of sampling points. Thus the groundwater level simulated using hydrological parameters, such as porosity, saturated and unsaturated hydraulic conductivities, macropores, etc. can also be affected; (2) the temporal variability of soil material caused by rainfall, long-term erosion etc., which either cannot be represented by intermittent sampling and laboratory test; (3) the limitations of measurement techniques which can result in error and bias.

Geometric parameters, including the parameters that control the position and the shape of the potential slip surface, belong to internal model parameters. Uncertainty regarding the geometric parameters is introduced by the pre-definition of the slip surface, for example, some models assume a deep-seated, ellipsoidal slip surface, and some models assume a shallow, planar slip surface. Meanwhile, geotechnical uncertainties and site-specific features, such as tension cracks and external loads could also contribute to the geometric uncertainty.

3. DESCRIPTIONS OF THE TWO MODELS: OPENLISEM AND SCOOPS3D

Two models: OpenLISEM and Scoosp3D, were compared in this study. These two models can be directly used to predict landslide volume, which is relevant to the research objectives. Although some other models can be applied to perform landslide volume simulation, such as the three-dimensional models mentioned in section 2.2.2.3, they are not the spatially distributed models. OpenLISEM and Scoops3D are GIS-based distributed models, which can be applied to a large area. The r.slope.stability model can also be applied to predict landslide volumes for a large area. At the beginning, we tried to incorporate r.slope.stability into our study, however, it has been run on Linux system, which is not so convenient. Thus this study selected OpenLISEM and Scoops3D to perform landslide volume simulation.

3.1. OpenLISEM

OpenLISEM is the abbreviation of the Open source Limburg Soil Erosion Model. Originally, it was a physically based soil erosion model De Roo et al., 1996). Based on a single rainfall event, it calculates the runoff from a surface water balance within a catchment and coupled to sediment transport equations. A series of dynamic hydrological processes, including rainfall interception, through fall, infiltration, surface flow, detachment, etc. are included in OpenLISEM. Later on, the infinite slope model was incorporated into the model (Van den Bout et al., 2017), and based on infinite slope model, an iterative method for progressive slope failure was developed from which landslide volume can be derived.

3.1.1. The iterative method

The iterative method is based on a modified infinite slope model. The conventional infinite slope model predefines the bottom of the soil layer as the potential slip surface (Fig. 2-3), whereas the iterative method iteratively searches the potential slip surface. The equation to calculate the FoS is (Van Beek, 2002):

$$\mathrm{FoS} = \frac{c' + \Delta c' + [(Z - Z_w) \cdot \gamma + Z_w \cdot \gamma'] cos^2\beta tan\phi'}{[(Z - Z_w) \cdot \gamma + Z_w \gamma_s] sin\beta cos\beta} \quad [3\text{-}1]$$

With c' and Δc' (kPa) the effective soil cohesion and root cohesion; Z (m) the soil depth; Z_w (m) the depth of the "pseudo-groundwater level"; γ, γ', and γ_s (kN/m^3) the soil unit weight, buoyant unit weight, and saturated unit weight, respectively, and $\gamma' = \gamma_s - \gamma_w$ (γ_w (kN/m^3) is the water density); β (°) the slope angle; ϕ' (°) the effective internal friction angle. Notably, the depth of pseudo-groundwater level in equation 3-1 can be calculated using equation 3-4. It is not the hydrological groundwater level, but a function of the initial, saturated, and residual soil moisture and soil depth (will be described in section 3.1.3).

OpenLISEM is a dynamic model, which means the calculations are performed for every time step. The time step can be defined by users. Fig. 3-1 and the following descriptions explain the procedures of the iterative method to calculate landside volume:

(1) At time step 1: the stabilities of all pixels over the entire DEM map will be calculated using the equation 3-1, and the unstable pixels with FoS less than 1 will be picked out. The corresponding illustration of this step in Fig. 3-1 is FoS map on the left. The red pixels indicate the calculated unstable pixels.

(2) At time step 2: every unstable pixel have 8 surrounding pixels in a 3×3 window. For the centered unstable pixels, the stabilizing forces R are less than the destabilizing forces T. There is a force unbalance. The iterative method assumes that the balance could be achieved by decreasing the elevations (removing failure depths) of those unstable pixels. The iterative method calculates the failure depths and removes them so that the FoS of those unstable pixels becomes greater than 1. The corresponding illustration of this step in Fig. 3-1 is iteration 1. The unstable pixel 1 experienced a decrease in depth and become stable. At this time step, all the unstable pixels calculated at time step 1 will be processed until become stable.

(3) At time step 3: due to the removal of the failure depths for unstable pixels at time step 2, the slopes between the centered pixels and the surrounding 8 pixels will be increased at the same time, which may lead to slope failures for previously stable pixels. So iterative method will repeat the steps (1) and (2). The corresponding illustration of this step in Fig. 3-1 is iteration 2 and 3. The pixels 3 and 4 were previously stable, due to the decrease of depth of pixel 2, the pixel 3 became unstable. After removing the failure depth for pixel 3, the pixel 4 became unstable.

(4) Repeat the steps (1), (2) and (3) until no unstable pixels exist in the whole map.

For each time step, the groundwater level is also dynamic and updated in the calculation of FoS.

Notably, there are two user-defined parameters that may affect the simulated landslide volume, the maximum factor of safety (F_i) and the resulting factor of safety (F_r). The F_i is the cut-off value of slope failure initiation. All the pixels with FoS less than F_i is regarded as unstable and will be failed. The F_r is the FoS used to calculate how much failure depths should be removed from those unstable pixels. By substituting FoS with F_r and calculating the soil depth Z in equation 3-1, failure depth can be calculated. Thus the F_r indicates the FoS after failure.

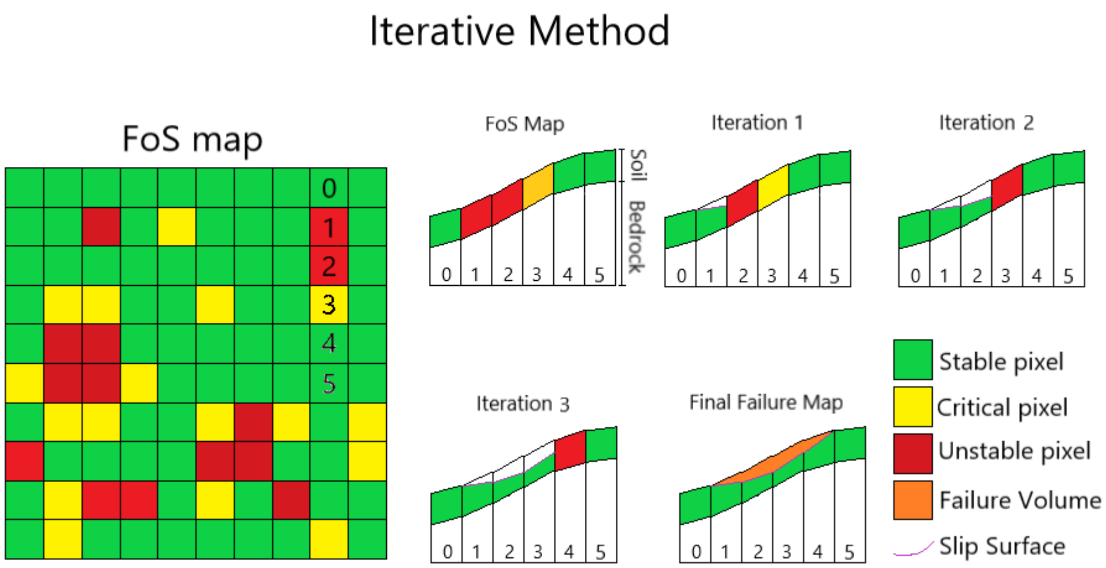

Fig. 3-1: *Example of the iterative method to calculate potential landslide volume. Firstly, the FoS map indicates overall stabilities of all pixels. For group 0-5, slope failure start from the pixel 1, and a failure depth is calculated (using equation 3-1) and removed from pixel 1 in order to become stable. The slope between 1 and 2 is changed due to the removal of failure depth of pixel 1, making that pixel 2 becomes unstable. Based on the changed slope, the failure depths for pixel 2 is calculated and removed as well. After pixel 2 becomes stable, the stability of pixel 3 is also changed and the failure depth of it is also removed. After pixel 1, 2, 3, and 4 all become stable, the slip surface can be determined, and the volume can be calculated.*

3.1.2. Input for OpenLISEM

Table 3-1 shows the input data required by OpenLISEM for performing a landslide simulation. The first column of this table indicates the names of model input data, the second column describes how the input parameters obtained. OpenLISEM requires the raster data in PCRaster map format (extended by ".map"). The format of rainfall data is ASCII text file (Jetten and Van den Bout, 2017).

***Table 3-1**: The input data of OpenLISEM for landslide simulation.*

Input data	Data source
Digital Elevation Model (DEM)	DEM represents the local topography. DEM can be obtained from some free global DEM data sources including Space Shuttle Radar Topography Mission (SRTM) and Advanced Spaceborne Thermal Emission and Reflection Radiometer (ASTER), etc. The resolutions of DEMs vary in different data sources.
Soil and root cohesion (kPa) Internal friction angle (rad) Bulk density (kg/m^3) Soil porosity(-) Initial soil moisture(-) Residual soil moisture(-) Saturated hydraulic conductivity (mm/h)	Each soil parameter is assigned to a horizontal soil class. The vertical variations of soil properties within the soil layer are not supported by OpenLISEM. The best ways to obtain these soil-related parameters are laboratory tests and field measurements. By interpolating measured soil samples, the spatially distributed soil properties can be obtained. If the laboratory tests and field measurements cannot be achieved, the literature values can also be used. In this case, the soil types should be known in advance. For some hydrological parameters like soil porosity and saturated hydraulic conductivity, an empirical model named Soil Water Characteristics (Saxton and Rawls, 2006) can be used. To apply this empirical model, soil particle size distribution (PSD), organic matter content, salinity, gravel content, compaction should be known or estimated in advanced.
Soil thickness (m)	The best ways to obtain soil thickness are field measurements using boreholes or geophysical techniques, etc. These measurements can derive depth of sampling points, and coupled with the spatial interpolations, soil thickness can be derived. If the field measurements cannot be achieved, an empirical model developed by Kuriakose et al. (2009) can be applied to model the spatial soil thickness. In this model, several environmental parameters such as slope steepness, curvature, soil wetness, distance to the coast or channel may be used.
Rainfall data	The rainfall duration (min) and intensity (mm/h) are required (Jetten and Van den Bout, 2017). The best rainfall data with high temporal resolutions may come from local rainfall stations. If rainfall station data is not accessible, the satellite rainfall data may be a substitute. The Tropical Rainfall Measuring Mission (TRMM) and Global Precipitation Measurement (GPM) could provide needed rainfall information. The TRMM provides rainfall data during the period from 1997 to 2015, with the maximum spatial and temporal resolutions of 0.25° and 3h; whereas the GPM provides rainfall data since 2014, with the maximum spatial and temporal resolutions of 0.1° and 30 min. The satellite rainfall data should be validated using measured data before putting into use.
Land cover data	Within OpenLISEM, objects on the ground surface such as vegetation and buildings can result in rainfall interception. The building map and vegetation cover map are needed in OpenLISEM to calculate rainfall interceptions. Building footprints as a shapefile or polygons can be extracted from OpenStreetMap database using GIS software like QGIS. Vegetation cover, or leaf area index, can be calculated using some empirical equations which are described in Jetten and Van den Bout, (2017).

3.1.3. Hydrological component in OpenLISEM

OpenLISEM provides dynamic rainfall input options. The landslide triggering mechanism is wetting front infiltration. The wetting front may affect slope stability by means of increasing total soil weight and (or) increasing groundwater level.

- If the infiltrated wetting front does not reach the groundwater level, then only the total soil weight is increased. The effect of the wetting front on FoS can be expressed using the equation:

$$\mathrm{FoS} = \frac{c' + \Delta c' + [(Z - Z_w - Z') \cdot \gamma + Z' \cdot \gamma_s + Z_w \cdot \gamma']cos^2\beta tan\phi'}{[(Z - Z_w - Z') \cdot \gamma + Z' \cdot \gamma_s + Z_w \gamma_s]sin\beta cos\beta} \quad [3\text{-}2]$$

  where Z' (m) is the depth of wetting front, γ_s (kN/m^3) is the saturated soil unit weight. The units of the other terms can be found in equation 3-1. Although the increase of total soil weight can increase the inter-particle friction at slip surface and thus increase shear resistance, the shear stress is increased much more, leading to a final decrease of FoS.

- If the infiltrated wetting front reaches the groundwater table, there is a connection between the wetting front and groundwater, then both total soil weight and groundwater table are increased. The change of total soil weight is described in equation 3-2. The increase of groundwater table is expressed by the increase of the Z_w in equation 3-2. This rise of groundwater level leads to a decrease of the friction forces at slip surface, resulting in a decrease of FoS.

The Green & Ampt model is used to simulate wetting front infiltration. This model assumes that a wetting front moves downwards into the soil, above this wetting front, the soil is saturated, beneath this wetting front it is completely dry. The infiltration rate is calculated using the equation:

$$\mathrm{f} = -K_{sat}\left(\frac{h_f - h_0}{z_f} - 1\right) \quad [3\text{-}3]$$

With f (m/s) the infiltration rate; K_{sat} (mm/h) the saturated hydraulic conductivity; h_f (m) the suction head at the wetting front; h_0 (m) the suction head at the soil surface; z_f (m) the depth of the wetting front. The infiltration depths can be calculated by multiplying the infiltration rate and infiltration time.

In OpenLISEM, the initial groundwater level is considered as the linear interpolation of initial soil moisture (Fig. 3-2; Van Beek, 2002). The initial groundwater level Z_w (m) is calculated using the equation:

$$Z_w = \frac{\theta_i - \theta_r}{\theta_s - \theta_r} Z \quad [3\text{-}4]$$

With θ_i (-) the initial soil moisture; θr (-) the residual soil moisture; θ_s (-) the soil porosity; Z (m) the soil depth. The residual soil moisture, porosity are the constants, and soil depth are constants.

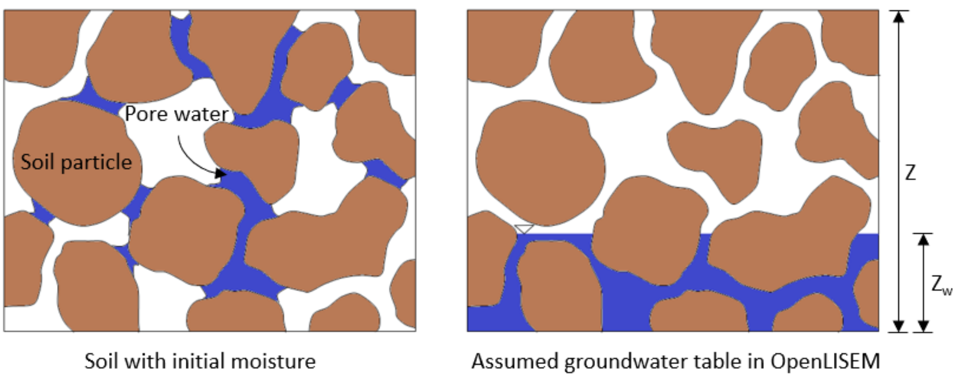

Fig. 3-2: *the initial soil moisture and the assumed groundwater table calculated based on initial soil moisture.*

3.1.4. Model assumptions

The model assumptions for landslide volume simulation can be summarized as the following aspects:

- Assumptions related to slope stability analysis;
- Assumptions related to the iterative method;
- Assumptions related to triggering mechanisms.

The slope stability analysis in OpenLISEM is based on the infinite slope model, thus it is also subjected to the assumptions of the infinite slope model. These assumptions have been discussed in section 2.2.2.1. The failure plane for each pixel is planar and parallel to the ground surface. The forces between pixels are ignored due to the length of the slope is infinitely long compared with the soil depth.

OpenLISEM adopts an iterative method to calculate slope failure. This method assumes that the slope failure is caused by the change of the surrounding slope. In reality, the slope failure is not caused by the change of surrounding slope, but by the change of force propagation through the subsurface.

OpenLISEM assumes that the groundwater level is a function of the initial and residual soil moisture, porosity, and soil depth (equation 3-4). During the rainfall events, the groundwater level will keep the initial groundwater level and not be changed until the wetting front reaches to the groundwater level. Once the wetting front reaches the groundwater level, the groundwater will be supplied by wetting front and the level will be raised. However, in reality, soil can be partially saturated everywhere above the bedrock or above the groundwater level. This assumption results in a completely dry soil above groundwater level, but the partially pore water pressure and saturated pore water pressure are different. This assumption may lead to an underestimation of FoS.

3.1.5. Calibration options

The calibrations of models can improve model behaviors so as to put to use for further prediction. OpenLISEM is very user-friendly for performing calibrations because the model results in-time are displayed in the model and users can monitor the model behaviors during running. The factor of safety map and slope failure map should be monitored when calibrating.

To calibrate the OpenLISEM model, the measured landslide locations and the corresponding landslide volumes are needed. The calibration options in terms of input parameters include soil cohesion, internal friction angle, saturated hydraulic conductivity, initial soil moisture, and soil depth. The calibration options in terms of model internal parameters include the maximum factor of safety (F_i) and resulting factor of safety (F_r) which are mentioned in section 3.1.1.

The calibrations of the models should be based on the sensitivity analysis of parameters and field observations. Some sensitivity analysis and calibrations for OpenLISEM have been done for some areas. De Roo and Jetten (1999) applied OpenLISEM for a catchment in the Netherlands and a catchment in South Africa for soil erosion simulation and concluded that the model is very sensitive to initial soil moisture and saturated hydraulic conductivity. Baartman et al. (2012) simulated soil erosion using OpenLISEM for a catchment in SE Spain. However, these sensitivity analyses and calibrations are performed for soil erosion, none of them is for landslides.

When performing a calibration, it is worthwhile to first analyze the datasets that are used to calibrate the model. OpenLISEM can simulate landslides at the initiation (depletion) areas, as well as the entrainments of the slip pathways. It is better to have information on landslide locations and volumes at initiation areas and the total landslide volumes, which include initiation volumes plus entrainment. Moreover, the model calibration should also take grid size and catchment characteristics into consideration (Jetten et al., 2003).

3.2. Scoops3D

Scoops3D was developed by Reid et al. (2015). It was originally designed to simulate volcanic edifice failures, thus contributing to the understanding of the long-term volcano evolution and the forecasting of the imminent volcanic hazards (Reid et al., 2000, 2010). It utilizes spheres as the potential slip surface and is capable of taking into account a number of soil layers with different properties, several different groundwater inputs (dry, piezometric surface, pore-pressure ratio etc.), and simplified earthquake effect when simulating landslide volumes.

3.2.1. Landslide volume simulation

Scoops3D applies the three-dimensional limit equilibrium method to analyze slope stability. The calculation of FoS can be found in Reid et al. (2015). The use of spheres as predefined potential slip surfaces makes it take into account the three-dimensional characteristics of topography. The steps of Scoops3D to calculate potential landslide volume are:

(1) Search the potential slip surfaces throughout the terrain by using a method called the complete searching method. This method utilizes a considerable number of (millions of) spheres to cut the terrain so as to generate a number of intersections (each intersection corresponds to a trial surface) between those spheres and the terrain. These spatially distributed spheres can be defined by a series of model parameters (will be described in section 3.2.2).

(2) Analyze the stability of each trial surface using two different limit equilibrium methods (the Ordinary method (Fellenius, 1936) and the Bishop's simplified method (Bishop, 1955)). For each intersection, the FoS is uniformly distributed along the trail surface, which means all the pixels within this intersection have the same FoS. Each pixel will probably be analyzed by a number of different trial surfaces until the lowest FoS is found for that pixel.

(3) Find the trial surface with the lowest FoS for each pixel. As each pixel may be cut by many different spheres, the trial surface with lowest FoS (of course should be lower than the landslide cut-off FoS) will be determined as the potential slip surface for that pixel. So the final slip surface for an individual landslide is determined by a combination of many small part of spheres which represent least stability for every pixels.

(4) Generate a new terrain map with all the materials above the potential slip surface removed. Thus the failure height map can be the subtraction between the previous terrain map and the new terrain map. The volume can be calculated using failure height map.

3.2.2. Internal model parameters

Scoops3D use several searching parameters to control the searching process. These parameters may affect the final volume results because they determine if the thorough search of terrain is performed. These searching parameters mainly include volume limits, the horizontal and vertical extent of searching nodes, and the search resolutions. The descriptions of these parameters are shown in Table 3-2. Fig. 3-3 schematically illustrates the meaning of these search parameters from a two-dimensional perspective. Table 3-2 also gives the recommendations of these parameters derived from Reid et al. (2015). These recommendations should be referred coupled with the characteristics of the study area.

3.2.3. Input and output for Scoops3D

Table 3-3 shows the input data required by Scoops3D for performing a landslide simulation. The first column of Table 3-3 indicates the names of model inputs, the second column of Table 3-3 describes how are the input parameters obtained. Scoops3D requires the raster data in ASCII raster grid format (extended by ".asc"). Other data formats should be transformed into ASCII raster format.

Table 3-2: *The definitions of searching parameters for Scoops3D.*

Search parameters		Descriptions
Search-lattice extent	Horizontal search lattice Vertical search lattice	The searching spheres are centered by a number of nodes above the terrain. Each node may emit a number of spheres (the number is determined by the volume limits introduced below). The horizontal and vertical boundaries of these nodes equal to the horizontal and vertical search-lattice extents. The size of the search-lattice cell equals to the pixel size of the Digital Elevation Model (DEM).
Search resolution	Horizontal resolution (m)	The horizontal density of the searching nodes. The minimum unit of horizontal density equals to the pixel size of DEM.
	Vertical resolution (m)	The vertical density of the searching nodes.
	Radius increment (m)	A single node may emit a number of spheres. Radius increment defines the increment between two adjacent spheres.
Volume limit	Minimum (m^3) Maximum (m^3)	This pair of parameters indicates the volume limit of intersected material for each search. If the intersected volume between one sphere and terrain is less than the minimum volume limit, the node will continually emit searching spheres until the volume achieves that goal. If the intersected volume is greater than the maximum volume limit for the first time, the search based on that node will be stopped and move to the next node. Notably, the volume limit is not the limitation of the final potential landslide volume.
Search parameters		**Recommendations**
Search-lattice extent	Horizontal search lattice	Initially, it is recommended that the horizontal extent of the search lattice is an extent equal to that of the DEM. If there is the case with steep slopes near a DEM boundary, the horizontal extent of search lattice should be beyond the DEM limits.
	Horizontal search lattice	The lower vertical limit to the search lattice is recommended to be slighter greater than the lowest DEM elevation. The upper vertical limit to the search lattice is initially recommended to the half of the relief above the lowest point in the topography.
Search resolution (m)	Horizontal resolution (m)	If the runtime and memory requirement is not a limitation, use the horizontal spacing equal to the DEM cell size. If excessive runtime is an issue, perhaps use 4 times the DEM cell size.
	Vertical resolution (m)	If the runtime and memory requirement is not a limitation, use the horizontal spacing equal to the DEM cell size. If excessive runtime is an issue, perhaps use 4 times the DEM cell size.
	Radius increment (m)	If the runtime and memory requirement is not a limitation, use the radius increment equal to the cell size. Decreasing radius increment is more effective to increase vertical resolution than increasing the vertical resolution.
Volume limit	Minimum (m^3) Maximum (m^3)	An unrestrictive size range is recommended to find the ultimate minimum FoS for each DEM cell. If a restrictive range is selected, we may miss the critical slip surface which may be outside of this range.

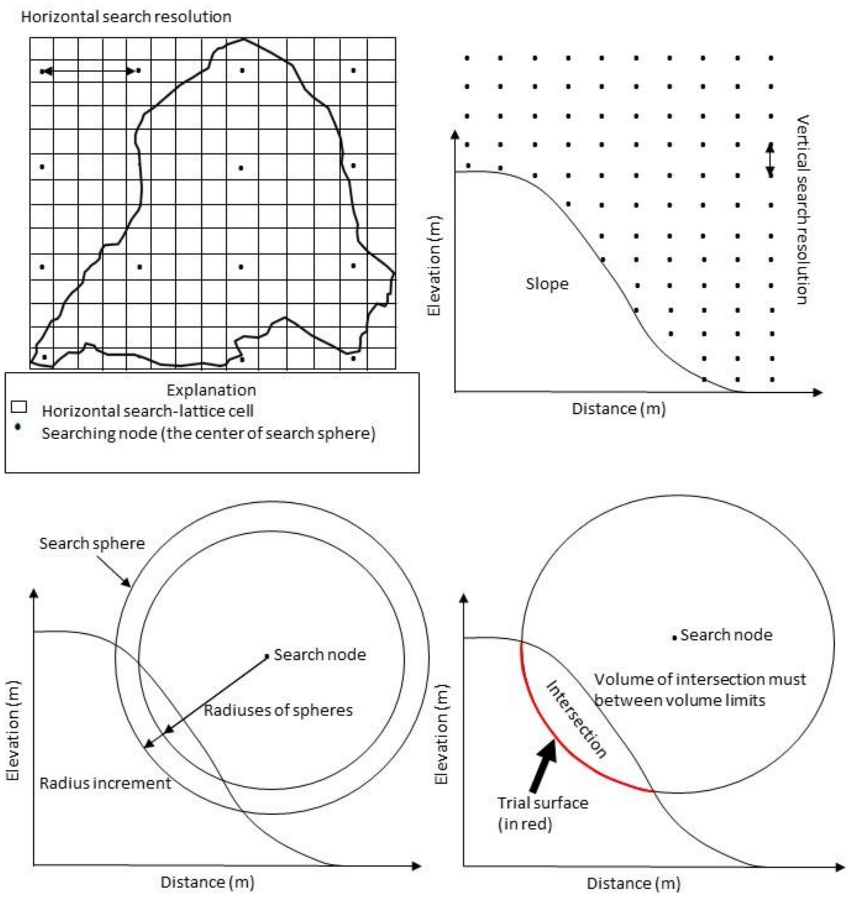

Fig. 3-3: *The definition of the searching parameters in Scoops3D.*

Table 3-3: *The input data for Scoops3D.*

Input data	Descriptions
Digital Elevation Model (DEM)	DEM represents the local topography. The ways to obtain DEM are introduced in Table 3-1.
Underground soil layers	A number of soil layers are defined by a set of raster maps of elevations of layer bottoms. The geometry of these soil layers may be irregular. The soil layers may reach the terrain surface or disappear in depth. The ways to obtain the underground conditions are boreholes, geotechnical techniques, etc.
Soil parameters (c, φ, γ)	Each soil layer has its own soil properties. The ways to obtain the soil parameters are introduced in Table 3-1.
Pore-water pressure inputs	Scoops3D provides three different ways to include the pore water pressures on slope stability. (1) No groundwater pressure. Dry underground condition. (2) Pore pressure ratio, r_u. r_u is defined as the ratio of pore pressure to vertical stress at a point. Each soil layer have its own r_u. (3) Piezometric surface. Piezometric surface represents the groundwater surface with vertically hydrostatic heads.
Earthquake loading	Scoops3D includes the horizontal seismic loading using a pseudo-acceleration coefficient k_{eq} (-). In the calculation of FoS, the k_{eq} multiplied by soil weight represents the horizontal seismic force.

3.2.4. Landslide triggering mechanisms in Scoops3D

Scoops3D includes two different triggering factors, pore water pressure caused by groundwater and earthquake loading. As mentioned in Table 3-3, three different options can be selected to simulate the groundwater conditions, and the dry condition is the simplest one.

If the pore pressure ratio option is selected, the pore water pressure can be calculated using the equation:

$$\mathrm{u} = r_u \cdot W \qquad [3\text{-}5]$$

Where u (kPa) is the pore water pressure; γ_u (m^{-2}) is the pore water pressure ratio; W (kN) is the total soil weight of the overlying material. Pore-water pressure ratio is assumed to be the same within one material layer, so the water pressure linearly increases from ground surface to the material layer bottom.

If the piezometric surface option is selected, the pore water pressure can be calculated using the equation:

$$\mathrm{u} = \mathrm{Z}' \cdot \gamma_w \qquad [3\text{-}6]$$

Where u (kPa) is the pore water pressure; Z' (m) is the depth of piezometric surface; γ_w (kN/m^3) is the water unit weight. This option is more realistic than pore-water pressure ratio option, but the accurate piezometric surface can be hard to acquire.

The seismic loading is restricted to a horizontal force. It equals to k_{eq} multiplied by total soil weight.

3.2.5. Model assumptions

The main model assumption for landslide volume simulation in Scoops3D is about slope stability analysis. Scoops3D adopts two different limit equilibrium methods (the Ordinary method (Fellenius, 1936) and the Bishop's simplified method (Bishop, 1955)) to analyze slope stability. Both methods ignore inter-column forces. The assumptions about limit equilibrium methods have been described in section 2.2.2.

3.2.6. Calibration options

Scoops3D can be calibrated by modifying the soil cohesion, internal friction angle, and soil bulk density. The information on locations and area of the historical landslides can be used to calibrate and validate the model. But the users cannot monitor the model behavior during the running. The results can only be seen until the model finish running, which is not convenient for model calibrations.

4. METHODOLOGY

The comparisons between OpenLISEM and Scoops3D should be based on the datasets where the soil thickness and soil properties are sufficiently known spatially. At the beginning, we tried to find such datasets, but we could not find a suitable dataset. As it is very difficult to have such a dataset, we decided to apply the comparison in a hypothetical environment, representing a volcanic environment. A hypothetical and volcanic environment here means the geotechnical and hydrological parameters are from literature values related to the volcanic environment, and the soil thickness is assumed. The detailed information about this hypothetical environment will be described in section 4.1. For the volcanic environment, three scenarios were considered.

This chapter consists of six sections. In the first, the reasons for using hypothetical datasets for the volcanic environment of the analysis are described. Then the characteristics of the volcanic environment and the scenario designs are introduced. Next, the preparation of input data for each simulation is described. After that, the model set up for OpenLISEM and Scoops3D is illustrated. Fourthly, the methods for model outputs processing and volume calculation are described. The methods for model outputs processing and volume calculation are described as well. Lastly, the comparison criteria are developed and applied to the results.

4.1. The use of hypothetical datasets in this work

4.1.1. Why we use Hypothetical datasets?

The reasons for choosing hypothetical synthetic scenarios are:

- The lack of input data in the original planned study area near Yingxiu, Sichuan province, China. Reliable input data, such as geotechnical and hydrological parameters should be determined by laboratory tests with enough soil samples with good spatial distribution, which are not available. The important input data, soil depth data is unknown. On the other hand, for heterogeneous areas such as the Yingxiu area, even if a good soil sampling and accurate tests are available, we still cannot ensure the reliability and the representability of the test results for that area because of a lot of uncertainties.
- A high resolution DEM is needed to perform a good landslide volume simulation because the resolutions of DEMs affects landslide volumes simulated by models (Reid et al., 2015). Coarse resolutions tend to give relatively big volumes. In order to minimize the effect of coarse resolution, DEM with relatively high resolution (i.e. 5m) should be guaranteed (depends on the potential sizes of the landslides).

4.1.2. Hypothetical datasets for the volcanic environment?

We selected a volcanic environment because of its relative homogeneity in terms of geotechnical and hydrological properties, which can theoretically be well represented by literature values. The geotechnical and hydrological parameters are critical for these two models in terms of volume simulation. This homogeneity of volcanic environment reduces the effects of many uncertainties mentioned in section 2.2.2.4, and simplify the model inputs a lot. Although we cannot validate our models using hypothetical datasets, we can still compare their behavior.

The volcanic environment used in the analysis presented here is based on hypothetical but controlled datasets. The controlled synthetic dataset has the following characteristics:

- Instead of using a DEM from a volcanic region, a DEM of a small catchment in the Yingxiu area, China was selected. The catchment covers about 4.5 km^2, with the elevation ranging from 1033 to 2144m (Fig. 4-1). The horizontal resolution of this DEM is 2m.
- The soil geotechnical and hydrological parameters are derived from the literature values. The soil cohesion, internal friction angle, and saturated hydraulic conductivity (Ksat) etc. are controlled within certain ranges to represent the volcanic environment.
- The soil thickness inputs are assumed based on a given hypothesis. For the first set of simulations, we assume that our catchment is near to a newly erupted volcano and that the eruption led to an ash deposition with 10m thickness. And for the second set of simulations, a critical soil thickness was calculated by subtracting failure depth in the first set of simulations from the 10m soil thickness. More information on critical soil thickness will be explained in section 4.3.2.
- The input rainfall events that are used as landslide triggering factors are artificial events created from rainfall statistics in a volcanic region (Saint Lucia, a small volcanic island country located at the eastern Caribbean Sea).

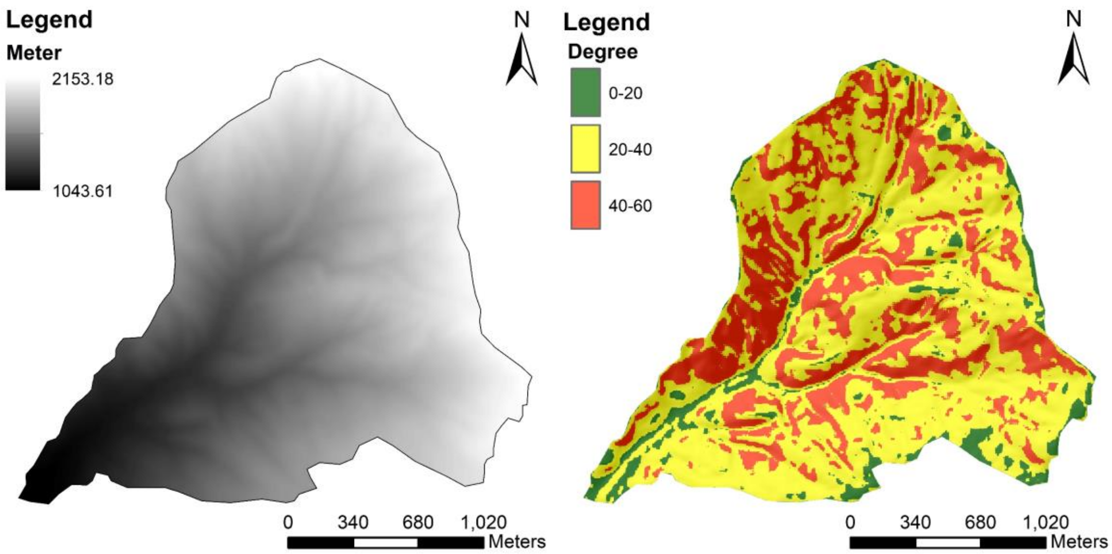

***Fig. 4-1**: Digital Elevation Model (left) and slope map (right) used in this study.*

4.2. Environment Description and Scenario Design

4.2.1. Environment Description

Volcanic eruptions can be generally categorized into two types: effusive eruptions and explosive eruptions, depending on the characteristics of the erupting magma, and the size and rate of magma emitting. The former type of eruption indicates basaltic magmas with low viscosity and (or) low gas content steadily reaching the surface, mainly resulting in different types of lava flows. The latter type of eruption indicates andesitic or rhyolitic magmas with high viscosity and (or) high gas content violently fragmenting into the air, resulting in volcanic ash cloud and pyroclastic flows, etc. (Degruyter et al., 2012). Compared with stream-like lava flows, volcanic ash fall is more uniform in terms of coverage and mechanical properties(Bilotta et al., 2005; Buytaert et al., 2007; Cecconi et al., 2010), so the volcanic ash fall caused by explosive eruptions were assumed in this study.

4.2.2. Scenario Design

In this section, we developed three different scenarios to perform our simulations. The design of scenarios begins with an understanding of the depositions of volcanic ashes and the erosion of volcanic ash soils (Fig. 4-2). After a major eruption, volcanic ash rains down and uniformly covers the whole terrain regardless of the terrain steepness (Fig. 4-2 (a)). However, with such a thick soil layer uniformly lying on top of the terrain, there might be a lot of instabilities caused by gravity even there is no interference from triggering factors. Thus the scenario 1 was derived: dry condition, with uniform soil thickness of 10 meters (UST).

In order to analyze the effect of rainfall or different groundwater levels on landslide volumes, a reduced soil thickness is calculated, corresponding to limit equilibrium conditions (FoS slightly higher than 1). The resultant soil thickness is called critical soil thickness (CST; Fig. 4-2(b)).

Based on the critical soil thickness (CST) calculated in scenario 1, the other two scenarios are developed. Scenario 2 is a rainfall event-based scenario, and the effect of wetting front on slope stability and potential landslide volume was evaluated in this scenario (Fig. 4-2 (c)). Four artificial rainfall scenarios, which will be described in section 4.3.3.1, were used in this scenario. There is no connection between the wetting front and groundwater level, and the initial soil moisture equals to residual soil moisture.

Scenario 3 is not an event-based scenario but a long-term analysis. The soil is initially assumed to be saturated due to a major rainfall event. As the terrain is too steep to keep the groundwater unchanged, the groundwater will flow from upslopes to downslopes. A groundwater flow model, developed in a GIS software, PCRaster, was used to simulate groundwater level variations. The outputs of this model are groundwater levels at different time steps. The further descriptions of this groundwater flow model can be found in section 4.3.3.2. In this scenario, we selected groundwater levels which correspond to the period of 10 and 20 days after the saturation to perform landslide simulation (Fig. 4-2(d)). All the soil parameters used in these three scenarios are the same. Table 4-1 summarizes these three scenarios.

Table 4-1: *The summary of three scenarios.*

Scenarios	Soil thickness	Soil parameters	Water-related landslide triggering
Scenario 1	10m uniform thickness	Homogeneous	Dry condition
Scenario 2	Critical soil thickness	Homogeneous	Wetting front
Scenario 3	Critical soil thickness	Homogeneous	Pore water pressure caused by groundwater

For all three scenarios the following assumptions were made:

(1) The distributions of the deposited ash particle size and thickness were assumed to be uniform in the catchment. In reality, the spatial Particle Size Distribution (PSD) and ash thickness are correlated with ash travel distance: coarser ashes (blocks or bombs with diameter D greater than 64 mm) are normally existing at shorter distances, middle size ashes (lapilli with D between 2mm to 64 mm) are also not far away from volcano, while the finer ashes (with D less than 2 mm) are existing at larger distances (Herrera and Lizcano, 2007). So there are reductions in the PSD and thickness with ash travel distance (Fig. 4-2). In this study, we assume that the catchment is located in the middle of the ash range, and is small enough for the ash height to be uniform everywhere.

(2) A thickness of 10m ash is considered in scenario 1. This assumption is based on the hypothesis of a catastrophic volcanic eruption that resulted in a very thick deposition of ash, in such a way that its availability, for the stability analysis, can be taken as unlimited.

4.3. Input Data Preparation

The input data for OpenLISEM can be mainly divided into five types: DEM, geotechnical parameters (soil cohesion, soil internal friction angle, and soil bulk density), hydrological parameters (saturated hydraulic conductivity, soil porosity, residual soil moisture, and initial soil moisture), soil thickness, and rainfall (with

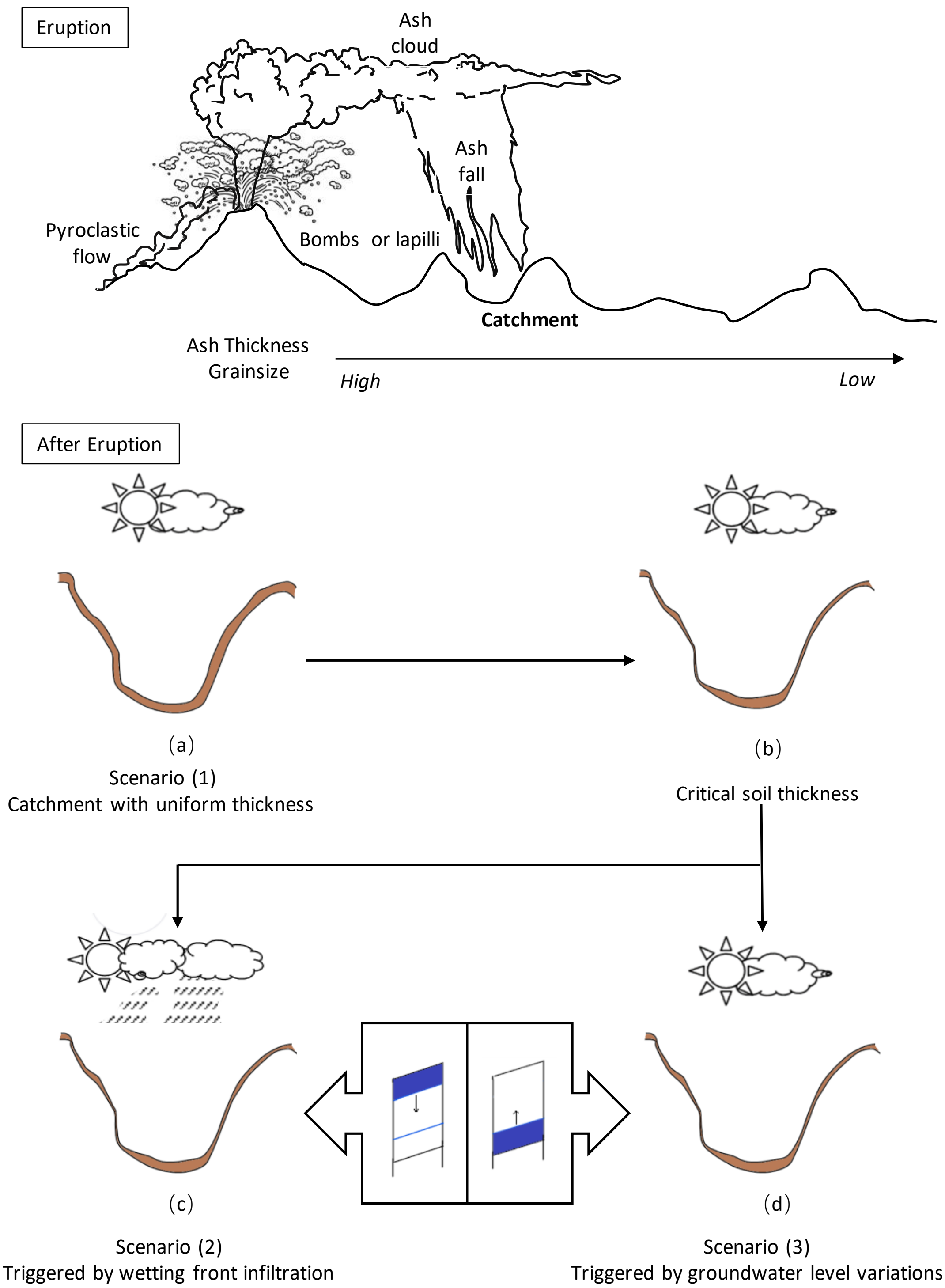

Fig. 4-2: *The illustration of volcanic environment and the corresponding three scenarios.*

time step of minutes). The input data for Scoops3D can be mainly divided into three types, DEM, geotechnical parameters, soil thickness, and different soil layers (optional). This section consists of four sub sections, illustrating how the input data was collected or determined. The sub-section 4.3.1 shows the determination of geotechnical and hydrological parameters; the sub-section 4.3.2 shows the determination of the critical soil thickness (CST) for scenario 2 and 3; the sub-section 4.3.3 describes the inputs of the triggering factors for scenario 2 and 3; the sub-section 4.3.4 describes the data conversion and processing environments for OpenLISEM and Scoops3D.

4.3.1. Geotechnical and Hydrological Parameters

The geotechnical and part of hydrological parameters were calculated based on literature values (Table 4-2). Some hydrological parameters could not be found in literature, so a model named Soil Water Characteristics was applied to calculate the hydrological parameters. This empirical model is developed by Saxton and Rawls (2006), who investigated statistical relationships between soil water characteristics and soil texture and organic matter (OM) using the USDA soil database. Through this model, hydrological parameters can be estimated using grain size distribution (GSD) and OM as input.

A number of literature values about geotechnical and hydrological properties were collected (Table 4-2), and the most suitable ones for the analysis were explored. Uncertainties in the definition of the geotechnical parameters are, amongst others, related to:

a) the soil properties are related to their parent material, their formation environments and mechanisms (Cecconi et al., 2010). Thus the properties of volcanic ash soils can vary a lot in different volcanoes and factors such as eruption type and history, degree of saturation, compaction, cementation status, and tillage history, and
b) The measured values also depend on the test methods. For example, the soil cohesion and internal friction angles can vary a lot when using two different methods: direct shear test and triaxial shear test.

The input parameters used in this study were calculated and shown in Table 4-3. Considering that the analysis assumes fresh volcanic ashes from a recently erupted volcano, for the soil cohesion, the approximate mean value of lower ranges, 8kPa was taken; the mean value of lower ranges, 32° and 1200kg/m^3 as internal friction angle and bulk density; and the mean value of Ksat and porosity, 19mm/h and 0.55(-) as input porosity. The saturated soil bulk density is 1500kg/m^3. The residual soil moisture is derived from Pagano et al. (2010).

4.3.2. Soil thickness

Scenario 1 uses the homogeneous 10m soil thickness. Scenario 2 and 3 use the critical soil thickness (CST). To calculate the CST, the critical failure depth in scenario 1 was firstly calculated using OpenLISEM and Scoosp3D. The CST is derived by subtracting the simulated failure depth from the 10m soil thickness. Ideally, with the CST, there should be no slope failure in dry condition. To investigate which model is capable of deriving CST, a cross- and self-checks of slope stability using new soil thickness were performed after assuming the CST, for scenario 1:

- Self-check: Use failure depth simulated by OpenLISEM (or Scoops3D) to calculate new soil depth, and use new calculated soil depth as input to analyze slope stability using OpenLISEM (or Scoops3D).
- Cross-check: Use failure depth simulated by OpenLISEM (or Scoops3D) to calculate new soil depth, and use new calculated soil depth as input to analyze slope stability using Scoops3D (or OpenLISEM), respectively.

The selected CST to apply for scenario 2 and 3 is chosen at the calculated CST using OpenLISEM or Scoops3D that results in the minimum number of slope instabilities for self- and cross-checks.

4.3.3. Triggering factors

4.3.3.1. Rainfall and Wetting Front

In scenario 2, rainfall results in a wetting front infiltration. Notably, only OpenLISEM integrates the rainfall infiltration into the landslide simulation, while Scoops3D cannot simulate that. To overcome this, we used the maximum depth of wetting front simulated by OpenLISEM during the rainfall as another soil layer input for Scoops3D. This infiltrated layer is saturated and considered as the first soil layer in Scoosp3D.

Table 4-2: *The physical properties of volcanic ash soils from literature.*

Description			c	φ	ρ	Grain size distribution			Ksat	Porosity	Ref.
Region	Soil		(kPa)	(°)	(kg/m³)	Clay (%)	Silt (%)	Sand (%)	(mm/h)	(-)	
San Salvador,	Pyroclastic		10	36	1300-1500	-	-	-	-	44-54	[1]
Salvador	(Tierra Blanca)		-	34	1391	0	45	55	**11.8**	46.1	[2]
			-	-	1302	0	3	97	**11.8**	51.7	[3]
			6	35	1498	18	40.5	41.5	**9.6**	44	[4]
			5	30	1370	24	28	48	**7**	53	
			-	-	1080-1290	-	-	-	-	47.5-62.3	[5]
			-	-	1370	0	10	90	**19.65**	49.2	[6]
Campania,	Pyroclastic		0-5	39	-	5	32-58	37-63	36	70	[7]
Southern Italy			4.7	32	730-1310	-	-	-	36	58	[8]
			1.5-5	30-41	8880-1659	-	-	-	20.88-72	53-74	[9]
			0-34	36-45	800-1300	-	-	-	0.36-36	-	[10]
			0-11	31-38	1400	-	-	-	21.6	50	[11]
Manizales,	Pyroclastic	Organic soil	15.6-42.2	24.8-36.6	1290	-	-	-	34.1	59	[12]
Colombia		Silty sand	0-33.6	29-39	1550	-	-	-	38.5	54	
		Sandy silt	17.7-53.9	22.4-29	1490	-	-	-	7	65	
		Saprolite	17.8-22.7	25.3-30	1850	-	-	-	14.7	50	
Chinandega, Nicaragua	Vitric Andosols		-	-	860-1410	6-36	21-49	21-73	-	-	[13]
Osorno,	Andosols		18.4-24.2	38-42	1000	39.1	50.9	10	-	-	[14]
Southern Chile	(Typic Hapludand)		5-32.3	35-36	800	32.9	55.0	12.1	-	-	

References: [1] Bommer et al., 2002; [2] Berdousis, 2001; [3] Mavrommati, 2000; [4] Amaya Dubón and Hayem Brevé, 2000; [5] Guzmán Urbina and Melara 1996; [6] Rolo 1998; [7] Pagano et al., 2010; [8] Cascini et al., 2003; [9] Bilotta et al., 2005; [10] Frattini et al., 2004 [11] Damiano et al., 2012) [12] Terlien, 1997; [13] Joergensen and Castillo, 2001; [14] Seguel and Horn, 2005. The values of Ksat in bold were calculated using Soil Water Characteristics Model developed by Saxton and Rawls (2006). The symbol "-" refers to no such data in the literature.

Table4-3: *The input parameters for OpenLISEM and Scoops3D. Where c' refers to effective cohesion; φ' to effective internal friction angle; ρ to soil bulk density; Z to soil thickness; UST to uniform soil thickness; CST to critical soil thickness; Ksat to saturated hydraulic conductivity; θi, θr, and θs to initial, residual and saturated soil moistures. Scoops3D only needs input parameters in bold.*

Parameters		Scenarios		
		(1)	(2)	(3)
Geotechnical Parameters	**c' (kPa)**	8	8	8
	φ' (°)	32	32	32
	ρ (kg/m³)	1200	Dry:1200 Wet:1500	Dry:1200 Wet:1500
	Z (m)	UST	CST	CST
Hydrological Parameters	Ksat(mm/h)	19	19	19
	θi (-)	0.13	0.13	0.55
	θr (-)	0.13	0.13	0.13
	θs (-)	0.55	0.55	0.55

Four rainfall scenarios are used in scenario 2, namely scenario a, b, c, and d. From scenario a to d, the magnitudes are increasing. These four rainfall scenarios are artificial events derived from rainfall statistics on the island of Saint Lucia. The rainfall curve and the scenario characteristics are shown in Fig. 4-3.

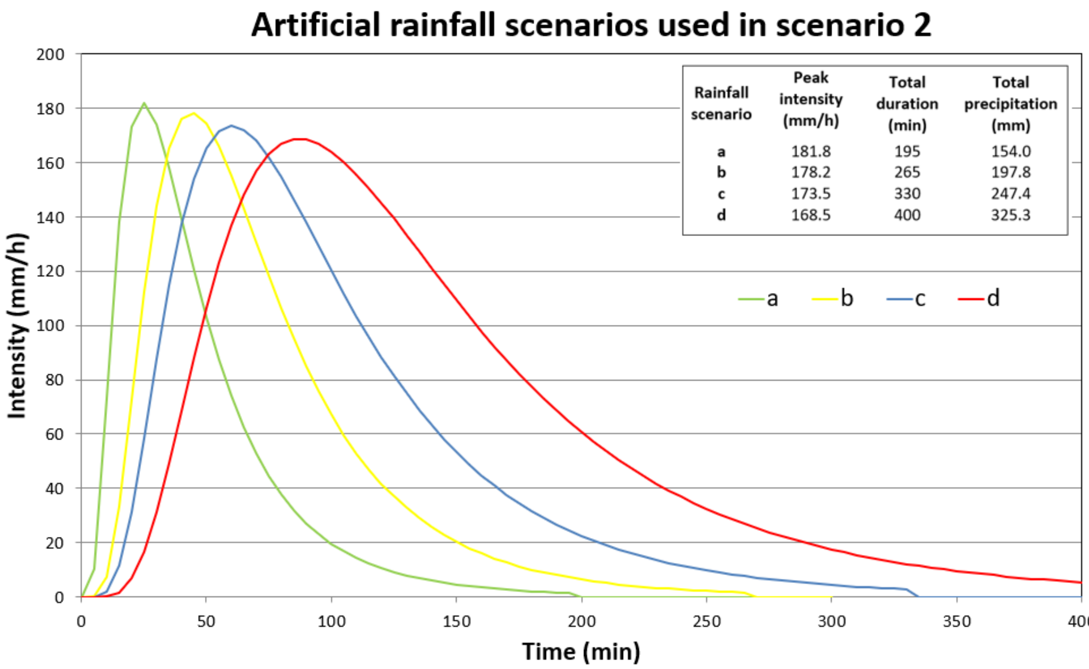

Fig. 4-3: *Designed rainfall events in Sant Lucia with their event characteristics.*

4.3.3.2. Groundwater Simulation

In scenario 3, landslides are triggered by pore water pressure due to groundwater. Neither OpenLISEM nor Scoops3D integrates the evolution of groundwater level inside the soil. Thus in our study, a simple groundwater flow model, developed in a GIS software, PCRaster, was used to simulate groundwater level variations. The inputs of this model consist of a DEM, soil thickness, soil porosity, initial soil moisture, residual soil moisture, and saturated hydraulic conductivity (Ksat). The outputs of this model are groundwater levels at different time steps. The script (Van den Bout, 2017) is detailed in Annex A. In this scenario, we took groundwater levels at three-time steps: the first one is with saturated soil moisture, the second one is 10 days after saturation, and the last one is 20 days after saturation. The resulting groundwater levels were then introduced as inputs at OpenLISEM and Scoops3D.

4.3.4. Data Conversion and Processing Environments

For OpenLISEM, the data processing and calculation were done in PCRaster with the raster data format of ".map". The data with other raster formats should be transformed to ".map", which can be done in Q-GIS using the raster data conversion tool (Convert Format). The conversion from PCRaster maps to GeoTiff maps needs a software named Geospatial Data Abstraction Library (GDAL; www.gdal.org). For Scoops3D, the pre-processing of input data was done in ArcMap. The required raster data format is ".asc", the conversions from other raster formats to ".asc" were done in ArcMap using data conversion tools (from raster to ASCII).

4.4. The Model Set Up

As mentioned and described in chapter 3, there are many internal model parameters that may influence the simulated landslide volumes. OpenLISEM has two major model parameters: the maximum factor of safety (F_i) and the resulting factor of safety (F_r). Scoops3D has many model parameters (described in section 3.2.2) that are used to define search process for unstable slopes. Reid et al. (2015) provided some recommendations for those parameters, but the recommendations concerning about search volume limit are not specific. They only mentioned that unrestricted volume limits can ensure a thorough search of the terrain.

In this study, the model parameters F_r for OpenLISEM, and volume limit for Scoops3D are determined through sensitivity analysis. Four different F_r values, 1.1, 1.2, 1.3, and 1.4 were tested for OpenLISEM in scenario 1. Three different volume ranges, 1-5000 m^3, 1-50000 m^3, and 1-100000 m^3 were tested for Scoops3D in scenario 1. Based on sensitivity analysis, the model parameters corresponding to the most overlapped landslide distributions between OpenLISEM and Scoops3D were determined as Fr for OpenLISEM and volume limit for Scoosp3D. The other model parameters of Scoops3D were determined based on the recommendations in Table 3-2 coupled with the catchment characteristics. Table 4-4 shows the determined model parameters except for volume limit.

Table 4-4: *The search parameters for Scoops3D.*

Search -lattice extent (m)		Search resolution (m)		
Horizontal	Vertical	Horizontal	Vertical	Radius increment
DEM extent	1043-4514	8	8	2

4.5. Calculation of Landslide Volume

The outputs of OpenLISEM and Scoops3D are failure depth maps (in raster format) indicating failure height for each raster cell and FoS maps (in raster format) indicating the slope stability for each DEM raster cell. The steps from model outputs to landslide volume include: 1) individual landslide polygon depicting, and 2) individual landslide volume calculation. Both steps were done in ArcMap.

4.5.1. The generation of landslide polygons

By using failure height map as a based map and FoS map as a reference map, polygons indicating the locations of the individual landslides were manually created. A hill shade map was also used to identify mountain ridges so that the incorrect merge of two landslides can be avoided. Fig. 4-4 gives an example where FoS maps (Fig. 4-4 (a) and (b)) and failure height maps (Fig. 4-4 (c) and (d)) were used to depict landslide polygons (Fig. 4-4 (e) and (f)). This example is from scenario 1 with 10m soil thickness. The cut-off FoS was determined as 1, which means areas with FoS less than 1 were regarded as unstable areas. The cut-off slope value for slope failure height was determined as 0.5m to avoid the generation of the very tiny landslide (i.e. at centimeter scale). From the landslide hazard perspective, we considered that landslide with depth less than 0.5m cannot cause loss.

In Fig. 4-4, the failure height maps were used to distinguish individual landslides. The adjacent pixel cells which are failed were regarded as one group and outlined using polygons. The FoS maps were used to ensure all failed pixel cells are included. Because on the edge of the groups, failure height may be not so visible, the FoS, which clearly indicate all the failed pixel cells, can be used to determine the group boundaries.

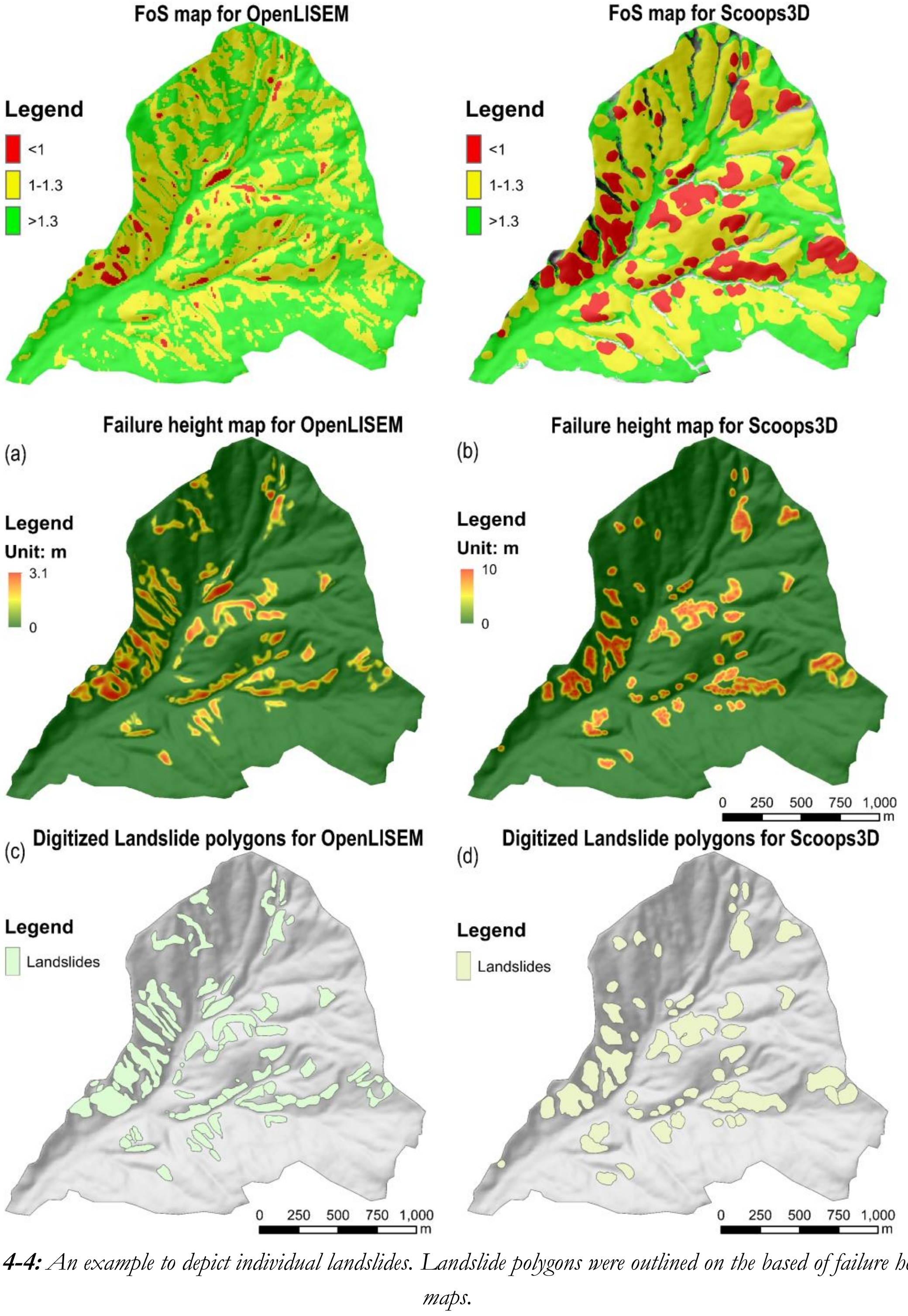

Fig. 4-4: *An example to depict individual landslides. Landslide polygons were outlined on the based of failure height maps.*

4.5.2. Landslide volume calculation

After depicting individual landslide polygons, the volume of each landslide was calculated using the zonal statistics tool in ArcMap. The equation to calculate volume is:

$$V = R^2 \sum_{i=0}^{n} H_i \qquad [4\text{-}1]$$

With V (m^3) is the volume of the individual landslide; R (m) the cell size; H_i (m) the failure height of the unstable cell i; n the number of unstable cells in this group.

4.6. The Model Comparison

The comparisons within the same model and between two different models were performed. Particularly, for each comparison, we concern about the following aspects:

(1) Number: the total number of landslides that the model predicted;

(2) Location: the spatial distribution of potential failures (including overlapping degree);

(3) Volume: the maximum and minimum volume predicted by OpenLISEM and Scoops3D; the volume difference between two models at the same location; the size distribution of potential failures;

(4) The area-volume relationship of predicted landslides.

To investigate the overlap degree between landslide polygons predicted by OpenLISEM and Scoops3D, a method proposed by Carrara et al. (1992) was adopted and the match index, M, was computed. The basic principle of this method is shown in Fig. 4-5. High M values indicate high-level overlap of landslide spatial distributions.

Fig. 4-6 Summarizes all the comparisons. The single arrow lines indicate the comparisons were performed within one model between different scenarios. The double arrow lines indicate the comparisons were performed between different models for the same scenario.

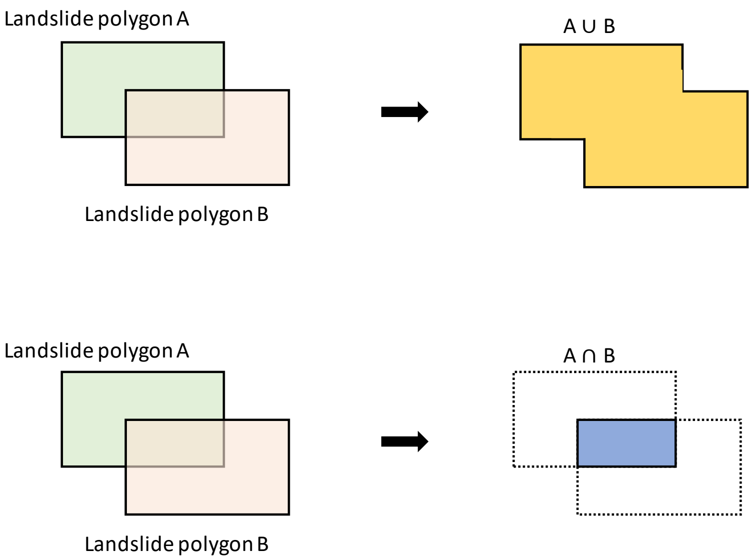

$$M = 1 - \frac{(A_1 \cup A_2) - (A_1 \cap A_2)}{(A_1 \cup A_2)}, \quad (0 \le M \le 1)$$

Fig. 4-5: *The method to calculate match index M.*

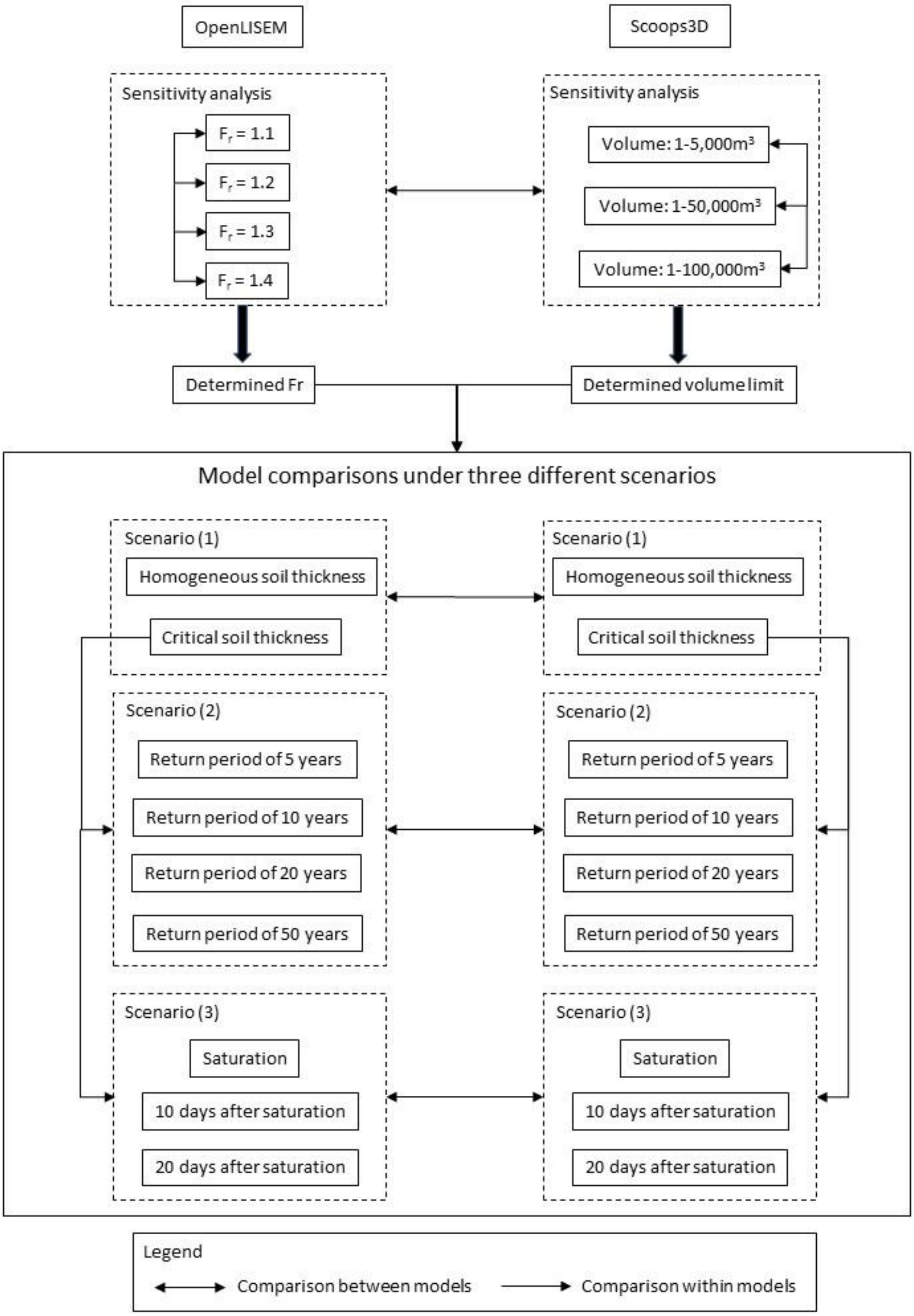

Fig. 4-6: *The sensitivity analysis of OpenLISEM and Scoops3D and comparisons within and between two models.*

5. RESULT AND ANALYSIS

This chapter shows all the results from OpenLISEM and Scoops3D. Section 5.1 describes the determination of the internal model parameters for OpenLISEM and Scoops3D, section 5.2 presents the determination of critical soil thickness, and section 5.3 compares the simulated volumes of the two models under three different scenarios.

5.1. The determination of internal model parameters

5.1.1. The sensitivity analysis on internal model parameters for OpenLISEM

Fig. 5-1 (a) shows the landslides simulated by OpenLISEM using four different resulting FoS (F_r) values, 1.1, 1.2, 1.3, and 1.4 in dry condition with 10m soil thickness. Fig. 5-1 (b) shows that all these four cases have the same initiating FoS (F_i). When F_r equals to 1.1, the failures begin at locations with FoS less than 1, and the failure end up with the FoS equal to 1.1. The resultant failures of F_r =1.1 tend to be less and smaller than those with the bigger F_r. The failures initially occurred at locations where FoS less than 1, however some locations with FoS less than 1 do not indicate any slope failure because the failure depths of those areas are less than 0.5m, which are not considered as slope failures in this study.

When F_r equal to 1.2, more landslides are produced. Although the landslides are initiated at the same location as was the case with Fr =1.1, the landslide areas are much bigger. This is because in the iterative failure process, the initial small failures changed the local terrain, leading to the subsequent failures of the surrounding pixels. Such influence can be downslope or upslope. In some places, some small separate failures are joined together, forming integral landslides.

When F_r values increased to 1.3 and 1.4, many landslides occurred at new locations, and the previous landslides are gradually enclosed by the bigger landslides. Compared with the initiating FoS map (Fig. 5-1 (b)), it is obvious that the originally stable areas (with FoS greater than 1) are significantly affected by the iterative failures, leading to an extensive failure distribution for the whole terrain.

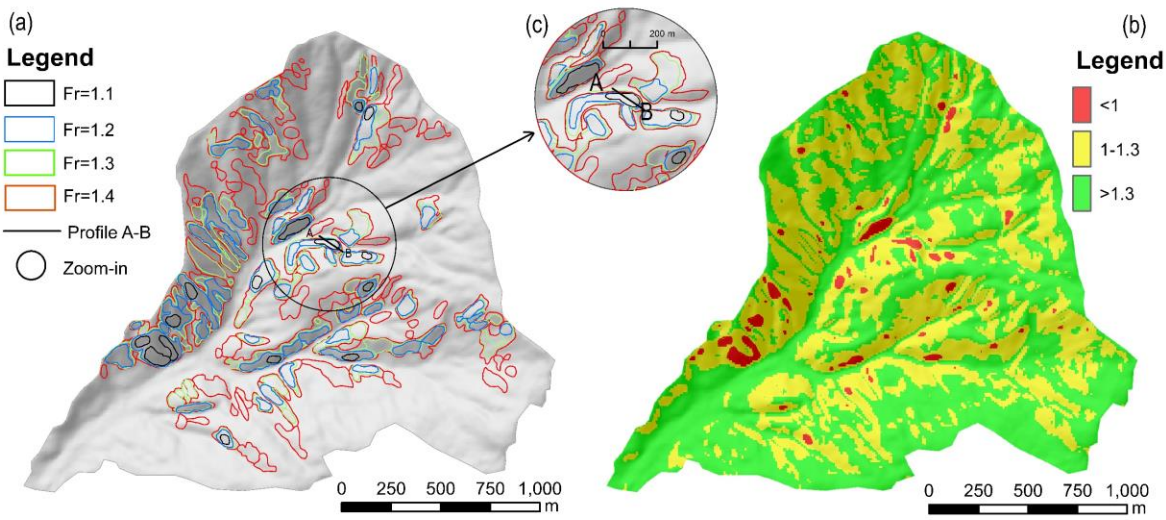

Fig. 5-1: *The landslides and the corresponding FoS map simulated by OpenLISEM. (a) shows four different landslide distributions in corresponding with four different F_r values (1.1, 1.2 , 1.3, and 1.4); (b) shows the FoS map for these four cases; (c) shows a zoom-in window for the middle part of map (a), thick black line A-B indicates a profile location which will explain in the following part.*

Table 5-1 shows the statistics of the simulated landslides with four different F_r values. Compared with the small F_r values, the bigger F_r values not only tend to produce larger landslide areas but also produce larger landslide volumes. From this table, it is found that only 1.3% of the total catchment area is affected by landslides when F_r=1.1, whereas 28.5% of the total area is affected by landslides when F_r=1.4. The average landslide volumes can be 10 ten times bigger when F_r increases from 1.1 to 1.4.

Table 5-1: *Summary of simulated landslides with four different F_r values.*

F_r	Total number of landslides	Maximum landslide volume (m^3)	Minimum landslide volume (m^3)	Total landslide volume (m^3)	Total landslide area (m^2)	Percentage of the affected area (%)	Average landslide area (m^2)	Average landslide volume (m^3)
1.1	15	4856	451	24989	47096	1.3	3140	1666
1.2	54	36521	583	268766	331576	9.4	6140	4977
1.3	75	70970	151	860136	577592	16.3	7701	11469
1.4	109	102683	209	1943451	1009060	28. 5	9257	17830

Fig. 5-2 shows a profile A-B indicated in Fig. 5-1 (a) and (c). It has been found that from F_r=1.1 to F_r =1.4, the failures become deeper and wider. This can be explained by the iterative failure process. When an initially unstable raster cell has been detected, the failure depth has to be removed to reach a stable status. When calculating failure depth in dry condition, the equation 3-1 can be simplified and transformed as:

$$Z = \frac{c'}{\Upsilon(FoS \cdot \, sin\alpha \, cos\alpha \; - \; cos^2\alpha \, sin\alpha)} \qquad [5\text{-}1]$$

Where c' (kPa) is the effective cohesion, z (m) the soil depth, γ(kN/m^3) the soil unit weight, α (°) the slope angle, φ (°) the internal friction angle. In equation 5-1, the soil depth z is inversely proportional to FoS, and the failure depth equal to 10 minus soil depth z. Thus the failure depth is in proportional to FoS. Using 1.1, 1.2, 1.3, and 1.4 to substitute the FoS in equation 5-1, it can be found that larger F_r leads to deeper failures. And the more failure depths that are removed from unstable cells, the steeper slope of surrounding cells can result in, leading to a wider propagation of slope instabilities.

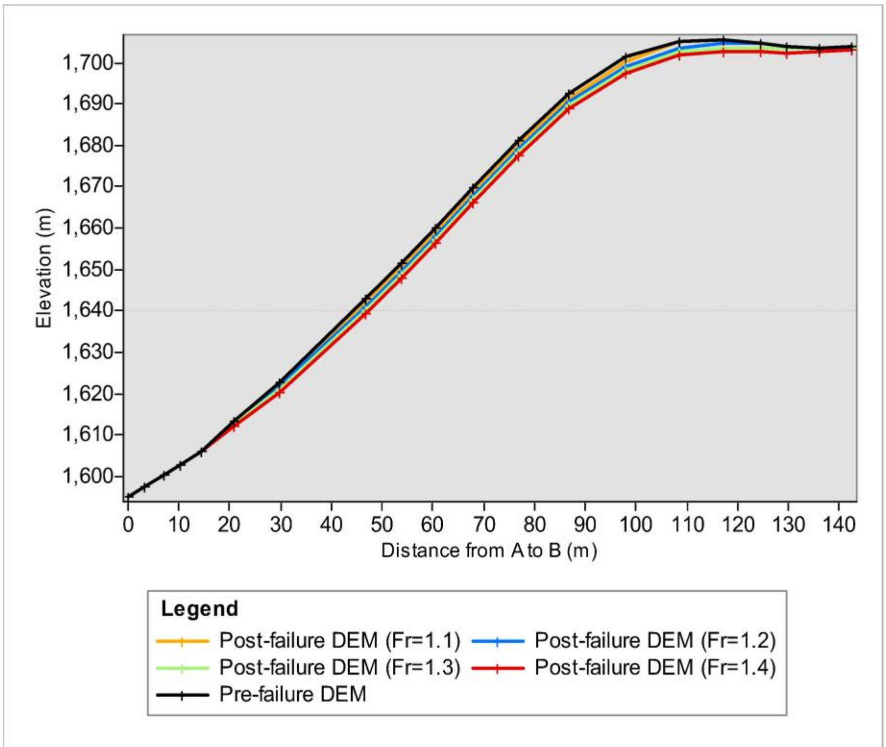

Fig. 5-2: *Profile A-B indicating a location marked with black thick line in Fig. 5-1 (c).*

5.1.2. The sensitivity analysis on internal model parameters for Scoops3D

Fig. 5-3 shows the landslide distribution maps (a1, b1, and c1) and the corresponding FoS maps (a2, b2, and c2) simulated by Scoops3D with three different volume limits, 1-5000, 1-50000, and 1-100000m^3 in dry condition with 10m soil thickness. Small volume limit requires less model runtime and memory requirement. But a large range of volumes indicates a complete search of the whole terrain, thus the volume limit of 1-100000m^3 is supposed to be better than the other two volume limits. Compared with the volume limits of 1-50000 and 1-100000m^3, the volume limit of 1-5000m^3 obviously simulated less and smaller landslides, even in some steep areas, no slope failure was simulated. Table 5-2 shows the overlap degree between these three volume ranges. The match index of 1-5000m^3 with the volume limit of 1-100000m^3 is only 0.07 (low overlap degree). However, when comparing the volume limits 1-50000m^3 with 1-100000m^3, the spatial distributions of the simulated landslides are similar. The match index between them is as high as 0.85, indicating a high degree of overlap.

Table 5-2: *The match index between volume limit 1-100000m^3 and another two limits.*

Volume limits	1-100000m^3
1-5000m^3	M=0.07
1-50000m^3	M=0.85

Table 5-3 shows the statistics of the simulated landslides, as well as the runtime and the number of the analyzed slip surfaces in Scoops3D. It can be found from Table 5-3 that the volume limit of 1-100000m^3 predicts the slightly bigger landslides than volume limit of 1-50000m^3, but the number, percentage of the affected area, total volume can be very similar, indicating the volume 1-50000m^3 a relatively complete search of the terrain. However, this small difference needs excessive runtime and memory requirements. It is also clear that only 20 landslides were simulated with the volume limit 1-5000m^3, accounting for the 1.4% of the whole area, indicating that it is not enough to perform a complete search of the terrain.

Table 5-3: *Statistics of landslides simulated by Scoops3D using three different volume limits.*

	Volume limits (m^3)		
	1-5000	1-50000	1-100000
Number	20	51	50
Min. volume (m^3)	2844	8447	9045
Max. Volume (m^3)	25090	273933	310863
Total area (m^2)	43292	549656	586552
Percentage of the affected area (%)	1.4	15.5	16.5
Total volume(m^3)	158214	2989547	3237586
Mean area (m^2)	2165	10778	11731
Mean volume (m^3)	7911	58619	64752
Runtime (h)	13	16	29
Number of analyzed potential slip surface	418903	623853	734751

Notably, although the large volume limits can ensure a thorough search of instabilities of the whole terrain, it does not mean that the bigger the volume limits, the better the search results. To illustrate this, a profile (indicated by a thick black line A-B in Fig. 5-3 (c1)) shown in Fig. 5-4 was made at a landslide position simulated using volume range 1-100000m^3. It can be found that the failure depth of this landslide exceeds the maximum soil depth 10m, and in deepest point, the failure depth can be as deep as 27m. This result means that the bedrock is cut by searching spheres, which is unexpected and against our scenario assumption mentioned in section 4.2.2. Thus the volume limit 1-100000m^3 is not suitable for this environment.

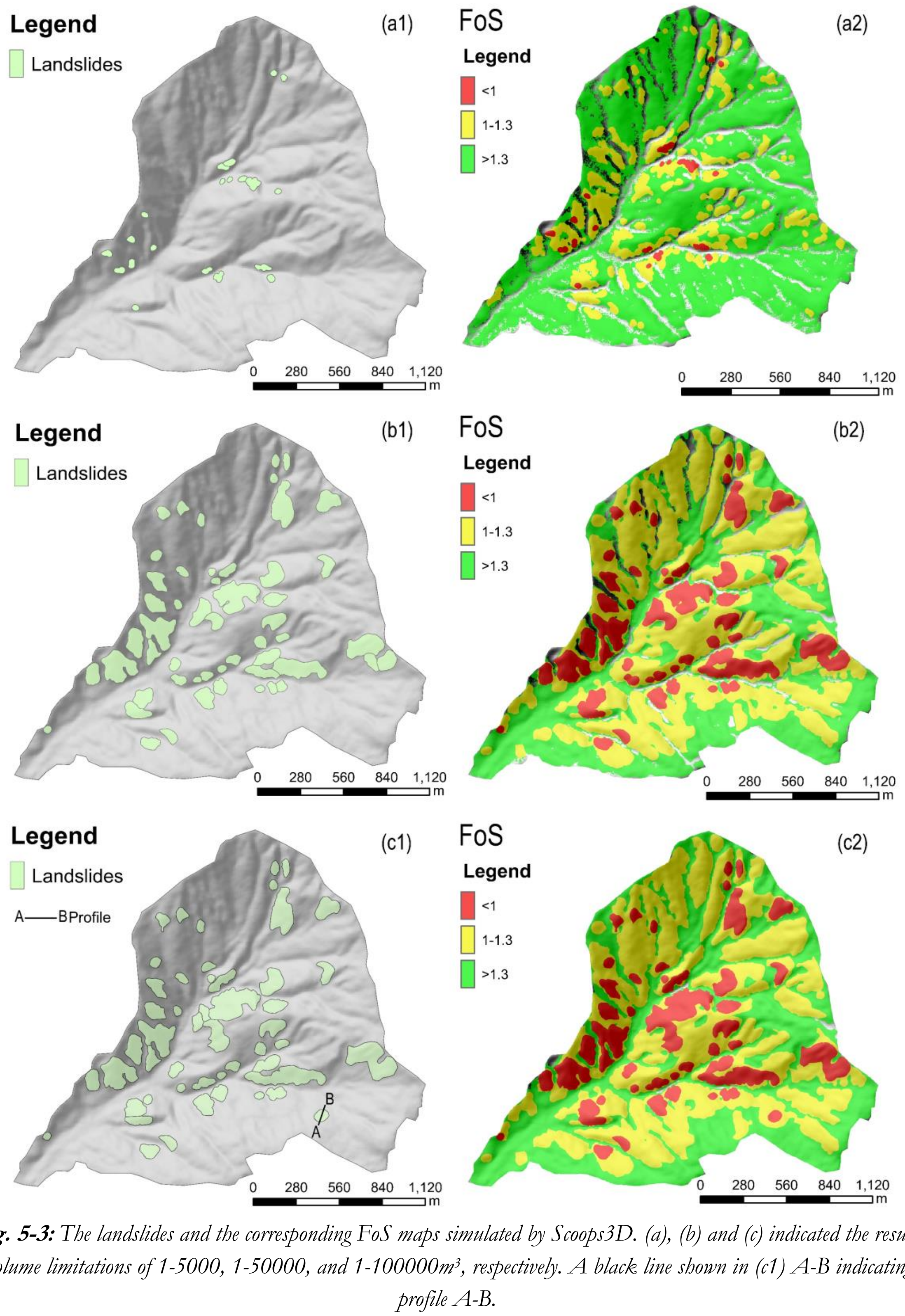

Fig. 5-3: *The landslides and the corresponding FoS maps simulated by Scoops3D. (a), (b) and (c) indicated the results of volume limitations of 1-5000, 1-50000, and 1-100000m³, respectively. A black line shown in (c1) A-B indicating a profile A-B.*

5.1.3. The determination of internal model parameters

Given the fact that volume limit 1-5000m³ failed to perform a complete search, whereas the volume limit 1-100000m³ would cut the bedrock and lead to unexpected results, the volume limit in this study is determined as 1-50000m³. In order to make OpenLISEM and Scoops3D comparable for predicting

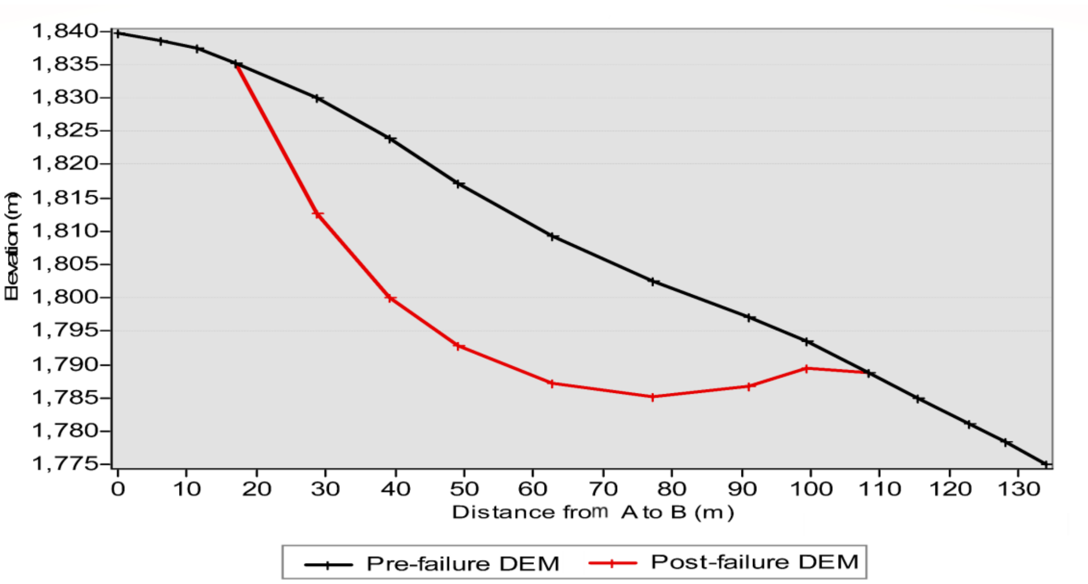

Fig. 5-4: *Profile A-B (marked with a black thick line shown in Fig. 5-3 (c1)).*

landslide volume, the spatial distributions of landslides simulated by OpenLISEM and Scoops3D are compared. Fig. 5-5 shows the comparison of match index (M) between Scoops3D (volume limits is 1-50000m^3) and OpenLISEM (Fr is 1.1, 1.2, 1.3, and 1.4). From Fig. 5-5 it is found that F_r=1.3 gives the highest overlapping degree (49%) with Scoops3D. Thus 1.3 is used as resulting FoS in this study.

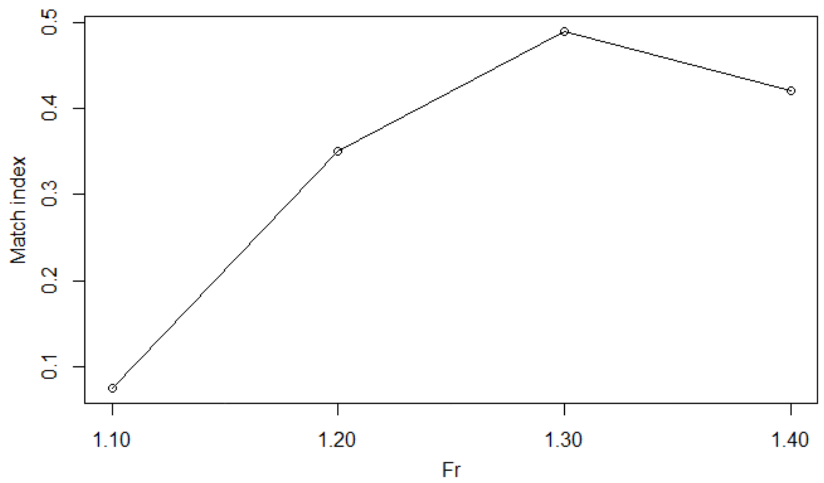

Fig. 5-5: *The match index between landslides simulated by OpenLISEM with four different Fr values and landslides simulated by Scoops3D with volume limit 1-50000m^3.*

5.2. Critical Soil Thickness

The determination of critical soil thickness (CST) needs self-check within the same model and cross-check between different models of the slope stability of the post-failure terrain. Fig. 5-6 shows the Factor of Safety maps of self- and cross-checks for OpenLISEM and Scoops3D.

Fig. 5-6 (a1) and (a2) show the FoS maps simulated by OpenLISEM and Scoops3D, respectively, using the OpenLISEM-derived new soil thickness. Fig. 5-6 (a1) indicates that using the OpenLISEM-derived new soil thickness, there is no unstable slope in OpenLISEM anymore. Fig. 5-6 (a2) indicate that there are still many unstable slopes in Scoops3D with this new soil thickness.

Fig. 5-6 (b1) and (b2) show the FoS maps simulated by OpenLISEM and Scoops3D, respectively, using the Scoops3D-derived new soil thickness. Using the Scoops3D-derived new soil thickness, both models predict unstable slopes. When checking the positions of the unstable slopes in Fig. 5-6 (b1), it is found that the unstable areas are just around the edges of the previous slope failures (previous slope failures are shown in Fig. 5-3 (b1)). From Fig. 5-6 (b2) it can be found that Scoops3D cannot ensure that all the slopes are stable after "cleaning" the unstable slopes, which means Scoops3D may produce successive slope failures due to the change of the terrain caused by landslides.

To summary, using the new soil thickness map produced by Scoops3D, there are still many unstable slopes in OpenLISEM, and many unstable slopes in Scoops3D, and the geometries of the landslides in Fig. 5-6 (b1) are unexpected. Using the new soil thickness produced by OpenLISEM, there is no slope failure in OpenLISEM, but till there are many unstable slopes in Scoops3D. The new soil thickness map derived by OpenLISEM was determined as critical soil thickness map because at least this thickness map can ensure all the slopes are stable (FoS >1) in OpenLISEM.

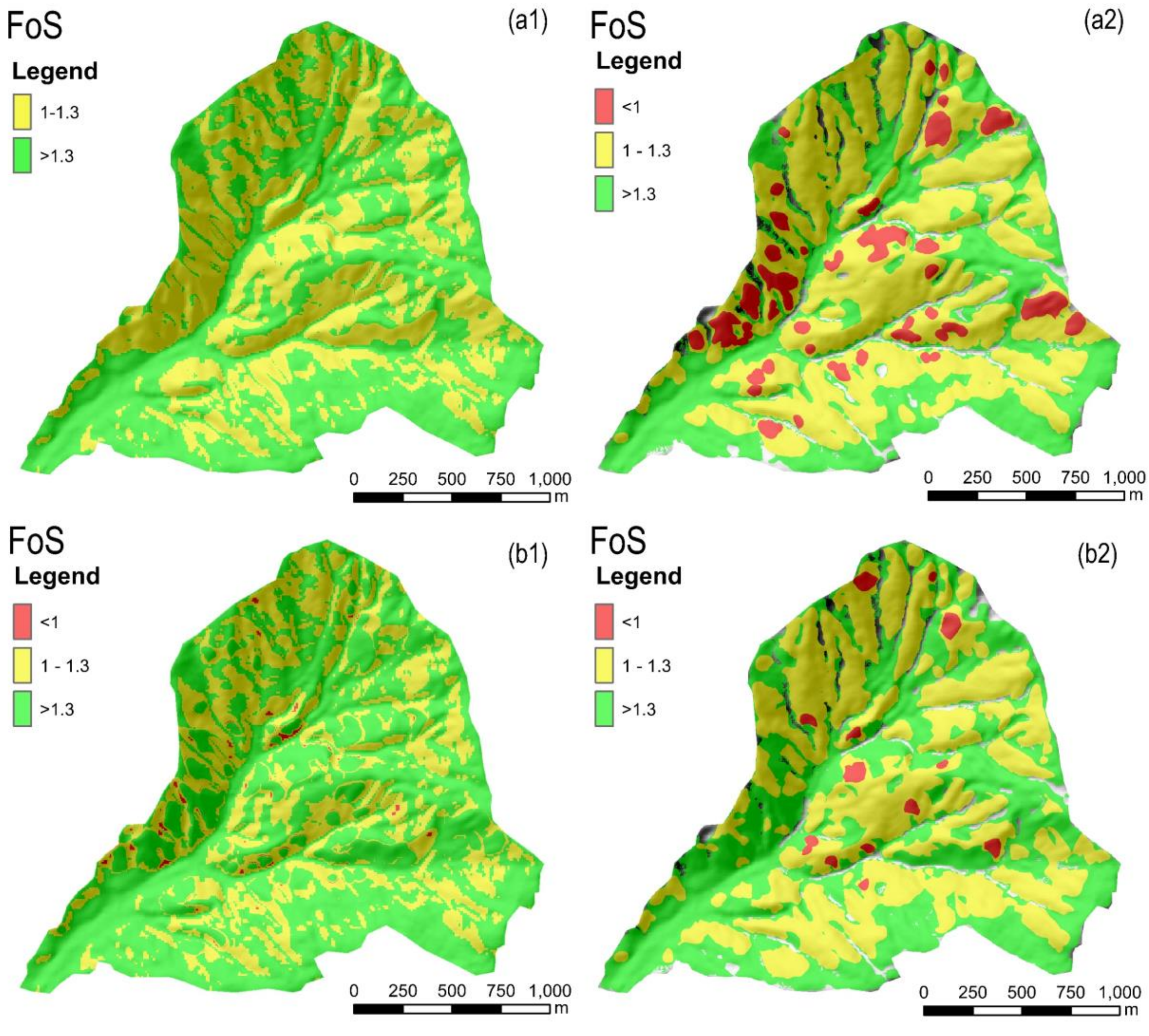

Fig. 5-6: *The self-check and cross-check of OpenLISEM and Scoops3D. (a1) FoS map simulated by OpenLISEM using OpenLISEM-derived new soil thickness (self-check); (a2) FoS map by Scoops3D using OpenLISEM-derived new soil thickness (cross-check); (b1) FoS map by OpenLISEM using Scoops3D-derived new soil thickness (cross-check); (b2) FoS map by Scoops3D using Scoops3D-derived new soil thickness (self-check).*

5.3. Model Comparisons Under Different Scenarios

5.3.1. Scenario 1

For this scenario, some results were shown already in section 5.1 when dealing with the determination of internal model parameters. In this section, the model comparisons in terms of number, location, area, and volume are discussed.

The locations and areas of the simulated landslides are firstly compared. Table 5-4 shows the statistics of the landslides simulated by OpenLISEM and Scoops3D. The percentage of landslide affected area in OpenLISEM and Scoops3D are 16.3% and 15.5%, respectively. However, the match index between them is only 49%. This means that over half of the landslides between these two models are mismatched. This can also be seen in Fig. 5-7, which shows the distributions of the simulated landslides. According to the landslide locations, the landslides can be classified into three types, the landslides which are only simulated by OpenLISEM (take the locations of O1, O2, and O3 in Fig. 5-7 as examples), the landslides which are only simulated by Scoops3D (take the locations of S1, S2, and S3 in Fig. 5-7 as examples), and the landslides which are simulated by both OpenLISEM and Scoops3D (take the locations of OS1, OS2, and OS3 in Fig. 5-7 as examples).

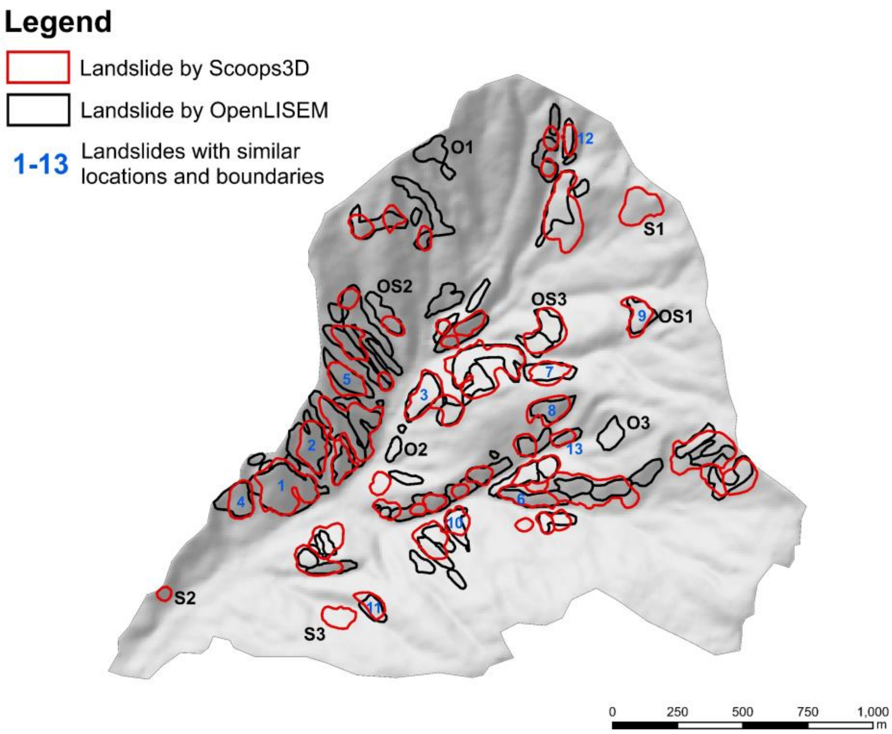

***Fig.5-7**: The landslides simulated by OpenLISEM and Scoops3D in scenario 1. Number 1-13 indicate 13 pairs of landslides whose volumes will be compared later. The S, O, as OS indicate locations where only predicted by Scoops3D, OpenLISEM, or by both models, respectively.*

***Table 5-4**: The statistic of simulated landslides in dry scenario.*

Models	Total number of landslides	Total landslide area (m^2)	Percentage of the affected area (%)	Total volume (m^3)	Mean area (m^2)	Mean volume (m^3)	Match index (%)
OpenLISEM	75	577592	16.3	860136	7701	11469	49
Scoops3D	51	549656	15.5	2989547	10778	58619	

For landslides which are simulated both by OpenLISEM and Scoops3D, there are big differences. Taking the landslides at locations of OS1, OS2, and OS3 as three examples. At OS1 position, the landslide areas simulated by both models show a high accordance. At OS2 position, Scoops3D simulated a smaller landslide locating at the lower part of the landslide which is simulated by OpenLISEM. The difference, in this case, can be explained by the dynamic failure process in OpenLISEM. Both models may initially simulate small failures, but due to the small failures, the surrounding failures may be initiated in OpenLISEM. This type of difference mainly occurred in the very steep area where small landslides may easily propagate upwards or joint together.

At OS3 position, two landslides which are simulated by OpenLISEM are wrapped by a single landslide which is simulated by Scoops3D. The difference arises when delimiting the boundaries of the landslides. In the output (failure height map) of OpenLISEM at this position, there is a clear distinction in failure height between these two adjacent landslides. In Scoops3D, however, only an integral failure displayed. Fig. 5-8 schematically depicting this difference from a two-dimensional perspective. OpenLISEM simulated landslides on both sides of the ridge, whereas Scoops3D cut the whole terrain, which seems unreasonable under the assumed volcanic environment in this study.

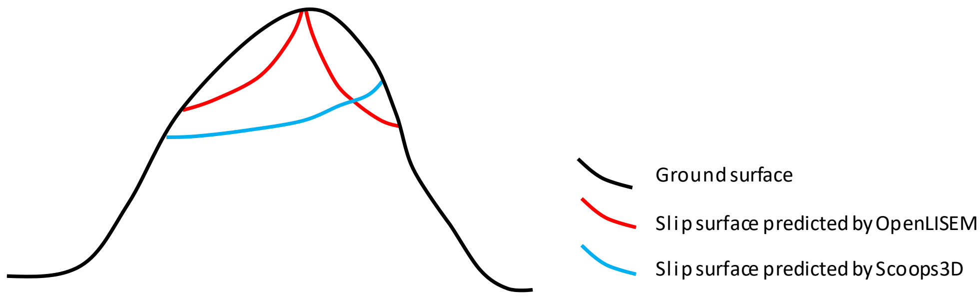

Fig. 5-8: *Two-dimensional sketch showing the landslides at OS2 position.*

To investigate the landslides which are only simulated by OpenLISEM or Scoops3D (at locations of O1, O2, and O3 or S1, S2, and S3), the relationships between landslide initiations and the average slope angles of landslides were analyzed (Fig. 5-9). The average slope angles were calculated by averaging the slopes within individual landslide polygons. Form Fig. 5-9 it is found that Scoops3D simulated landslides with average slope angles ranging from 42-48°, and OpenLISEM with average slope angles ranging from 40-49°. The landslide O1 and O2, which were only simulated by OpenLISEM have an average slope angle of 41.8° and 41.9. However, landslide O3, which is also simulated only by OpenLISEM has an average slope angle of 44°. The average slope angles of landslide S1, S2, and S3 are 42.06, 44.67, and 42.63, respectively. Given that in the dry scenario, only the slope angle affected the spatial variability in slope stability in OpenLISEM, the landslide S1, S2, and S3 should also have been detected by OpenLISEM.

The volumes of 13 pairs of individual landslides, identified by numbers from 1 to 13 in blue shown in Fig. 5-7, have also been compared. These 13 pairs of landslides have been selected due to their similar locations and boundaries with their counterparts. Fig. 5-10 shows the volume comparisons of those 13 pairs of landslides. It is clear that Scoops3D predicts much deeper landslides than OpenLISEM at the same locations, but they have the similar volume variation trend. The large landslides in OpenLISEM are also the large landslides in Scoops3D.

The non-cumulative and cumulative volume-frequency distributions for landslides simulated by OpenLISEM and Scoops3D in scenario 1 are shown in Fig. 5-11 (x- and y-axis at logarithmic scale) and Fig. 5-12 (x-axis at logarithmic scale), respectively. The non-cumulative frequency distribution shows the relation between the proportions of landslides of different volumes. It is clear from Fig. 5-11 that OpenLISEM simulated a large number of landslides of small and medium volumes, and a small number of landslides of larger volumes in this scenario. Scoops3D severely underestimated the number of landslides

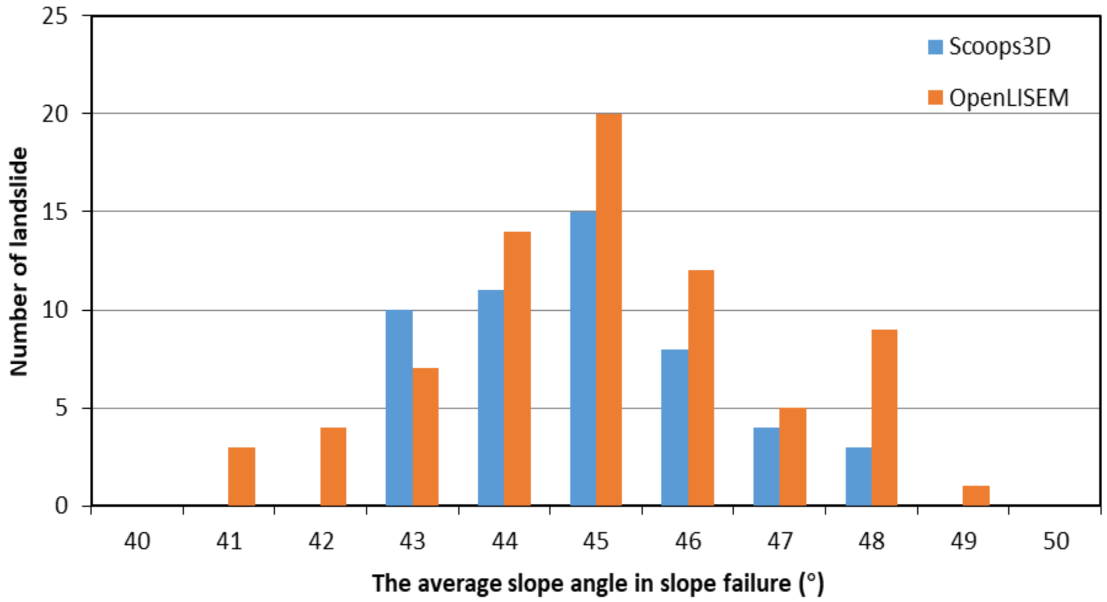

Fig. 5-9: *The relationships between landslide frequency and the average slope angles within slope failures.*

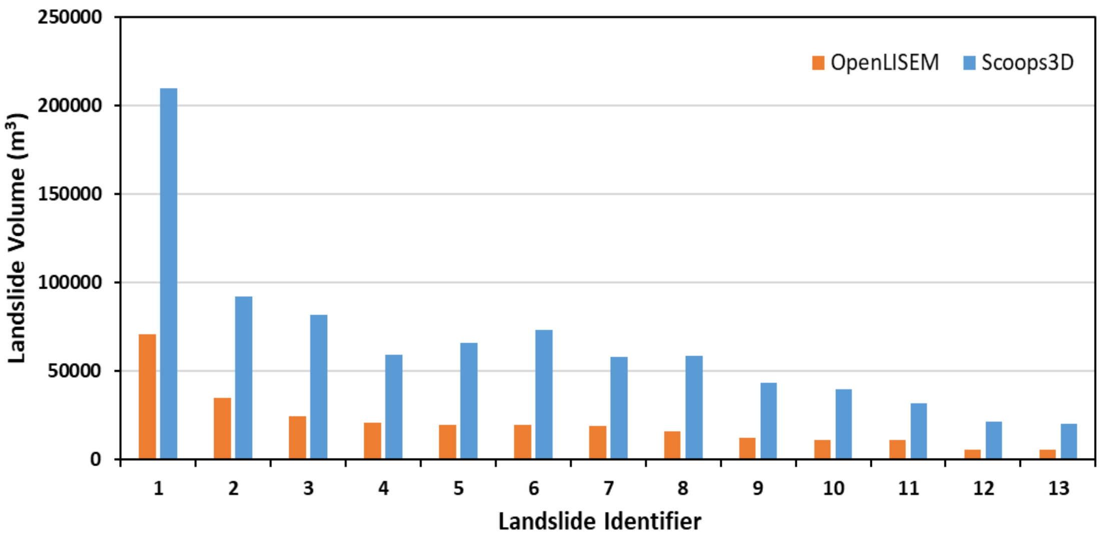

Fig. 5-10: *The volumes of 13 pairs of individual landslides simulated by OpenLISEM and Scoops3D. These 13 pairs of landslides are shown in Fig. 5-7 (marked by blue numbers).*

of small volumes and simulated a relatively large number of landslides with larger volumes in this scenario. Besides, OpenLISEM predicted a larger volume range, whereas Scoops3D predicted a small volume range.

The cumulative frequency distribution shows the relation between the cumulative number of landslides with volumes greater than a certain volume plotted at x-axis. Fig. 5-12 shows that about 40 % number of landslides simulated by OpenLISEM have volumes greater than 10000m^3, whereas about 50% number of landslides simulated by Scoops3D have volumes greater than 10000m^3. It can also be found that no landslide has a volume greater than 100000m^3 in OpenLISEM, but about 10% number of landslides have volumes greater than 100000m^3. For each large volume level at x-axis, Scoops3D predicted more number than OpenLISEM.

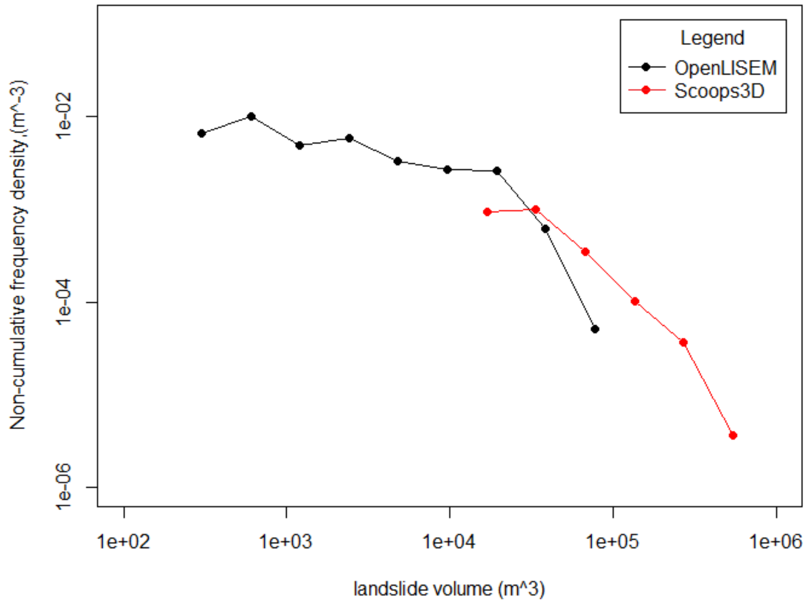

Fig. 5-11: *The non-cumulative volume frequency-density distribution of landslides in scenario 1 (x-axis at logarithmic scale).*

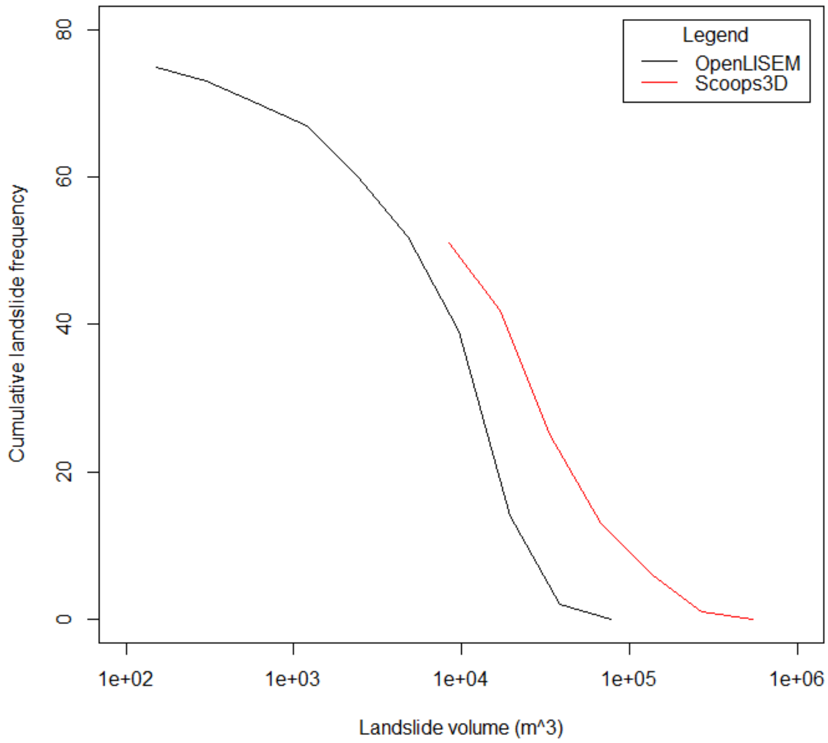

Fig. 5-12: *The cumulative frequency-density distribution of landslides in scenario 1 (x-axis at logarithmic scale).*

5.3.2. Scenario 2

In this scenario, landslides are caused by wetting front infiltration. Initially, the soil is completely dry, the initial soil moisture equals to residual soil moisture, and no pore water pressure used in this scenario. The wetting front only changes the total soil weight. The modeled results show that Scoops3D simulated a number of landslides in scenario 2, but the rainfall magnitude shows almost no influence on landslide locations and landslide volumes. OpenLISEM does not produce any landslide in this scenario.

Fig. 5-13 shows the landslides simulated by Scoops3D. Before wetting front infiltration there are already a number of landslides in dry condition delimited by black polygons in Fig. 5-13 (also mentioned in section 5.2). The red polygons indicate the landslides after the wetting front infiltration, so the red polygons are not the landslides that are purely induced by wetting front, they equal to the effect of wetting front infiltration plus landslides in dry conditions. For convenience, the red polygons in Fig. 5-13 are still named wetting font induced landslides. Fig. 5-13 (a), (b), (c), and (d) stand for four different rainfall scenarios with the rainfall intensity increasing.

When comparing the wetting front induced landslides between these four maps, it is found that the landslide distributions with respect to four different rainfall intensities are almost the same. The only major difference is that rainfall with the smallest intensity failed to trigger a small landslide which is highlighted by a blue rectangle in Fig. 5-13 (b), (c) and (d). Table 5-5 shows the statistics of the landslides simulated by Scoops3D for scenario 2, as well as for dry scenario which the critical soil thickness was used. From Table 5-5 it is found that not only the landslide locations but also the landslide volumes are similar among these four scenarios. The magnitude of the rainfall events cannot have a big influence on simulated landslide volume.

However, when comparing the landslides induced by wetting front with the landslides in dry condition with critical soil thickness, there is a relatively big difference in terms of landslide surface areas and landslide volumes. About 11 new landslides initiated by the wetting front in each rainfall scenario and about 9.5% of

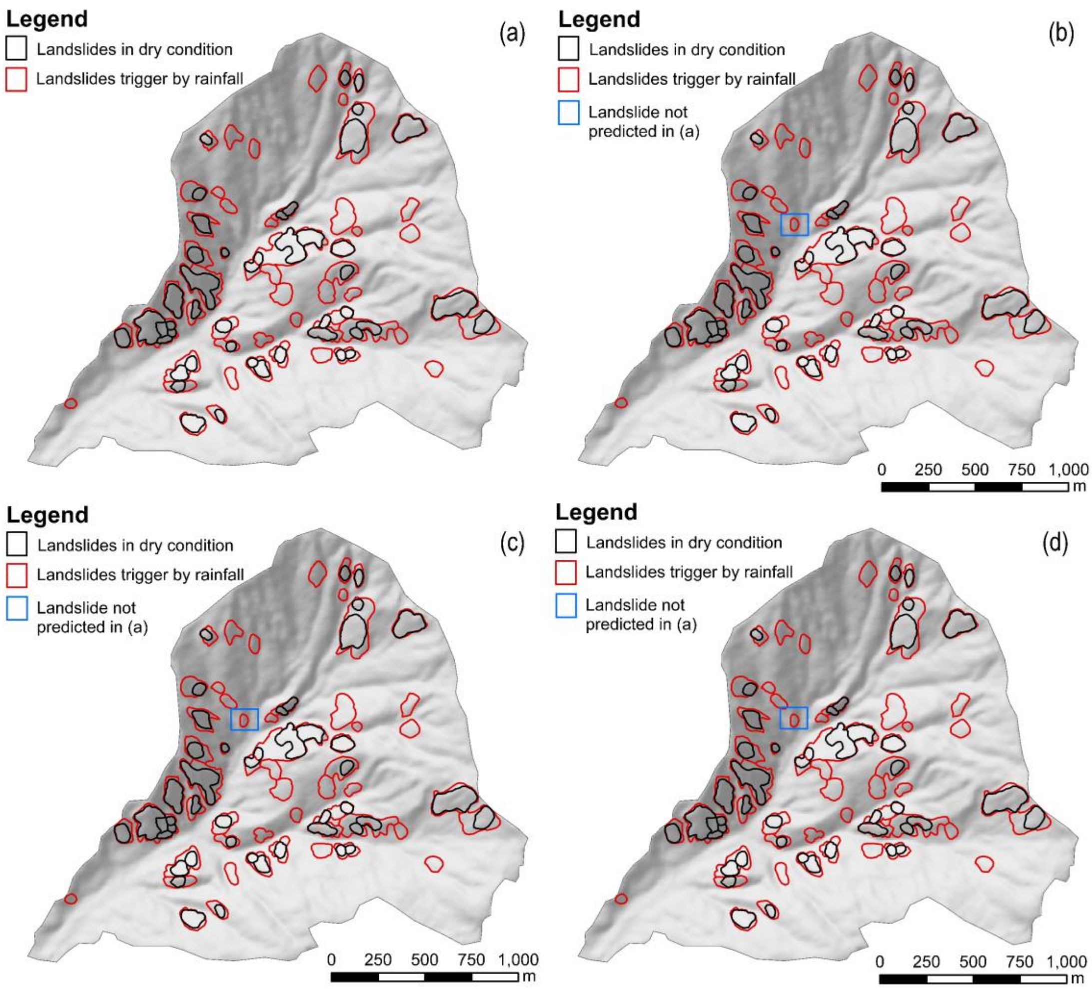

Fig. 5-13: *Landslide simulated by Scoops3D in scenario 2 (red polygons) and scenario 1 (black polygons; with critical soil thickness). (a), (b), (c), and (d) represent rainfall scenarios a, b, c, and d, respectively.*

Table 5-5: *The statistics of the simulated landslides by Scoops3D in scenario 2 and scenario 1 (with critical soil thickness). In scenario 2, rainfall scenario a, b, c, and d indicate an increasing rainfall magnitude.*

	Rainfall intensity level				
	Dry	a	b	c	d
Total number of landslides	44	55	56	56	56
Minimum landslide volume (m^3)	5520	7173	7173	7173	7173
Maximum landslide volume (m^3)	115885	284849	297366	297643	298644
Total landslide area (m^2)	284444	619184	624312	624912	627344
Percentage of the affected area (%)	8.0	17.5	17.6	17.6	17.7
Total landslide volume (m^3)	1352920	3015147	3050233	3056641	3073434
Average landslide area (m^2)	6465	11258	11148	11159	11203
Average landslide volume (m^3)	30748	54821	54468	54583	54883

the total catchment area is affected by these new landslides. And the total failure volume increased by 123% compared with the total landslide volume in dry condition with critical soil thickness.

From the Table 5-5, it is also found that the slope failures are not determined by the magnitude of the rainfall events, but by the presence of the rainfall. Such behavior of Scoops3D perhaps because of the intersection size between searching spheres and the terrain. When a searching sphere initially meets the slope, the radius of that sphere is relatively small, and the initial intersection is superficial. The depth of the wetting front, in this case, account for a relatively big proportion of the whole intersected depth. When analyzing the slope stability of this shallow intersection, the FoS can be very small.

OpenLISEM cannot produce any slope failure in this scenario. The FoS maps with respect to four rainfall events are almost the same, and they are all greater than 1. The wetting front does not have a visible influence on slope stability. In order to investigate the reason of this behavior, a simple stand-alone calculation of FoS has been made to simulate the worst case (worst case means the calculation use the steepest slope angle, maximum soil thickness 10m, and the maximum infiltration depth of 0.7m during the most intensive rainfall event) in this scenario. In totally dry conditions, the equation to calculate FoS in OpenLISEM is (a simplification of equation 3-1 for dry condition):

$$\text{FoS} = \frac{c' + Z \cdot \gamma \cdot cos^2\alpha \; tan\phi'}{Z \cdot \gamma \cdot sin\alpha cos\alpha} \quad [5\text{–}2]$$

For the worst case, the soil effective cohesion c'=8kpa; dry soil depth Z=10m; moisture soil unit weight γ=12 kN/m^3; the steepest slope angle α=58°; soil effective internal friction angle ϕ'=32°. The calculated FoS is about 0.54. When wetting front infiltrates, the equation to calculate FoS becomes:

$$\text{FoS} = \frac{c' + [Z \cdot \gamma + Z' \cdot \gamma_s] cos^2\alpha \; tan\phi'}{[Z \cdot \gamma + Z' \cdot \gamma_s] sin\alpha cos\alpha} \quad [5\text{–}3]$$

Where the depth of the wetting front Z' = 0.7m; dry soil depth Z = 10-0.7=9.3m; soil saturated bulk density γ_s = 15kN/m^3. The other parameters remain the same. The calculated FoS, in this case, is about 0.53. The decrease rate of FoS can be calculated as: ΔFoS=(0.54-0.53)/0.54=1.8%. Given such a steep slope angle, with the maximum wetting front infiltration and soil depth, the change of the FoS is only about 1.8%. It is clear from the result that the effect of the wetting front on slope stability is very small in this study when there is no connection between the wetting front and the groundwater level.

To summarize, it is hard to compare the landslide volume in this scenario because no landslide is produced by OpenLISEM. OpenLISEM did not produce landslides because the wetting front has no connection with groundwater, thus the wetting front only changes the total weight of the soil, rather than increasing the pore water pressure. For OpenLISEM, the soil depth from bedrock to the ground surface is used in the calculation of FoS. Compared with the soil depth, the wetting front depth is too small to have a large influence on slope stability. The stand-alone calculation of FoS has proven this analysis. For Scoops3D, the intersected soil depth (between searching spheres and ground surface) is used in the calculation of FoS. When a sphere slightly cuts the terrain, the wetting front depth may be almost similar to the intersected soil depth. This means that wetting front has a relatively large influence on the slope stability.

5.3.3. Scenario 3

In this scenario, landslides are triggered by pore-water pressure caused by two different groundwater table. A groundwater flow model was used to simulate the groundwater level that varied from near the surface (saturated soil), to 10days and 20 days after soil saturation. The groundwater level which corresponds to 10 days after soil saturation is regarded as high groundwater level, and the groundwater level which corresponds to 20 days after soil saturation is regarded as low groundwater level, the pore-water pressures caused by these two groundwater levels were used in this scenario to simulate landslides.

Fig. 5-14 shows the simulated landslides by OpenLISEM (left) and Scoops3D (right) in scenario 3. It is clear from Fig. 5-14 that under such groundwater levels, both models simulated a number of landslides widely distributed on the whole terrain. The high groundwater level (the red polygons) lead to more extensive landslides than low groundwater level (the black polygons). Many new landslides were predicted using high groundwater level in both models.

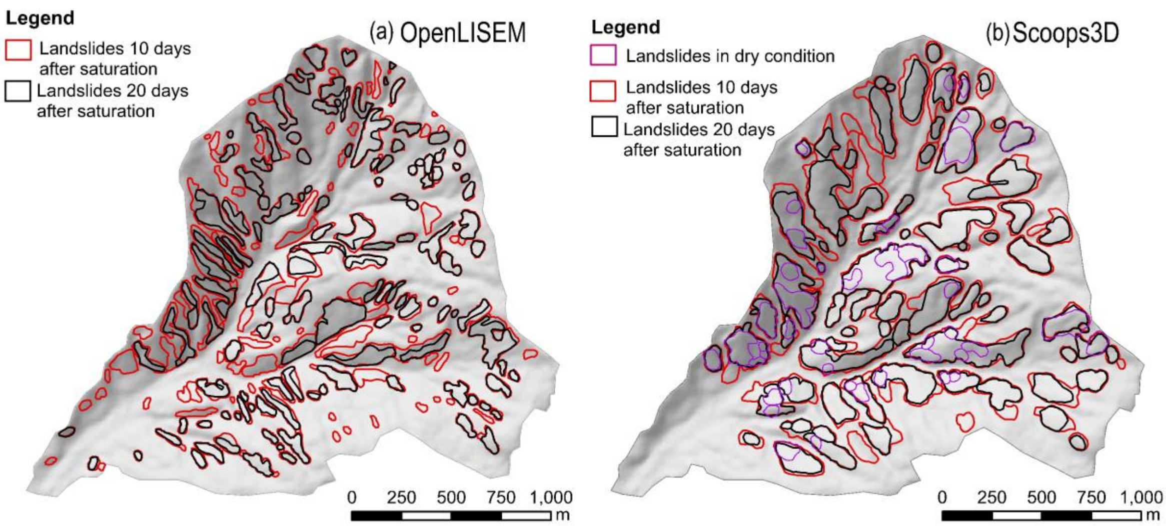

Fig. 5-14: *The landslide simulated by OpenLISEM (left) and Scoops3D (right) in scenario 3.*

Table 5-6 shows the statistics of landslides shown in Fig. 5-14. For OpenLISEM, 53 new landslides were simulated using the high groundwater level, and about 12% of new areas are affected by these new landslides. The total volume of these new landslides is 199558m^3, which account for about 33.6% of the total landslide volume. For Scoops3D, the number of landslides was decreased by 4 when the high groundwater level was used, but about 10% new areas were affected due to the groundwater level rise. This means some small landslides joined together and form larger ones. The total volume of these new landslides is 1984360m^3, which account for about 21.6% of the total landslide volume. The results show that different groundwater levels have influence on slope stabilities for both models, but using the different groundwater levels have a relatively bigger influence on OpenLISEM than on Scoops3D.

Table 5-6: *The statistics of the landslides simulated by OpenLISEM and Scoops3D in scenario* 3.

	OpenLISEM		Scoops3D	
	High water table	Low water table	High water table	Low water table
Total landslide number	179	126	72	76
Minimum landslide volume (m^3)	109	217	3074	3135
Maximum landslide volume (m^3)	19321	16604	536288	454599
Total landslide area (m^2)	1079416	652388	1495572	1107456
Percentage of the affected area (%)	30.4	18.4	42.2	31.2
Total landslide volume (m^3)	593804	394246	9189022	7204662
Average landslide area (m^2)	6030	5178	20772	14572
Average landslide volume (m^3)	3317	3129	127625	94798

Fig. 5-15 shows the landslides in OpenLISEM overlapped with landslides in Scoops3D. The match index between OpenLISEM and Scoops3D is 41.1% for high groundwater level, and 25% for low groundwater level. It can also be found that the OpenLISEM tends to produce more discrete landslides, whereas Scoops3D produces more integral landslides. It is hard to find a comparable individual landslide with similar boundary and location.

To compare the failure volumes at the same locations, the intersections (overlapped locations) between landslides from OpenLISEM and landslides from Scoops3D have been made based on Fig. 5-15 (a) and (b). Fig. 5-16 (a) and (b) show the intersected landslides for high and low groundwater level, respectively. Among these intersections, 8 intersections for each groundwater level, which marked by blue numbers in Fig. 5-16, were selected to perform the volume comparison.

Fig. 5-17 shows the volume comparison results. It can be found that at the same locations, Scoops3D simulated far bigger landslides than the OpenLISEM. All the volumes simulated by OpenLISEM at these intersections are less than 20000m^3, while only one intersection has the volume less than 20000m^3 in Scoops3D. At some locations (i.e. the number 4 location in Fig. 5-16 (b)), the difference can be more than 10 times.

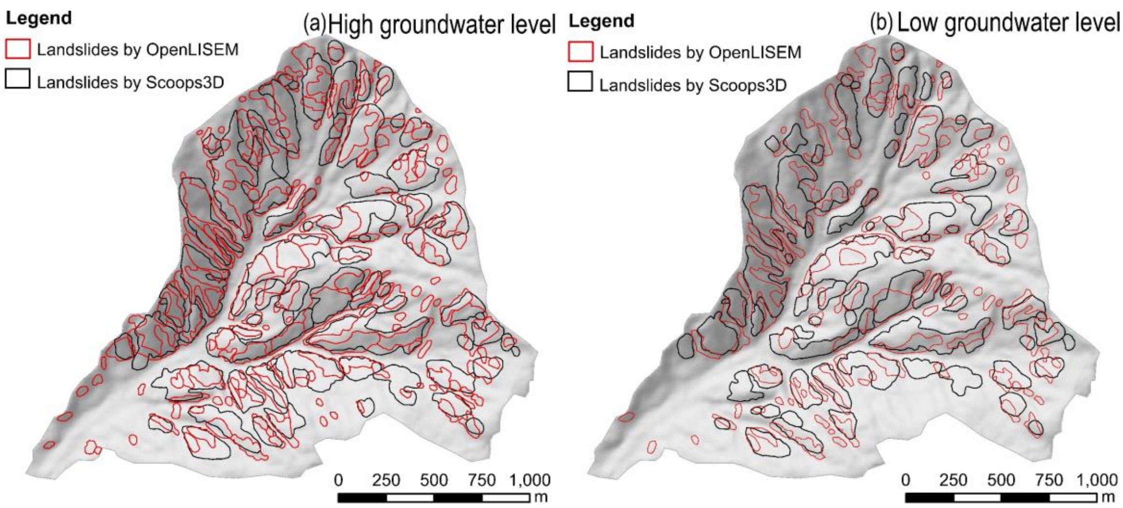

Fig. 5-15: *Simulated landslides when groundwater are high (a) and low (b).*

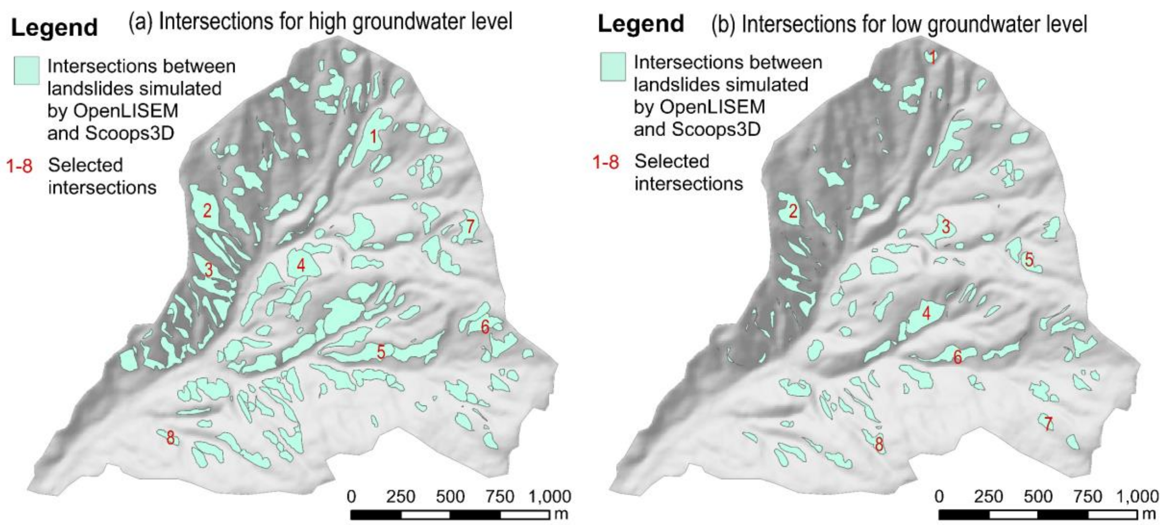

Fig. 5-16: *The intersections (overlapped sections) between OpenLISEM and Scoops3D corresponding to high groundwater level (a) and low groundwater level (b). The numbers in red indicate the selected locations which will be used to perform volume comparisons.*

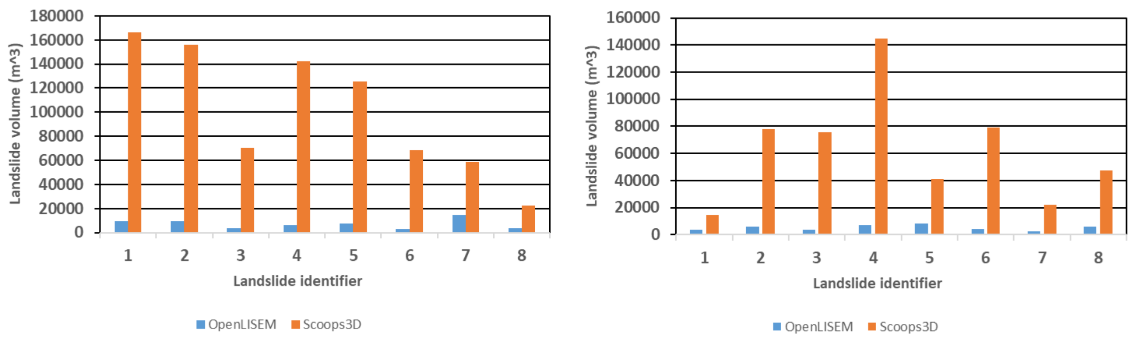

Fig. 5-17: *The comparisons of volumes at 8 overlapped locations for high groundwater level (left) and 8 overlapped locations for low groundwater level (right).*

The non-cumulative volume-frequency distributions for landslides simulated by OpenLISEM and Scoops3D in scenario 3 are shown in Fig. 5-18. The x-axis and y-axis are given at logarithmic scale. It is clear that the increase of groundwater level in OpenLISEM led to relatively more landslides with both small and large volumes. Whereas the increase of groundwater level in Scoops3D led to more landslides with large volumes, but fewer landslides with small volumes. When checking the landslide distributions in Fig. 5-15, it can be found that some relatively large landslides joined together and formed an even larger landslide in Scoops3D, but such merging did not occur in OpenLISEM. When Comparing frequency density results of Scoops3D and OpenLISEM, it can be found that the OpenLISEM simulated more landslide with small and medium volumes, whereas Scoops3D simulated much bigger landslides.

For an overall comparison, the relationships linking landslide areas and volumes for all three scenarios were plotted in log-log coordinates in Fig. 5-19. All the relationships were then fitted by power laws. Table 5-7 details the information on these power-law relationships and the corresponding exponents (β). Notably, for scenario 2, only Scoops3D produced landslides, and the magnitude of the rainfall events did not have a big influence on landslide volumes and areas. To avoid replicated plotting, only the most intensive rainfall triggered landslides were used. Additionally, the areas and volumes of all the landslides produced by OpenLISEM and Scoops3D were respectively merged and integrally plotted in Fig. 5-19. The merged relation for OpenLISEM was plotted using a thick green dash line, and the merged relation for Scoops3D was plotted using a thick red dash line.

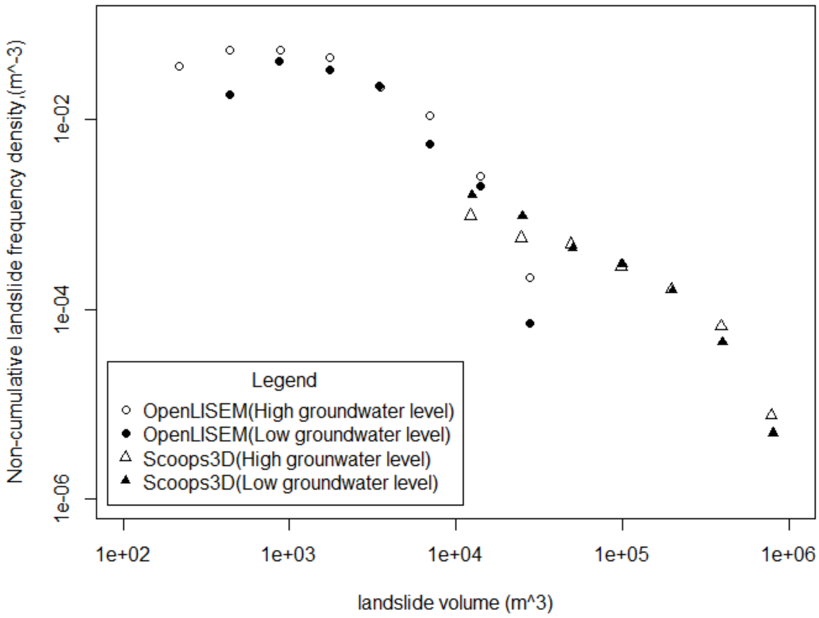

Fig. 5-18: *The volume-frequency distributions of simulated landslides in scenario 3.*

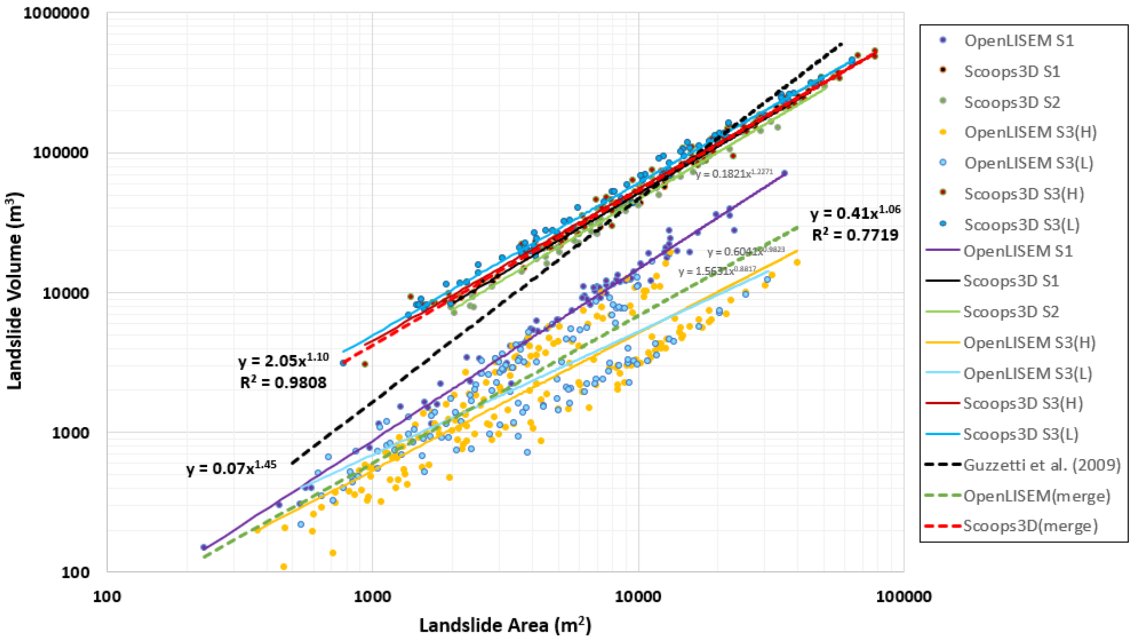

Fig. 5-19: *The volume-area relationships for all the scenarios. Thin solid lines indicate the relationships for individual scenarios, and the dash lines (in green and red) indicate the integral relationships for three scenarios for OpenLISEM and Scoops3D. The black dashed line indicates the internal relationship proposed by Guzzetti et al. (2009).*

The scaling exponents of two merged relationships were then compared with the international scaling exponent proposed by Guzzetti et al. (2009), which is mentioned in section 2.1.3. The international scaling exponent equal to 1.45. The scaling exponents of merged landslides from OpenLISEM and Scoops3D are 1.06 and 1.10, respectively. The area-volume relationship for Scoops3D is closer to the international landslide area-volume relationship. But Scoops3D produce more narrow relationships than OpenLISEM. It is hard to make a judgment which model predict more realistic landslide volume because the scaling exponent depends on many factors such as geological environment and triggering mechanism (section 2.1.3).

Table 5-7: *The descriptions of the legend in Fig. 5-19 and the corresponding fit equations and exponents.*

Legend	Descriptions	Fit equations	Exponent (β)
OpenLISEM S1	Scenario 1: 10m soil thickness	$y = 0.18x^{1.23}$	1.23
Scoops3D S1	Scenario 1: 10m soil thickness	$y = 1.66x^{1.12}$	1.12
Scoops3D S2	Scenario 2: critical soil thickness	$y = 1.44x^{1.13}$	1.13
	Wetting front infiltration		
OpenLISEM S3(H)	Scenario 3: critical soil thickness, high groundwater level	$y = 0.60x^{0.98}$	0.98
OpenLISEM S3(L)	Scenario 3: critical soil thickness, low groundwater level	$y = 1.56x^{0.88}$	0.88
Scoops3D S3(H)	Scenario 3: critical soil thickness, high groundwater level	$y = 2.45x^{1.09}$	1.09
Scoops3D S3(L)	Scenario 3: critical soil thickness, high groundwater level	$y = 2.71x^{1.09}$	1.09
OpenLISEM (merge)	All landslides simulated by OpenLISEM in three scenarios	$y = 0.41x^{1.06}$	1.06
Scoops3D (merge)	All landslides simulated by Scoops3D in three scenarios	$y = 2.05x^{1.10}$	1.10

6. DISCUSSION, CONCLUSIONS, AND RECOMMENDATIONS

6.1. Discussion

This section discusses main limitations of this study, which hindered the comparisons between the two models. The major limitations of this study are related to the following aspects:

(1) The lack of adequate input data and validation data;

(2) The mimicked volcanic environment;

(3) Errors and uncertainties related to the model outputs processing;

(4) The limitations of the models caused by the model assumptions.

6.1.1. Lack of adequate input data and validation data

This study is firstly hindered by the lack of adequate input data. To overcome this, the dummy datasets were adopted to mimic the volcanic environment. In dummy datasets, the topographic data (DEM) was not from volcanic areas but was taken from the originally planned study area in Yingxiu, Sichuan province, China, near to the epicenter of the 2008 Wenchuan Earthquake. The soils are assumed to be homogeneous everywhere and initially have 10-meter thickness. The soil geotechnical and hydrological properties are averages taken from literature values. However, can such dummy datasets extracted from many different sources represent a volcanic environment? Or even approximately represent a real environment?

Besides, this study did not take full advantage of OpenLISEM because some input characteristics were ignored. OpenLISEM integrates many factors with slope stability analysis. These factors include vegetation cover or other surface objects on the slopes that can intercept rainfall, the root cohesion of different vegetation species, the spatial variations of soil properties, etc. These elements probably affect the final slope stabilities. Moreover, in reality, real occurred landslide volume may be larger than initiation volumes because of the entrainment of path material. OpenLISEM can simulate not only initiation landslide volumes but also the entrainment of path material. But this option was not included in this study.

Neither did this study take full advantage of Scoops3D. Scoops3D can simulate different soil layers with different soil properties. To some extent, this characteristic makes the simulation more realistic when multiple soil layers exist underground.

However, to make these two models comparable, some compromises had to be made for both models by abandoning the specific inputs. Otherwise, the models will be compared based on different benchmarks. For example, Scoops3D cannot incorporate the surficial elements that may influence the rainfall infiltration, which will in turn influence slope stability. OpenLISEM cannot include multiple soil layers in the simulation, which is not realistic in a complex area. Thus no vegetation cover and only one layer of soil were considered in this study. Thus comparisons can be hardly reasonable since both models were not fully explored in this study.

The lack of calibration and validation data also restricts the model comparisons. The calibration and validation data should include historical landslide distributions and landslide volumes at the depletion zones. With calibration and validation data, both models can achieve the best performances under the given datasets. By comparing the best performances of these two models, the answer to which model is better than another for the specific environment can be concluded. Initially, together with the supervisors, we searched for datasets where both soil thickness distribution and geotechnical parameters are sufficiently known, and where landslide locations, dates, and volumes are known, but we could not find a suitable dataset. Due to such a major limitation of input data in this study, there is no strong evidence to prove which model is better than another. Consequently, the comparisons mainly focus on the differences of the model results.

To perform an overall comparison, optimal input data and calibration and validation data should be guaranteed. Specifically, a pre-event DEM with relatively high resolution (i.e. 5m) is needed. The soil samples on landslides should be collected from the field and the corresponding laboratory tests should be done to derive geotechnical and hydrological parameters. The soil properties and thickness should be derived from borehole data coupled with the proper interpolation methods. Empirical models can also be used to derive spatial soil thickness distributions if there are strong links between environmental factors like slope, distance from the valley, wet index, etc. and soil thickness. The most reliable and accurate rainfall data is from rainfall stations with the date of occurrence, satellite data such as Tropical Rainfall Measuring Mission satellite (TRMM) and Global Precipitation Measurement (GPM) can also be used when validation data is available. The locations (in the form of polygons) and the volumes of depletion zones of historical landslides can be used as validation data. And the historical landslides should be linked to the corresponding triggering factors.

6.1.2. The mimicked volcanic environment

Whether the mimicked environment is appropriate to perform a reasonable comparison between OpenLISEM and Scoops3D? As mentioned in chapter 3, OpenLISEM was probably suitable for shallow and translational landslides due to the assumptions in terms of slope stability analysis, whereas Scoops3D is more suitable for rotational and deep-seated landslides due to the assumptions of slip geometry. In this study, the simulations were based on the mimicked volcanic environment. But what will be the performance of OpenLISEM and Scoops3D if given a totally different environment? Fig. 6-1 Shows an example of another geologic environment: Loess Plateau environment.

Loess Plateau is characterized by very thick soil and steep terrain. Loess Plateau is prone to landslides especially in monsoon season due to the geotechnical sensitivity to water (Wen and Yan, 2013). The current

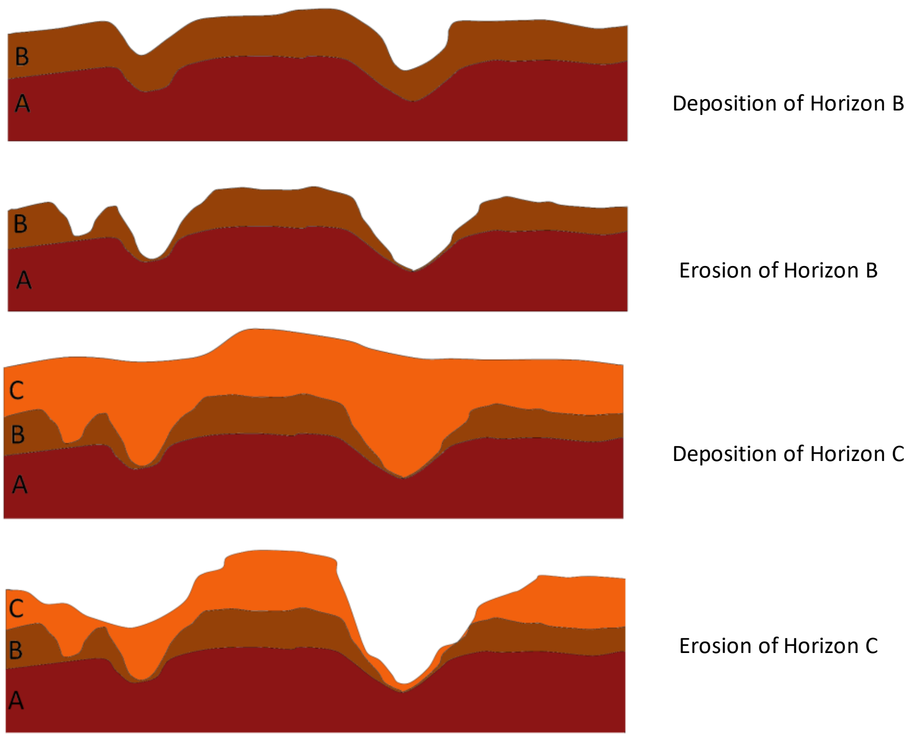

Fig. 6-1: *Different phases of loess deposition and erosion and our simplified situation.*

topography of Loess Plateau is shaped by deposition and erosion of loess layers in the different geologic period. Fig. 3-1 briefly depicts different phases of loess deposition and erosion. Initially, layer B deposits on top of eroded layer A. After a long period of time when layer B has also been eroded, layer C deposits on layer B. Finally the eroded layer C forms the current topography. Under such environment when underground soil layers are known, Scoops3D can easily incorporate different soil layers by inputting the elevation of the bottom of each layer, however, OpenLISEM can only consider one layer of soil. Which model is more realistic for landslide simulation? This question is unresolved.

6.1.3. Errors and uncertainties related to the model outputs processing

Errors and uncertainties are also involved when transforming the model outputs to the landslide volumes. The major outputs related to landslide volumes are failure maps, which indicate the failures of every individual pixels. Transforming the pixel failures to the individual slope failures can be extremely difficult when a cluster of failed pixels is weakly joined together and some indistinct boundaries can be found among them. Fig. 6-2 shows failure height maps and the final landslide maps in scenario 1 simulated by OpenLISEM and Scoosp3D. The final landslide maps were derived from digitizing polygons using failure height maps (sometimes also coupled with FoS map). In Fig. 6-2 (a), within a red circle, there are some several groups of failure pixels weakly linked with each other, we considered them as several individual landslides which are shown in Fig. 6-2 (b). Whereas in Fig. 6-2 (c), within a red circle at the same location, it is very hard to distinguish whether they are separate landslides or integral landslides. We considered them as integral landslides. Subjective judgment may be required when digitizing the landslide polygons from the combined maps of failure depth and Factor of Safety. Wrong combinations or separations of failed pixels will result in totally different landslide areas and volumes. The total landslide area and volume, in this case, is more trustful than the individual landslide areas and volumes.

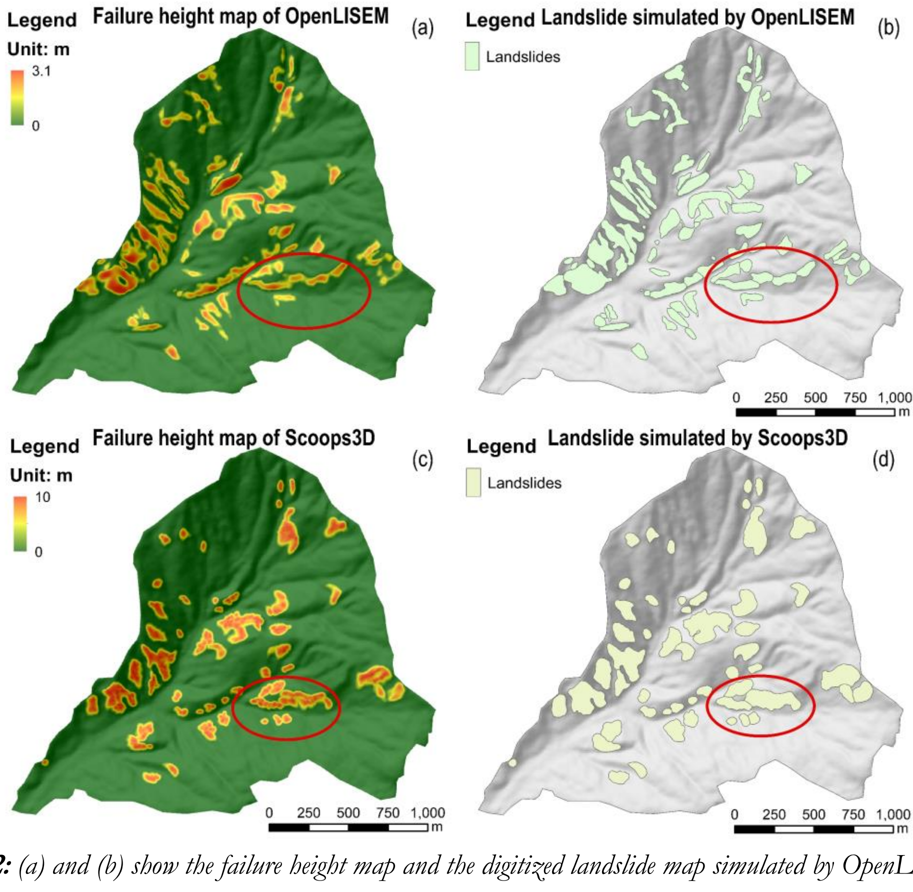

Fig. 6-2: *(a) and (b) show the failure height map and the digitized landslide map simulated by OpenLISEM in scenario 1. (c) and (d) show the failure height map and the digitized landslide map simulated by Scoops3D in scenario 1.*

6.1.4. The limitations of the models

The limitations of the models themselves also affect the model results. The limitations are mainly caused by the model assumptions described in chapter 3.

- For slope stability analysis, both OpenLISEM and Scoops3D apply limit equilibrium methods. No progressive failure can be simulated in limit equilibrium methods, and failure occurs simultaneously along one single failure surface. For landslide monitoring and more complex slip geometry, OpenLISEM and Scoops3D are not appropriate anymore.
- Neither OpenLISEM nor Scoops3D takes site-specific features such as tension cracks and local soil layer discontinuities, etc. into consideration. However, such features are very important because most rainfall-induced landslides are not simply caused by slow infiltration of wetting front, but rather by rainfall infiltrating into the tension cracks or macropores. And the earthquake-induced landslides are probably caused by the internal strata discontinuities. When such site-specific features are important, OpenLISEM and Scoops3D are not appropriate anymore. Then other models such as TSLOPE (Baum, 2000), CLARA-W (Hungr, 2001), or SVSlope (Fredlund et al., 2009) could be applied.
- The triggering mechanisms in OpenLISEM. OpenLISEM assumes an unrealistic or fake groundwater level. The equation 3-1 of FoS described in section 3.1 is:

$$\mathrm{FoS} = \frac{c' + \Delta c' + [(Z - Z_w) \cdot \gamma + Z_w \cdot \gamma'] cos^2\beta tan\phi'}{[(Z - Z_w) \cdot \gamma + Z_w \gamma_s] sin\beta cos\beta}$$

  Fig. 3-3 (left) shows the real soil situation, and based on the real soil situation, Z_w should be 0. However, as shown in Fig. 3-3 (left), OpenLISEM assumes that there is a groundwater table, and the depth can be calculated using equation 3-4, the Z_w is then greater than 0, and according to equation 3-1, FoS will be decreased.
- Notably, the version of OpenLISEM we used in this study is an untested beta version, the unexpected behavior may have also been due to bugs in the system that still need to be corrected.

6.2. Conclusions and recommendations

The principal purpose of this study was to compare and evaluate two physical models in terms of landslide volume prediction. To achieve this goal, a "virtual volcanic environment" was developed. The input geotechnical and hydrological parameters were derived from literature. The soil depth was initially assumed to be homogeneous everywhere on the terrain. Based on the homogeneous soil depth, scenario 1 (totally dry scenario) was developed. The critical soil depth was also derived using OpenLISEM in scenario 1. Based on the critical soil depth, scenario 2 and 3 with different trigger factors were developed. The similarities and differences between these two models were compared under three developed scenarios.

The first important conclusion in this study can be drawn after learning the models: the data requirements for the successful application of both models are problematic. For calibration and validation, the historical topography, soil data, as well as triggering factors are required. However, when dealing with the unexpected landslide hazards, the qualities of such data are probably poor. The pre-event topography may be derived from digitizing existing hardcopy topographic maps, which can result in errors. The dates and related landslides are probably unknown if a good event-based landslide inventory is not available. For prediction, also the topography and reliable underground information on soil depth, soil characteristics, and groundwater system is required. Many inputs for the physically-based modelling often comes from empirical modelling (e.g. statistical soil depth modelling). However, the significant uncertainties from the approximation of such data will result in large uncertainties for model results, especially for a heterogeneous area at a large scale. Let alone groundwater may be varied with time or seasons. The applications of these two physical models for landslide volume prediction should be regarded with caution.

The internal model parameters can significantly affect the landslide locations and volumes. Sometimes, the effect of these parameters can be bigger than soil parameters or soil depth. The internal model parameters should be carefully selected when one plan to apply these two models in one area. Sensitivity analysis is helpful to determine these parameters.

This study also compared the similarities and differences of simulated landslides between OpenLISEM and Scoops3D. With regards to similarities, both models predict landslides initiation zones. In reality, the real landslide volumes should be bigger than the volumes at the initiation zones due to the entrainment of path material, especially for rapid landslides (McDougall and Hungr, 2004).

The differences of simulated landslides can be summarized as follows:

- <u>The location</u>: the locations of the landslides simulated by OpenLISEM and Scoops3D can be overlapped or non-overlapped. The match index was used to measure the overlapping degree. The match indexes of three scenarios are all less than 0.5, indicating a large difference between two models for detecting potential landslides.
- <u>The landslide density</u>: in scenario 1, the percentage of landslide affected area (the total area of landslides divided by the total area of the catchment) for OpenLISEM is almost the same with the percentage for Scoops3D, they are 16.3% and 15.5%, respectively. In scenario 2, the percentage of landslide affected area for OpenLISEM is 0% whereas the percentage for Scoops3D is about 18%. In scenario 3, the percentage for OpenLISEM is smaller than the percentage for Scoops3D, the difference is about 12%. It can be concluded that Scoops3D tends to affect more area than OpenLISEM in this environment. More importantly, in scenario 2, OpenLISEM did not produce any landslides. This is probably because the extensive runoff due to the low Ksat and steep terrain, the infiltration depths for different rainfall scenarios are more or less the same.
- <u>Landslide morphology</u>: OpenLISEM can produce both narrow and wide landslides discretely distributed on the terrain, the shapes of landslides may be controlled by the failure propagation along the slope. Whereas Scoops3D can only produce relatively round landslides, and sometimes distributed across the whole slope.
- <u>The volume</u>: Scoops3D tends to produce landslides with much larger volumes than OpenLISEM. The potential slip surfaces of landslides from OpenLISEM are pretty shallow, whereas the slip surfaces of landslides from Scoops3D are very deep. For many landslides in Scoops3D, the failure depth can equal to or even exceed the predefined soil depth.
- <u>Successive slope failure</u>: For OpenLISEM, once the slope failures are removed from the original terrain, there will be no more unstable area. Whereas for Scoops3D, the slope failure will continue to occur even if the previous slope failures are all removed from the terrain. Such behavior of successive slope failure is not realistic and should be with caution for its application.

This study also reveals that the internal model parameters can significantly affect the landslide volumes. In OpenLISEM, the maximum factor of safety (F_i) used as cut-off FoS for slope failures and the resultant factor of safety (F_r) used to indicate the post-failure stability should be determined by users. The lower the F_i, the larger the landslide volumes, and the larger the gap between F_i and F_r, the larger the landslide volumes can be produced by OpenLISEM. Meanwhile, in Scoops3D, a series of searching parameters should be determined by users. This study only tested the sensitivity of the volume limits on potential landslide volumes. The other searching parameters were determined by referring to the Scoops3D manual (Reid et al., 2015). It is found that a larger volume limit can ensure a thorough search of the terrain for unstable slopes. However, the bedrock may also be affected if the volume limit is too large, in which case lead to undesired results. The determination of the internal model parameters should be based on the calibration and validation of the models using the historical landslide datasets.

In general, it is hard to draw a conclusion on which model is better, to some degree it was comparing apples with pears. But it is clear that Scoops3D would sometimes exaggerate the slope failures and produce undesired results, and OpenLISEM can give more acceptable results than Scoops3D. To get the more comprehensive and robust comparison, real datasets of different environments should be used in the simulation.

LIST OF REFERENCES

Abramson, L. W., Lee, T. S., Sharma, S., & Boyce, G. M. (2002). Slope stability and stabilization methods. John Wiley & Sons.

Adegbe, M., Ako, T. A., Onoduku, U. S., Asema, A. I., Unubi, A. S., & Inyang, E. B. (2014). Determination of the Volume of Debrisfrom Yingxiu Landslides, Southwest China: Geomorphological and Field Observation Approaches. Journal of Natural Sciences, 2(1), 95-105. Amirahmadi, A., Pourhashemi, S., Karami, M., & Akbari, E. (2016). Modeling of landslide volume estimation. *Open Geosciences*, *8*(1), 360–370. https://doi.org/10.1515/geo-2016-0032

Baartman, J. E. M., Jetten, V. G., Ritsema, C. J., & de Vente, J. (2012). Exploring effects of rainfall intensity and duration on soil erosion at the catchment scale using openLISEM: Prado catchment, SE Spain. *Hydrological Processes*, *26*(7), 1034–1049. https://doi.org/10.1002/hyp.8196

Baldi, P., Fabris, M., Marsella, M., & Monticelli, R. (2005). Monitoring the morphological evolution of the Sciara del Fuoco during the 2002-2003 Stromboli eruption using multi-temporal photogrammetry. *ISPRS Journal of Photogrammetry and Remote Sensing*, *59*(4), 199–211. https://doi.org/10.1016/j.isprsjprs.2005.02.004

Baldo, M., Bicocchi, C., Chiocchini, U., Giordan, D., & Lollino, G. (2009). LIDAR monitoring of mass wasting processes: The Radicofani landslide, Province of Siena, Central Italy. *Geomorphology*, *105*(3–4), 193–201. https://doi.org/10.1016/j.geomorph.2008.09.015

Barbarella, M., Fazio, C., & Fiani, M. (2000). Evaluation of landslide volume using photogrammetric techniques. Int Arch Photogramm Remote Sens, 33(part B4), 278-282.

Bichler, A., Bobrowsky, P., Best, M., Douma, M., Hunter, J., Calvert, T., & Burns, R. (2004). Three-dimensional mapping of a landslide using a multi-geophysical approach: The Quesnel Forks landslide. *Landslides*, *1*(1), 29–40. https://doi.org/10.1007/s10346-003-0008-7

Bilotta, E., Cascini, L., Foresta, V., & Sorbino, G. (2005). Geotechnical characterisation of pyroclastic soils involved in huge flowslides. *Geotechnical and Geological Engineering*, *23*(4), 365–402. https://doi.org/10.1007/s10706-004-1607-3

Bommer, J. J., Rolo, R., Mitroulia, A., & Berdousis, P. (2002). Geotechnical properties and seismic slope stability of volcanic soils. In Proceedings of the 12th European Conference on Earthquake Engineering, London.

Brunetti, M., Guzzetti, F., & Rossi, M. (2009). Probability distributions of landslide volumes. *Nonlinear Processes in Geophysics*, *16*(2), 179–188. https://doi.org/10.5194/npg-16-179-2009

Buytaert, W., Deckers, J., & Wyseure, G. (2007). Regional variability of volcanic ash soils in south Ecuador: The relation with parent material, climate and land use. *Catena*, *70*(2), 143–154. https://doi.org/10.1016/j.catena.2006.08.003

Calvo, L., Haddad, B., Pastor, M., & Palacios, D. (2015). Runout and deposit morphology of Bingham fluid as a function of initial volume: implication for debris flow modelling. *Natural Hazards*, *75*(1), 489–513. https://doi.org/10.1007/s11069-014-1334-x

Cecconi, M., Scarapazzi, M., & Viggiani, G. M. B. (2010). On the geology and the geotechnical properties of pyroclastic flow deposits of the Colli Albani. *Bulletin of Engineering Geology and the Environment*, *69*(2), 185–206. https://doi.org/10.1007/s10064-009-0250-x

Chambers, J. E., Wilkinson, P. B., Kuras, O., Ford, J. R., Gunn, D. A., Meldrum, P. I., … Ogilvy, R. D. (2011). Three-dimensional geophysical anatomy of an active landslide in Lias Group mudrocks, Cleveland Basin, UK. *Geomorphology*, *125*(4), 472–484. https://doi.org/10.1016/j.geomorph.2010.09.017

Chen, R. F., Chang, K. J., Angelier, J., Chan, Y. C., Deffontaines, B., Lee, C. T., & Lin, M. L. (2006). Topographical changes revealed by high-resolution airborne LiDAR data: The 1999 Tsaoling landslide induced by the Chi-Chi earthquake. *Engineering Geology*, *88*(3–4), 160–172. https://doi.org/10.1016/j.enggeo.2006.09.008

Chen, Z., Zhang, B., Han, Y., Zuo, Z., & Zhang, X. (2014). Modeling accumulated volume of landslides using remote sensing and DTM data. *Remote Sensing*, *6*(2), 1514–1537. https://doi.org/10.3390/rs6021514

Chong Xu, Xiwei Xu, Tolga Gorum, Cees J. van Westen, and X. F., & Abstract. (2014). Did the 2008 Wenchuan Earthquake Lead to a Net Volume Loss?, *3*, 191–196. https://doi.org/10.1007/978-3-319-04999-1

Corominas, J., van Westen, C., Frattini, P., Cascini, L., Malet, J. P., Fotopoulou, S., … Smith, J. T. (2014).

Recommendations for the quantitative analysis of landslide risk. *Bulletin of Engineering Geology and the Environment*, *73*(2), 209–263. https://doi.org/10.1007/s10064-013-0538-8
Cruden, D. M. (1996). Landslides Types and Processes:. Landslides. Investigation and mitigation, 36-75.
Dai, F. ., Lee, C. ., & Ngai, Y. . (2002). Landslide risk assessment and management: an overview. *Engineering Geology*, *64*(1), 65–87. https://doi.org/10.1016/S0013-7952(01)00093-X
Dai, F. C., & Lee, C. F. (2001). Frequency-volume relation and prediction of rainfall-induced landslides. *Engineering Geology*, *59*(3–4), 253–266. https://doi.org/10.1016/S0013-7952(00)00077-6
Dai, F. C., Xu, C., Yao, X., Xu, L., Tu, X. B., & Gong, Q. M. (2011). Spatial distribution of landslides triggered by the 2008 Ms 8.0 Wenchuan earthquake, China. *Journal of Asian Earth Sciences*, *40*(4), 883–895. https://doi.org/10.1016/j.jseaes.2010.04.010
Damiano, E., Olivares, L., & Picarelli, L. (2012). Steep-slope monitoring in unsaturated pyroclastic soils. *Engineering Geology*, *137–138*, 1–12. https://doi.org/10.1016/j.enggeo.2012.03.002
Davis, T. J., & Keller, C. P. (1997). Modelling uncertainty in natural resource analysis using fuzzy sets and monte carlo simulation: Slope stability prediction. *International Journal of Geographical Information Science*, *11*(5), 409–434. https://doi.org/10.1080/136588197242239
de Bari, C., Lapenna, V., Perrone, A., Puglisi, C., & Sdao, F. (2011). Digital photogrammetric analysis and electrical resistivity tomography for investigating the Picerno landslide (Basilicata region, southern Italy). *Geomorphology*, *133*(1–2), 34–46. https://doi.org/10.1016/j.geomorph.2011.06.013
de Falco, M., Di Crescenzo, G., & Santo, A. (2012). Volume estimate of flow-type landslides along carbonatic and volcanic slopes in Campania (Southern Italy). *Natural Hazards*, *61*(1), 51–63. https://doi.org/10.1007/s11069-011-9782-z
De Roo, A. P. J., & Jetten, V. G. (1999). Calibrating and validating the LISEM model for two data sets from the Netherlands and South Africa. *Catena*, *37*(3–4), 477–493. https://doi.org/10.1016/S0341-8162(99)00034-X
De Roo, A. P. J., Offermans, R. J. E., & Cremers, N. H. D. T. (1996). LISEM: a single-event, physically based hydrological and soil erosion model for drainage basins. II: sensitivity analysis, validation and application. *Hydrological Processes*, *10*(8), 1119–1126. https://doi.org/10.1002/(SICI)1099-1085(199608)10:8<1119::AID-HYP416>3.0.CO;2-V
Degruyter, W., Bachmann, O., Burgisser, A., & Manga, M. (2012). The effects of outgassing on the transition between effusive and explosive silicic eruptions. *Earth and Planetary Science Letters*, *349–350*, 161–170. https://doi.org/10.1016/j.epsl.2012.06.056
Deparis, J., Fricout, B., Jongmans, D., Villemin, T., Effendiantz, L., & Mathy, A. (2008). Combined use of geophysical methods and remote techniques for characterizing the fracture network of a potentially unstable cliff site (the "Roche du Midi", Vercors massif, France). *Journal of Geophysics and Engineering*, *5*(2), 147–157. https://doi.org/10.1088/1742-2132/5/2/002
Dewitte, O., & Demoulin, a. (2005). Morphometry and kinematics of landslides inferred from precise DTMs in West Belgium. *Natural Hazards and Earth System Science*, *5*(2), 259–265. https://doi.org/10.5194/nhess-5-259-2005
Dewitte, O., Jasselette, J. C., Cornet, Y., Van Den Eeckhaut, M., Collignon, A., Poesen, J., & Demoulin, A. (2008). Tracking landslide displacements by multi-temporal DTMs: A combined aerial stereophotogrammetric and LIDAR approach in western Belgium. *Engineering Geology*, *99*(1–2), 11–22. https://doi.org/10.1016/j.enggeo.2008.02.006
Du, J., & Teng, H. (2007). 3D laser scanning and GPS technology for landslide earthwork volume estimation, *16*, 657–663. https://doi.org/10.1016/j.autcon.2006.11.002
Duncan, J. M., Wright, S. G., & Brandon, T. L. (2014). *Soil Strength and Slope Stability*. Retrieved from http://site.ebrary.com/lib/istanbulteknik/reader.action?docID=10909566&ppg=1
Fan, X., van Westen, C. J., Xu, Q., Gorum, T., & Dai, F. (2012). Analysis of landslide dams induced by the 2008 Wenchuan earthquake. *Journal of Asian Earth Sciences*, *57*, 25–37. https://doi.org/10.1016/j.jseaes.2012.06.002
Fell, R., Corominas, J., Bonnard, C., Cascini, L., Leroi, E., & Savage, W. Z. (2008). Guidelines for landslide susceptibility, hazard and risk zoning for land use planning. *Engineering Geology*, *102*(3–4), 85–98. https://doi.org/10.1016/j.enggeo.2008.03.022
Frattini, P., Crosta, G. B., Fusi, N., & Dal Negro, P. (2004). Shallow landslides in pyroclastic soils: A distributed modelling approach for hazard assessment. *Engineering Geology*, *73*(3–4), 277–295. https://doi.org/10.1016/j.enggeo.2004.01.009
Fumitoshi Imaizumi, R. C. S. and R. K. (2009). High spatial resolution data acquisition for the geosciences: kite aerial photography. *Earth Surface Processes and Landforms*, *34*, 155–161.

https://doi.org/10.1002/esp
GEO-SLOPE International. (2010). Stability Modeling with SLOPE / W 2007, (February), 355.
Göktürkler, G., Balkaya, Ç., & Erhan, Z. (2008). Geophysical investigation of a landslide: The Altındağ landslide site, İzmir (western Turkey). Journal of Applied Geophysics, 65(2), 84-96. https://doi.org/10.1016/j.jappgeo.2008.05.008
Guthrie, R. H., & Evans, S. G. (2004). Analysis of landslide frequencies and characteristics in a natural system, coastal British Columbia. *Earth Surface Processes and Landforms*, *29*(11), 1321–1339. https://doi.org/10.1002/esp.1095
Guzzetti, F., Ardizzone, F., Cardinali, M., Galli, M., Reichenbach, P., & Rossi, M. (2008). Distribution of landslides in the Upper Tiber River basin , central Italy, *96*, 105–122. https://doi.org/10.1016/j.geomorph.2007.07.015
Guzzetti, F., Ardizzone, F., Cardinali, M., Rossi, M., & Valigi, D. (2009). Landslide volumes and landslide mobilization rates in Umbria , central Italy. *Earth and Planetary Science Letters*, *279*(3–4), 222–229. https://doi.org/10.1016/j.epsl.2009.01.005
Hack, R. (2000). Geophysics for slope stability. *Surveys in Geophysics*, *21*(4), 423–448. https://doi.org/10.1023/A:1006797126800
Hapke, C. J. (2005). Estimation of regional material yield from coastal landslides based on historical digital terrain modelling. *Earth Surface Processes and Landforms*, *30*(6), 679–697. https://doi.org/10.1002/esp.1168
Herrera, M. C., Lizcano, A., & Santamarina, J. C. (2007). Colombian volcanic ash soils. Characterization and engineering properties of natural soils, 2385-2409.
Hovius, N., Stark, C. P., & Allen, P. A. (1997). Sediment flux from a mountain belt derivedby landslide mapping. *Geology*, *25*(March), 231–234. https://doi.org/10.1130/0091-7613(1997)025<0231
Hungr, O., Salgado, F. M., & Byrne, P. M. (1989). Evaluation of a three-dimensional method of slope stability analysis. Canadian Geotechnical Journal, 26(4), 679-686.
Hungr, O., Corominas, J., & Eberhardt, E. (2005). Estimating landslide motion mechanism, travel distance and velocity. *Landslide Risk Management*, (February 2017), 99–128.
Imaizumi, F., & Sidle, R. C. (2007). Linkage of sediment supply and transport processes in Miyagawa Dam catchment, Japan. *Journal of Geophysical Research: Earth Surface*, *112*(3), 1–17. https://doi.org/10.1029/2006JF000495
Jetten, V., Govers, G., & Hessel, R. (2003). Erosion models: Quality of spatial predictions. *Hydrological Processes*, *17*(5), 887–900. https://doi.org/10.1002/hyp.1168
Jetten, V., & van den Bout, B. (2017). LISEM Limburg Soil Erosion model v 3.9x: Documentation & User Manual.
Joergensen, R. G., & Castillo, X. (2001). Interrelationships between microbial and soil properties in young volcanic ash soils of Nicaragua, *33*, 1581–1589.
Jongmans, D., Bièvre, G., Renalier, F., Schwartz, S., Beaurez, N., & Orengo, Y. (2009). Geophysical investigation of a large landslide in glaciolacustrine clays in the Trièves area (French Alps). *Engineering Geology*, *109*(1–2), 45–56. https://doi.org/10.1016/j.enggeo.2008.10.005
Jongmans, D., & Garambois, S. (2007). Geophysical investigation of landslides: A review. *Bulletin de La Societe Geologique de France*, *178*(2), 101–112. https://doi.org/10.2113/gssgfbull.178.2.101
Kasai, M., Ikeda, M., Asahina, T., & Fujisawa, K. (2009). LiDAR-derived DEM evaluation of deep-seated landslides in a steep and rocky region of Japan. *Geomorphology*, *113*(1–2), 57–69. https://doi.org/10.1016/j.geomorph.2009.06.004
Keefer, D. K. (1994). The importance of earthquake-induced landslides to long-term slope erosion and slope-failure hazards in seismically active regions. *Geomorphology*, *10*(1–4), 265–284. https://doi.org/10.1016/0169-555X(94)90021-3
Keller, G. V. (1986). An Introduction to Geophysical Exploration. *Eos, Transactions American Geophysical Union* (Vol. 67). https://doi.org/10.1029/EO067i011p00132-01
Kerle, N. (2002). Volume estimation of the 1998 flank collapse at Casita volcano, Nicaragua: A comparison of photogrammetric and conventional techniques. *Earth Surface Processes and Landforms*, *27*(7), 759–772. https://doi.org/10.1002/esp.351
Khazai, B., & Sitar, N. (2000). Assessment of seismic slope stability using gis modeling. *Geographic Information Sciences*, *6*(2), 121–128. https://doi.org/10.1080/10824000009480540
Klar, A., Aharonov, E., Asael, B. K., & Katz, O. (2011). Analytical and observational relations between landslide volume and surface area, *116*(December 2010), 1–10. https://doi.org/10.1029/2009JF001604

Korup, O. (2005). Distribution of landslides in southwest New Zealand. *Landslides*, *2*(1), 43–51. https://doi.org/10.1007/s10346-004-0042-0

Krahn, J. (2003). The 2001 R.M. Hardy Lecture: The limits of limit equilibrium analyses. *Canadian Geotechnical Journal*, *40*(3), 643–660. https://doi.org/10.1139/t03-024

Larsen, I. J., Montgomery, D. R., & Korup, O. (2010). Landslide erosion controlled by hillslope material. *Nature Geoscience*, *3*(4), 247–251. https://doi.org/10.1038/ngeo776

Lebourg, T., Binet, S., Tric, E., Jomard, H., & El Bedoui, S. (2005). Geophysical survey to estimate the 3D sliding surface and the 4D evolution of the water pressure on part of a deep seated landslide. *Terra Nova*, *17*(5), 399–406. https://doi.org/10.1111/j.1365-3121.2005.00623.x

Letters, P. S., Guzzetti, F., National, I., & King, B. D. M. (2002). Power-law correlations of landslide areas in central Italy Power-law correlations of landslide areas in central Italy, *195*(April 2014), 169–183. https://doi.org/10.1016/S0012-821X(01)00589-1

Loew, S., Gschwind, S., Gischig, V., Keller-Signer, A., & Valenti, G. (2017). Monitoring and early warning of the 2012 Preonzo catastrophic rockslope failure. *Landslides*, *14*(1), 141–154. https://doi.org/10.1007/s10346-016-0701-y

Lollino, G., Giordan, D., Crosta, G. B., Corominas, J., Azzam, R., Wasowski, J., & Sciarra, N. (2015). Engineering geology for society and territory – Volume 2: Landslide processes. *Engineering Geology for Society and Territory - Volume 2: Landslide Processes*, *2*, 1–2177. https://doi.org/10.1007/978-3-319-09057-3

Malamud, B. D., Turcotte, D. L., Guzzetti, F., & Reichenbach, P. (2004). Landslide inventories and their statistical properties. *Earth Surface Processes and Landforms*, *29*(6), 687–711. https://doi.org/10.1002/esp.1064

Marchesini, I., Cencetti, C., & De Rosa, P. (2009). A preliminary method for the evaluation of the landslides volume at a regional scale. *GeoInformatica*, *13*(3), 277–289. https://doi.org/10.1007/s10707-008-0060-5

McCann, D. M., & Forster, A. (1990). Reconnaissance geophysical methods in landslide investigations. *Engineering Geology*, *29*(1), 59–78. https://doi.org/10.1016/0013-7952(90)90082-C

Mergili, M., Marchesini, I., Alvioli, M., Metz, M., Schneider-Muntau, B., Rossi, M., & Guzzetti, F. (2014). A strategy for GIS-based 3-D slope stability modelling over large areas. *Geoscientific Model Development*, *7*(6), 2969–2982. https://doi.org/10.5194/gmd-7-2969-2014

Mergili, M., Marchesini, I., Rossi, M., Guzzetti, F., & Fellin, W. (2014). Spatially distributed three-dimensional slope stability modelling in a raster GIS. *Geomorphology*, *206*, 178–195. https://doi.org/10.1016/j.geomorph.2013.10.008

Meric, O., Garambois, S., Jongmans, D., Wathelet, M., Chatelain, J. L., & Vengeon, J. M. (2005). Application of geophysical methods for the investigation of the large gravitational mass movement of Séchilienne, France. *Canadian Geotechnical Journal*, *42*(4), 1105–1115. https://doi.org/10.1139/t05-034

Montgomery, D. R., & Dietrich, W. E. (1994). A physically based model for the topographic control on shallow landsliding. *Water Resources Research*, *30*(4), 1153–1171. https://doi.org/10.1029/93WR02979

Naudet, V., Lazzari, M., Perrone, A., Loperte, A., Piscitelli, S., & Lapenna, V. (2008). Integrated geophysical and geomorphological approach to investigate the snowmelt-triggered landslide of Bosco Piccolo village (Basilicata, southern Italy). *Engineering Geology*, *98*(3–4), 156–167. https://doi.org/10.1016/j.enggeo.2008.02.008

Nchez, a J. (1998). The frequency and distribution of Larsen, M.C., Torres Sa recent landslides in three montane tropical regions of Puerto Rico. *Geomorphology*, *24309e331*, 309–331.

Nikolaeva, E., Walter, T. R., Shirzaei, M., & Zschau, J. (2014). Landslide observation and volume estimation in central Georgia based on L-band InSAR. *Natural Hazards and Earth System Sciences*, *14*(3), 675–688. https://doi.org/10.5194/nhess-14-675-2014

Pack, R. T., Tarboton, D. G., & Goodwin, C. N. (2003). SINMAP - A stability index approach to terrain stability hazard mapping. *Manuel*, 1–75. https://doi.org/10.1007/SpringerReference_28001

Pagano, L., Picarelli, L., Rianna, G., & Urciuoli, G. (2010). A simple numerical procedure for timely prediction of precipitation-induced landslides in unsaturated pyroclastic soils. *Landslides*, *7*(3), 273–289. https://doi.org/10.1007/s10346-010-0216-x

Pazzi, V., Tanteri, L., Bicocchi, G., D'Ambrosio, M., Caselli, A., & Fanti, R. (2017). H/V measurements as an effective tool for the reliable detection of landslide slip surfaces: Case studies of Castagnola (La Spezia, Italy) and Roccalbegna (Grosseto, Italy). *Physics and Chemistry of the Earth*, *98*, 136–153. https://doi.org/10.1016/j.pce.2016.10.014

Pyke, R., 1991. TSLOPE3: User Guide. Taga Engineering System and Software, Lafayette.
Refice, A., & Capolongo, D. (2002). Probabilistic modeling of uncertainties in earthquake-induced landslide hazard assessment. *Computers and Geosciences*, *28*(6), 735–749. https://doi.org/10.1016/S0098-3004(01)00104-2
Reid, M. E., Christian, S. B., Brien, D. L., & Henderson, S. . (2015). Scoops3D—Software to Analyze Three-Dimensional Slope Stability Throughout a Digital Landscape. In *U.S. Geological Survey Techniques and Methods, book 14* (p. 218). https://doi.org/10.3133/tm14A1
Rice, R. M., Crobett, E. S., & Bailey, R. G. (1969). Soil Slips Related to Vegetation, Topography, and Soil in Southern California. *Water Resources Research*, *5*(3), 647–659. https://doi.org/10.1029/WR005i003p00647
Ritz, M. (1999). Electrical imaging of lateritic weathering mantles over granitic and metamorphic basement of eastern Senegal , West Africa, 335–344.
Robain, H., Descloitres, M., Ritz, M., & Yene, Q. (1996). IGIEI HIV51C5 A multiscale electrical survey of a lateritic soil system in the rain forest of Cameroon, *34*, 237–253.
Saxton, K. E., & Rawls, W. J. (2006). Soil Water Characteristic Estimates by Texture and Organic Matter for Hydrologic Solutions. *Soil Science Society of America Journal*, *70*(5), 1569. https://doi.org/10.2136/sssaj2005.0117
Seguel, O., & Horn, R. (2005). Mechanical behavior of a volcanic ash soil (Typic Hapludand) under static and dynamic loading, *82*, 109–116. https://doi.org/10.1016/j.still.2005.01.010
ten Brink, U. S., Geist, E. L., & Andrews, B. D. (2006). Size distribution of submarine landslides and its implication to tsunami hazard in Puerto Rico. *Geophysical Research Letters*, *33*(11), 23–26. https://doi.org/10.1029/2006GL026125
Terlien, M. T. J. (1997). Hydrological landslide triggering in ash-covered slopes of Manizales (Columbia). *Geomorphology*, *20*(1–2), 165–175. https://doi.org/10.1016/S0169-555X(97)00022-6
Tseng, C. M., Lin, C. W., Stark, C. P., Liu, J. K., Fei, L. Y., & Hsieh, Y. C. (2013). Application of a multi-temporal, LiDAR-derived, digital terrain model in a landslide-volume estimation. *Earth Surface Processes and Landforms*, *38*(13), 1587–1601. https://doi.org/10.1002/esp.3454
van Beek, L. P. H. (2002). *Assessment of the influence of changes in land use and climate on landslide activity in a Mediterranean environment.*
Van den Bout, B., L. Lombardo, C.J. van Westen, & Jetten, V., (2017). To be published. Submitted to EGU General Assembly 2018.
van Westen, C. J., & Lulie Getahun, F. (2003). Analyzing the evolution of the Tessina landslide using aerial photographs and digital elevation models. *Geomorphology*, *54*(1–2), 77–89. https://doi.org/10.1016/S0169-555X(03)00057-6
van Westen, C. J., & Terlien, M. T. J. (1996). An approach towards deterministic landslide hazard analysis in GIS. A case study from Manizales (Colombia). *Earth Surface Processes and Landforms*, *21*(21), 853–868. https://doi.org/10.1002/(SICI)1096-9837(199609)21:9<853::AID-ESP676>3.0.CO;2-C
Ventura, G., Vilardo, G., Terranova, C., & Sessa, E. B. (2011). Tracking and evolution of complex active landslides by multi-temporal airborne LiDAR data: The Montaguto landslide (Southern Italy). *Remote Sensing of Environment*, *115*(12), 3237–3248. https://doi.org/10.1016/j.rse.2011.07.007
Wang, H. B., Liu, G. J., Xu, W. Y., & Wang, G. H. (2005). GIS-based landslide hazard assessment: an overview. *Progress In Physical Geography*, *29*(4), 548–567. https://doi.org/10.1191/0309133305pp462ra
Wilson, J. P. (2012). Digital terrain modeling. *Geomorphology*, *137*(1), 107–121. https://doi.org/10.1016/j.geomorph.2011.03.012
Wu, W., & Sidle, R. C. (1995). A Distributed Slope Stability Model for Steep Forested Basins. *Water Resources Research*, *31*(8), 2097–2110. https://doi.org/10.1029/95WR01136
Xie, M. W., Esaki, T., Zhou, G. Y., & Mitani, Y. (2003). Three-dimensional stability evaluation of landslides and a sliding process simulation using a new geographic information systems component. *Environmental Geology*, *43*(5), 503–512. https://doi.org/10.1007/s00254-002-0655-3
Xu, C., Xu, X., Pourghasemi, H. R., Pradhan, B., & Iqbal, J. (2014). Volume, gravitational potential energy reduction, and regional centroid position change in the wake of landslides triggered by the 14 April 2010 Yushu earthquake of China. *Arabian Journal of Geosciences*, *7*(6), 2129–2138. https://doi.org/10.1007/s12517-013-1020-4
Xu, C., Xu, X., Shen, L., Yao, Q., Tan, X., Kang, W., … Li, K. (2016). Optimized volume models of earthquake-triggered landslides. *Scientific Reports*, *6*(March), 29797. https://doi.org/10.1038/srep29797
Zhan, W., Fan, X., Huang, R., Pei, X., Xu, Q., & Li, W. (2017). Empirical prediction for travel distance of

channelized rock avalanches in the Wenchuan earthquake area, (2015), 833–844.
Zhang, W., Chen, J., Zhang, W., Lü, Y., Ma, Y., & Xiong, H. (2013). Determination of critical slip surface of fractured rock slopes based on fracture orientation data. *Science China Technological Sciences*, *56*(5), 1248–1256. https://doi.org/10.1007/s11431-012-5129-6

Annex A

```
################################################
# Model: simple slope based groundwater flow                    #
# Author: Bastian van den Bout                                  #
################################################
binding
        DT = 6;                     ## timestep in hours
        SD = soildepth.map;         ## input soil depth, soildepth.map in mm
        ThetaS = thetas.map;        ## porosity (saturated) of the soil (-)
        ThetaI = thetai.map;        ## initial soil moisture content of the soil (-)
        ThetaR = thetar.map;        ## porosity (residual) of the soil (-)
        KSat = ksat.map;  ## saturated hyraulic conductivity of the soil (mm/h)
        DEM = dem.map;              ##  digital elevation model (m)
        Thetareport = thetaim;      ## bind output map
        Hreport = SoilH;  ## bind output map
        Hinitial = SoilHi.map;      ## bind initial output map
areamap
        mask.map;                   ## mask indicates the area for calculation

timer
1 80 1;                             ## start timestep, final timestep, increment
rep = 1, 1 + 1..endtime;

initial
        SD = SD/1000.0;         ## soil depth to meters
        KSat = KSat/1000.0;     ## saturated conductivity to meters per hour
        H = ThetaI * SD;        ## effective water height
        report SoilHi.map = H;

        Q = scalar(0.0);  ## total discharge
        Qx = scalar(0.0); ## x direction discharge
        Qy = scalar(0.0); ## y direction discharge
        Sx = scalar(0.0); ## x direction slope
        Sy = scalar(0.0); ## y direction slope

dynamic
        #R = min(KSat,timeinputscalar(Rainfall,1))* DT / 1000;
        #H = max(ThetaR * SD,min(ThetaS * SD, H + R / (ThetaS - ThetaR)));
        Sx = -(cover(shift(DEM + H,0,1),DEM) - cover(shift(DEM + H,0,-1),DEM))/celllength(); ## calculate
slope
        Sy = -(cover(shift(DEM + H,1,0),DEM) - cover(shift(DEM + H,-1,0),DEM))/celllength(); ## calculate
slope
        Qx = DT * KSat * Sx * H ; ## calculate groundwater discharge
        Qy = DT * KSat * Sy * H ; ## calculate groundwater discharge
        Qx = if(Qx gt 0.0,1.0,-1.0) * min(0.3 * H,abs(Qx));     ## limit by available water
        Qy = if(Qy gt 0.0,1.0,-1.0) * min(0.3 * H,abs(Qy));     ## limit by available water
        H = H + min(0.0, -abs(Qx) -abs(Qy));         ## subtract outflow
        H = H + abs(min(0.0,cover(shift(Qx,0,1),0.0)));         ## add inflow x direction
        H = H + abs(max(0.0,cover(shift(Qx,0,-1),0.0)));        ## add inflow x direction
        H = H + abs(min(0.0,cover(shift(Qy,1,0),0.0)));         ## add inflow y direction
        H = H + abs(max(0.0,cover(shift(Qy,-1,0),0.0)));        ## add inflow y direction

        H = max(ThetaR * SD,min(ThetaS * SD,H));  ## if oversaturation, remove
        H = windowaverage(H,celllength() * 2.0);      ## take spatial average of 2 cells width to smoothen
dem errors
        report (rep)  Hreport = H;                    ## reports map in SoilH.map
        report (rep)  Thetareport = max(ThetaR,min(ThetaS,H/SD)); ## reports map in thetaim.map
```